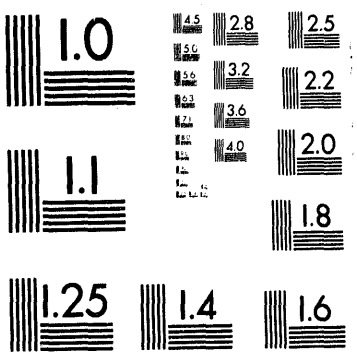
1.0
1.1
1.25
1.4
1.6
1.8
2.0
2.2
2.5
2.8
3.2
3.6
4.0
4.5
5.0
5.6
6.3

1 of 2

Sythesis,Characterization Phase Diagrams and Superconducting and normal State Magnetc Properties of La*2-x*CuO4 .....

by Fangcheg Chou

thesis submitted to Iowa State University

Ames Laboratory, U. S. DOE

Iowa State University

Ames, Iowa 50011

Date Transmitted: August 1993

Prepared for the U. S. Department of Energy

Under contract no. W-7405-eng-82.

DISCLAIMER

Synthesis, characterization, phase diagrams and superconducting and normal state magnetic properties of $La_{2-x}Sr_xCuO_4$ ($0 \le x \le 0.08$) and electrochemically oxidized $La_{2-x}Sr_xCuO_{4+\delta}$ ($0 \le x \le 0.33$, $0 \le \delta \le 0.12$)

Fangcheng Chou

Under the supervision of D. C. Johnston
From the Department of Physics and Astronomy
Iowa State University

$La_{2-x}Sr_xCuO_4$ ($0 \le x \le 0.15$) can all be intercalated with oxygen by an novel electrochemical oxidation method. Bulk superconductivity is found with an onset $T_c \approx 40$ K for the whole range $0.01 \le x \le 0.15$; for $x = 0.25$ and 0.33, the electrochemical oxidation did not improve the superconducting properties. The magnetic susceptibility χ(T = 50-320 K) data for $La_2CuO_{4.11}$ and $La_{1.92}Sr_{0.08}CuO_{4.07}$ are nearly identical with those of conventionally prepared $La_{1.85}Sr_{0.15}CuO_4$, indicating that the hole doping level (p) in the CuO_2 planes of the three compounds is nearly the same. Combined thermogravimetric analysis and iodometric titration experiments indicate that part of the intercalated oxygen has a formal valence close to -1. The maximum doped-hole concentration in the CuO_2 planes that can be achieved from combined Sr-doping and electrochemical oxygen doping for $0 \le x \le 0.15$ is $p \approx 0.16$ holes/formula unit.

Oxygen can also intercalate into single crystal La_2CuO_4 through a slow electrochemical oxidation process. The required low current and long time for the charging process reflects that the oxygen intercalation for a single crystal is limited by its small specific surface area and long diffusion distance. The anisotropic superconducting, magnetic and transport properties are summarized and compared with those of polycrystalline $La_2CuO_{4+\delta}$ as well as of $YBa_2Cu_3O_{7-\delta}$ and $La_{2-x}Sr_xCuO_4$ single crystals. The single crystal $La_2CuO_{4+\delta}$ has a maximum $T_C \approx 40$ K, which is lower than that ($T_C \approx 42$-45) of the corresponding polycrystalline samples.

The magnetic phase diagram of $La_{2-x}Sr_xCuO_4$ in the antiferromagnetic (AF) regime ($0 \leq x \leq 0.02$) has been derived from ^{139}La NQR studies from 4 to 250 K. The data demonstrate localization of the doped holes' charge below ~ 30 K, followed by freezing of the holes' effective spin degrees of freedom below $T_f \approx (815\ x)$ K into a spin-glass-like (SG) state which is superimposed on the AF background. These and previous results allow a detailed magnetic phase diagram to be constructed for $x \leq 0.05$ and reveal a distinct cross-over at $x \approx 0.02$ in the nature of the SG transition.

Synthesis, characterization, phase diagrams and superconducting and normal state magnetic properties of $La_{2-x}Sr_xCuO_4$ ($0 \leq x \leq 0.08$) and electrochemically oxidized $La_{2-x}Sr_xCuO_{4+\delta}$ ($0 \leq x \leq 0.33$, $0 \leq \delta \leq 0.12$)

by

Fangcheng Chou

A Dissertation Submitted to the
Graduate Faculty in Partial Fulfillment of the
Requirements for the Degree of
DOCTOR OF PHILOSOPHY

Department: Physics and Astronomy
Major: Condensed Matter Physics

Approved:

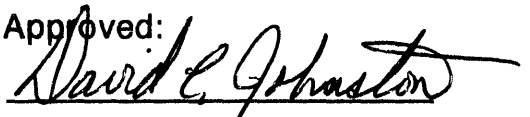

In Charge of Major Work

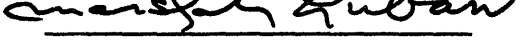

For the Major Department

For the Graduate College

Iowa State University
Ames, Iowa

1993

To my mother and my wife

TABLE OF CONTENTS

CHAPTER 1 INTRODUCTION

1.1. Scope of this work

The T-x phase diagram of $La_{2-x}Sr_xCuO_4$ and the δ-T phase diagram of $La_2CuO_{4+\delta}$ have led to important physical insights which may contain the answer of the origin of high-T_c superconductivity. In this work we used an electrochemical oxidation method to investigate more about the superconductivity, phase separation mechanism and the normal state magnetism of $La_2CuO_{4+\delta}$. The physical properties of the first electrochemically oxidized $La_2CuO_{4+\delta}$ single crystals will be reported. ^{139}La NQR spectroscopy has been used to investigate the dynamical and static magnetic properties of lightly doped $La_{2-x}Sr_xCuO_4$ ($x \leq 0.02$). A new phase boundary has been proposed within the Néel state at low temperature.

The format of this dissertation is as follows. In Chapter 1, a theoretical and experimental survey of the physical properties of La_2CuO_4 is given. In Chapter 2, some basics of electrochemistry as well as the nature of intercalated oxygen and its impact on physical properties of $La_{2-x}Sr_xCuO_{4+\delta}$ are discussed. In Chapter 3, anisotropic superconducting, transport and magnetic properties of electrochemically oxidized single crystal $La_2CuO_{4+\delta}$ are summarized. In Chapter 4, we introduce the theoretical background of ^{139}La NQR and summarize the dynamic and static magnetic properties of lightly doped

$La_{2-x}Sr_xCuO_4$. Finally we propose a complete phase diagram containing the additional information obtained in this study.

1.2. Literature review

Bednorz and Müller first showed that superconductivity occurs below T_c ~ 30 K in the La-Ba-Cu-O system [Bednorz, 1986]. A somewhat higher $T_c \leq 40$ K was later achieved by Sr substitution to the La site of La_2CuO_4 [Tarascon, 1987]. A number of authors reported traces or larger amounts of superconductivity in nominal La_2CuO_4 but later it was found that the oxygen stoichiometry plays a major role in the observed superconductivity [Grant, 1987][Beille, 1987]. Schirber et al. [1988] made superconducting $La_2CuO_{4+\delta}$ with $T_c \approx 34$ K by annealing La_2CuO_4 in an oxygen pressure of 3 kbar at 500-600 °C, where, oxidation of the La_2CuO_4 occurs due to oxygen insertion. Further studies on oxygen insertion by high oxygen pressure up to 23 kbar did not enhance T_c further [Zhou, 1989]. High oxygen pressure oxidation becomes less effective for Sr-doped La_2CuO_4 as shown in studies using oxygen pressure up to 400 bar [Oda, 1990]. Phase separation below phase separation temperature $T_{ps} \approx 320$ K in $La_2CuO_{4+\delta}$ was observed by Jorgensen et al. [1988] from powder neutron diffraction structural analysis, where nearly stoichiometric La_2CuO_4 was found to coexist with oxidized $La_2CuO_{4+\delta}$ ($\delta \approx 0.08$) below T_{ps} and the latter was deduced to be the superconducting phase.

Wattiaux et al. [1990] found that superconducting $La_2CuO_{4.09}$ with

$T_C \approx 44$ K can be synthesized from the antiferromagnetic insulator parent compound La_2CuO_4 using a unique electrochemical oxidation method [Grenier, 1991]. This electrochemical oxidation method surpasses earlier high-oxygen-pressure methods in three aspects. First, it can control the amount of intercalated oxygen accurately. Second, the experiment can be performed at room temperature and third, it has the capability to achieve single-phase samples with higher oxygen contents. After the development of oxygen intercalation by high-oxygen pressure annealing and electrochemical oxidation methods on La_2CuO_4, additional direct room temperature chemical oxidation by strong oxidants, such as $KMnO_4$ [T-Muromachi, 1993] and NaOBr [Rudolf, 1992], were found successful later.

It has been of great importance to clarify the role of magnetic interactions in the CuO_2 planes and of their modifications in the presence of holes introduced by Sr doping and/or by excess oxygen. The introduction of doped holes in the CuO_2 plane is known to reduce drastically the Néel temperature $T_N \approx 320$ K of the planar Heisenberg antiferromagnet (AF) La_2CuO_4, whereby T_N decreases to 0 K by $x \approx 0.02$. Throughout the low doping regime, $x < 0.08$, a rich phenomenology is observed below ~ 20 K in ^{139}La NQR relaxation rates [Kumagai, 1987][Watanabe, 1990], μSR [Harshman, 1988], neutron scattering [Sternlieb, 1990] and magnetic susceptibility $\chi(T)$ measurements [Filipkowski, 1990], which have been attributed to a low temperature magnetic phase similar to a spin-glass. In the "spin-glass regime" $0.02 \leq x \leq 0.08$, Cho et al. have inferred from ^{139}La NQR data that this phase

is an unconventional cluster-spin-glass [Cho, 1992]. In the AF regime $0 \leq x \leq 0.02$, on the other hand, the origin of these anomalies below T_N is obscure, although similarities in behavior to so-called re-entrant spin-glass systems have been noted [Harshman, 1988].

1.3. **Characterization of undoped La_2CuO_4**

1.3.1. Crystal structure

The high temperature tetragonal structure of undoped La_2CuO_4 with space group I4/mmm is shown in Fig. 1.1(a) At temperatures below ~ 530 K the crystal exhibits a second order transition to the orthorhombic structure with space group Cmca [Grande, 1977][Jorgensen, 1987], which is described by the double cell along the diagonal of the tetragonal structure as indicated in Fig. 1.1. This structural transition involves a tilt of CuO_6 octahedra about the tetragonal [110] axis by ~ 1.5° so that the CuO_2 plane is buckled [Grande, 1977].

1.3.2. Spin structure

The spin 1/2 antiferromagnetic Heisenberg model has been used to describe La_2CuO_4. Since La_2CuO_4 undergoes a high temperature tetragonal to a low temperature orthorhombic structure transition around ~530 K, the most important deviation from spin 1/2 2D Heisenberg Hamiltonian is the Dzyaloshinsky-Moriya (D-M) antisymmetric exchange interaction generated by the small tilting of

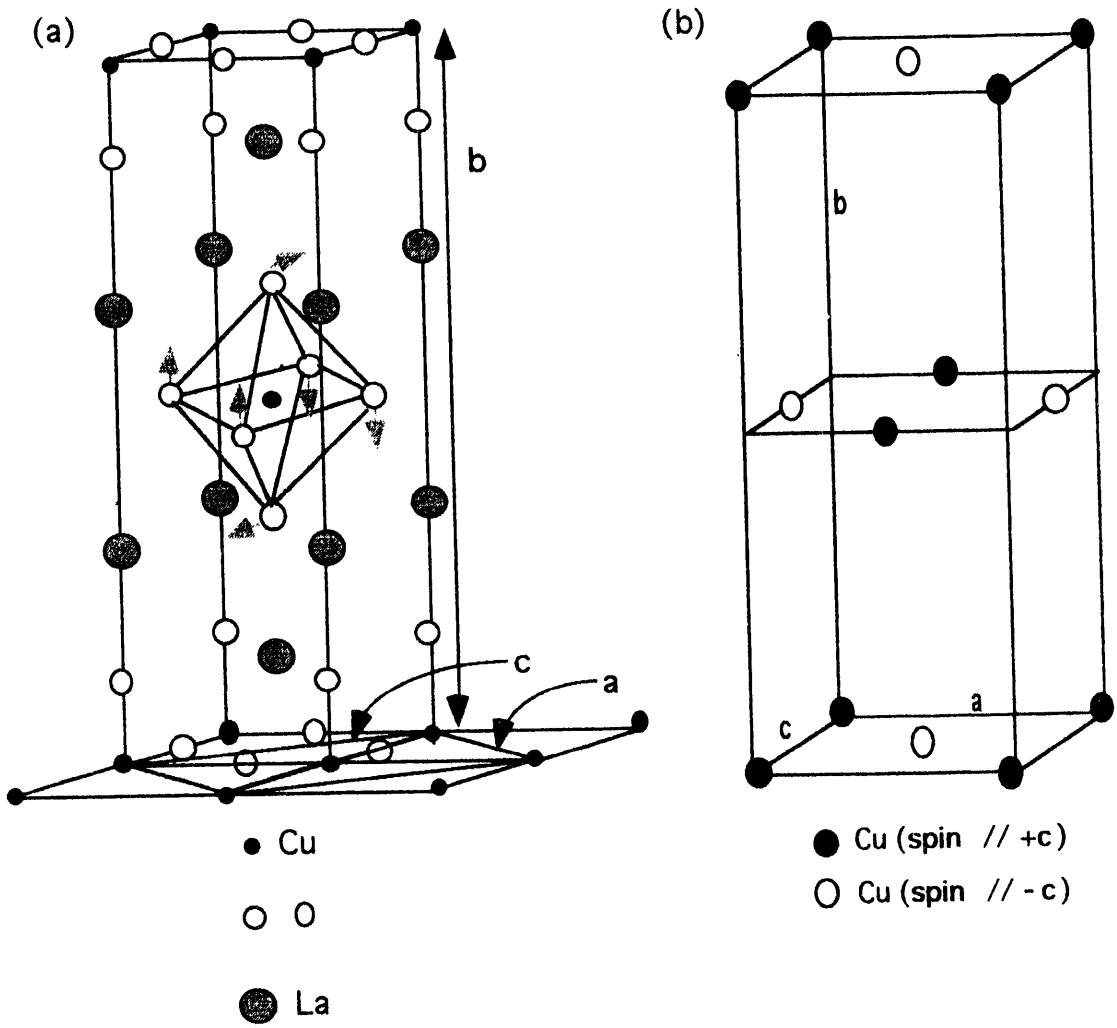

Fig. 1.1(a) Tetragonal structure of undoped La_2CuO_4. The CuO_6 rotation in the distorted orthorhombic structure is indicated by the dashed arrows. The orthorhombic a- and c-axes are chosen along the tetragonal [110] directions. (b) The Cu spin structure below the Néel temperature as proposed from neutron diffraction.

the CuO_6 octahedra [Thurston, 1989]. Theoretically, the Hamiltonian includes an antisymmetric term arising from the D-M interaction and a weak out-of-plane spin exchange anisotropy. The effective exchange coupling constant J' between the Cu^{2+} ions in adjacent CuO_2 layers was estimated to be ~ 10^{-5} J, where J ≈ 1500 K is the intraplane Cu-Cu exchange coupling constant [Johnston, 1991]. The Cu spin structure has been proposed from both magnetization [Thio, 1988] and neutron diffraction [Vaknin, 1987] studies as shown in Fig. 1.1(b). Within a given CuO_2 plane, the Cu^{2+} spins cant of the plane below T_N by ~ 0.17°, so that each plane has a small (~ 0.002 μ_B/Cu) ferromagnetic (FM) component to the ordered moment. The direction of the FM component alternates from layer to layer, producing a net AF structure in which FM component is hidden. The FM canted moments in all layers can be lined up above the critical field $H_c(T)$ [Cheong, 1989].

1.3.3. Electronic structure

Early one-electron band structure calculation predicts that undoped La_2CuO_4 is a nonmagnetic metal with a half filled Cu $3d_{x^2-y^2}$ - O $2p_{xy}$ band [Mattheiss, 1987]. However, the conductivity measurements indicate that La_2CuO_4 is essentially nonmetallic near room temperature and semiconducting below about 200K [Cheong, 1989]. Thus, there must exist strong electronic correlation effects which cannot be neglected. The Hubbard model description indicates that undoped La_2CuO_4 is not a metal but rather a charge transfer insulator [Nücker, 1992]. A strong on-site Coulomb repulsion U leads to

splitting of the Cu $3d_{x^2-y^2}$ band into an upper and a lower Hubbard band. An energy gap about 2 eV between the valence and conduction bands has been observed from optical spectra [Suzuki, 1989]. In the rigid band model for charge-transfer insulator, holes in the valence band with mainly O 2p character may be formed upon p-type doping. Other models predict the formation of partially filled "impurity" band [Nücker, 1992].

1.4. Phase separation and δ-T phase diagram of $La_2CuO_{4+\delta}$

Based on a t-J model calculation, it is shown that dilute holes in an antiferromagnet do not have a uniform density but separate into a hole-rich phase and a phase with no holes [Emery, 1990]. Two types of phase separation have been observed. Neutron diffraction studies of high oxygen pressure prepared $La_2CuO_{4+\delta}$ ($\delta \sim 0.03$) revealed that a reversible macroscopic phase separation occurs below about 320 K into two nearly identical orthorhombic phases of $\delta \sim 0.00$ and 0.08 [Jorgensen, 1988]. Fig. 1.2 shows a schematic T-δ phase diagram of $La_2CuO_{4+\delta}$ by Dabrowski et al., which is based on a neutron diffraction two-phase Rietveld refinement results of $La_2CuO_{4+\delta}$ and the isostructural $La_2NiO_{4+\delta}$ [Dabrowski, 1989]. A miscibility gap has been proposed to exist between $0.00 \leq \delta \leq 0.08$ to separate the superconducting phase with $\delta \approx 0.08$ and the stoichiometric AF insulator with $\delta \approx 0.00$. Herein, microscopic phase separation is proposed in lightly doped $La_{2-x}Sr_xCuO_4$ also, where the samples separate into undoped antiferromagnetic regions separated by hole rich

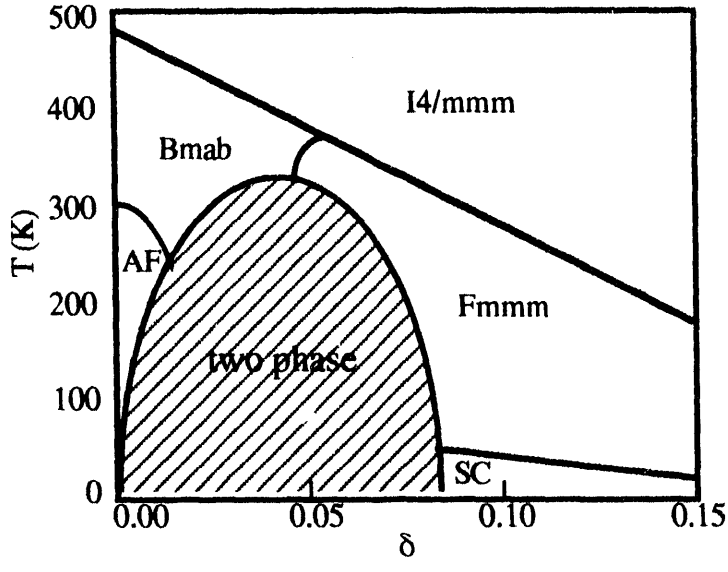

Fig. 1.2 A schematic T-δ phase diagram for $La_2CuO_{4+\delta}$ proposed by Dabrowski et al. [1989]. AF = antiferromagnetic phase. SC = superconducting phase.

domain walls [Cho, 1993].

In the macroscopic phase separation occurring in $La_2CuO_{4+\delta}$, an interstitial oxygen diffusion process always accompanies the hole phase separation motion above the oxygen freezing temperature ~190-210 K. The accompanied negative oxygen ion compensates the hole's charge and the "chargeless hole" (in Lab time scale) can move more freely [Emery, 1990]. The holes aggregate into a hole rich domain, which is energetically favorable due to its minimal surface that leads to minimal AF bond breaking. This oxygen-rich domain size of $La_2CuO_{4.03}$ has been estimated by Jorgensen et al. from neutron scattering line broadening to be $\geq$ 3000 Å [Jorgensen, 1988]. On the other hand, in $La_{2-x}Sr_xCuO_4$ ($0 < x < 0.02$), the hole motion is restricted close to the Sr sites in the microscopic phase separation, because the Sr^{2+} ions are immobile. The domain-wall type hole distribution requires less average travel distance and is evidently energetically more favorable in this case.

1.5. Magnetic phase diagram of $La_{2-x}Sr_xCuO_4$

A complete phase diagram of $La_{2-x}Sr_xCuO_4$ is summarized in Fig. 1.3, which shows the combined experimental results of the transition temperatures of orthorhombic-tetragonal structural transition ($T_{O/T}$), AF magnetic transition (T_N) and superconducting transition (T_C) versus x [Takagi, 1992; Sun, 1991; Cho, 1993; Filipkowski, 1990]. The Néel temperature T_N is extremely sensitive to the hole doping, which drops

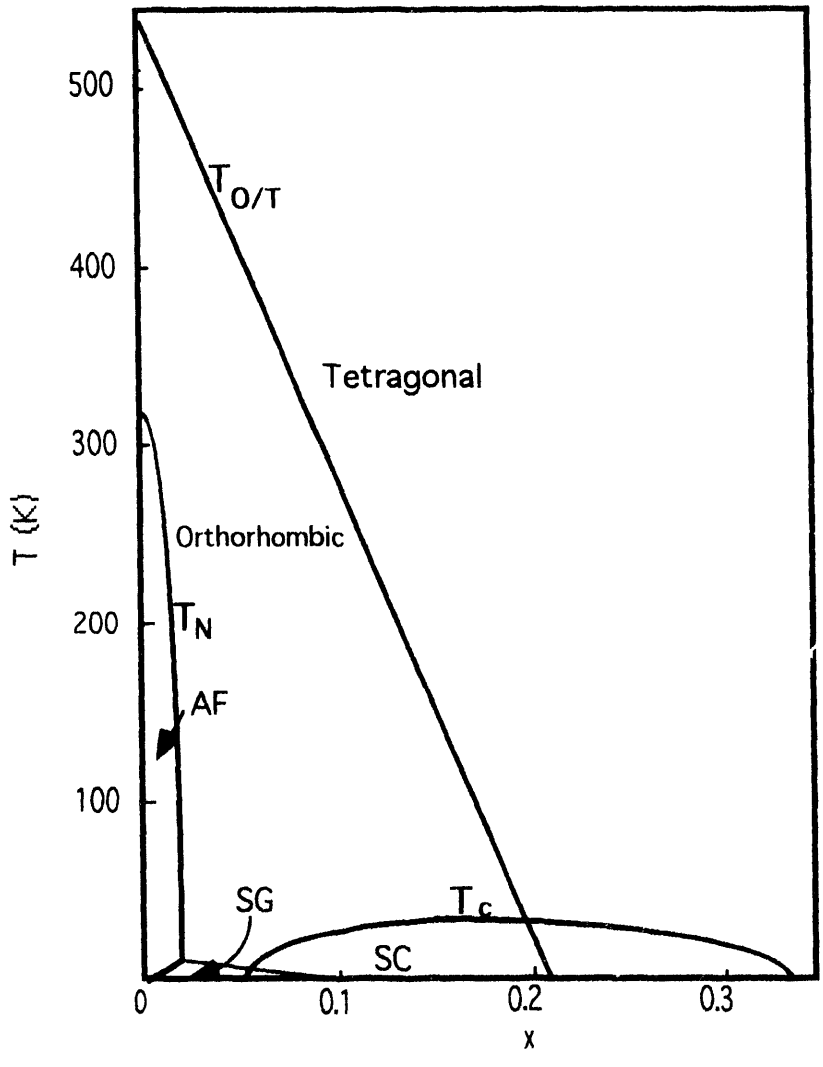

Fig. 1.3 Phase diagram of $La_{2-x}Sr_xCuO_4$ summarized from References [Takagi, 1992; Sun, 1991; Cho, 1993; Filipkowski, 1990]. $T_{O/T}$ is the orthorhombic to tetragonal structure transition temperature. T_N and T_C are respectively the antiferromagnetic (AF) and superconducting (SC) phase transition temperatures. SG = spin glass phase.

from about 320 K to 0 with only 1% Sr doping (x = 0.02). Such a drastic reduction in T_N has generated a lot of theoretical interest because it cannot be explained simply by the conventional percolation picture. Aharony et al. introduced a phenomenological model in which the (localized) doped holes generated an effective ferromagnetic coupling between adjacent Cu spins, which frustrate the 3D AF ordering [Aharony, 1988]. Cho et al. later proposed that microscopic doped-hole separation occurs, to explain the x dependence of T_N [Cho, 1993]. There is a spin-glass state at low temperature observed between the Néel state threshold (x = 0.02) and the onset of superconductivity (x ~ 0.05) from muon spin rotation μSR [Harshman, 1988]. ^{139}La NQR studies on Ba doped La_2CuO_4 revealed a new phase boundary for $x \leq 0.02$ below around 10 K also, which is believed to be a novel mixed phase [Watanabe, 1990]. Such re-entrant behavior in the AF phase at low T has been explained from long-range indirect interaction between the spins of localized holes [Ivanov, 1992].

CHAPTER 2. PREPARATION AND CHARACTERIZATION OF ELECTROCHEMICALLY OXIDIZED POLYCRYSTALLINE $La_{2-x}Sr_xCuO_{4+\delta}$ ($0.00 \leq x \leq 0.33$)

2.1. Introduction

Wattiaux et al. first found that superconducting $La_2CuO_{4.09}$ with $T_c \approx 44$ K can be synthesized from the antiferromagnetic insulator parent compound La_2CuO_4 using a unique electrochemical oxidation method [Wattiaux, 1990]. There are two intriguing physical properties of this new superconducting phase: (i) it shows a larger orthorhombic distortion compared with stoichiometric La_2CuO_4, instead of the smaller distortion found in the high pressure oxygenated samples [Zhou, 1989], and (ii) its $T_c \approx 44$ K surpasses the 40 K obtained by optimum Sr doping [Tarascon, 1987]. Herein, we confirm and extend this work on electrochemically oxidized $La_2CuO_{4+\delta}$, and report additional investigations on $La_{2-x}Sr_xCuO_{4+\delta}$ ($0 < x \leq 0.33$) synthesized using the same electrochemical method, including electrochemical, powder x-ray diffraction, thermogravimetric analysis, iodometric titration, pressure dependence of T_c, neutron diffraction study and SQUID magnetization measurement results.

2.2. Electrochemistry of Oxide Electrodes

2.2.1. Basics of electrochemistry

Electrochemical and chemical reactions are the same from an overall point of view. In the former method, electronic charge transfer reactions take place at the separated electrode/electrolyte interfaces, whereas chemical reactions need thermal collisional activation plus bond breaking [Bockris, 1973]. Usually the high T_c material is processed with high temperature solid state chemical reactions. Electrochemical reaction shows a better control of the redox reaction and is possible to perform at room temperature. Because of limitations of high overpotential, corrosion and its two dimensional nature, the electrochemical synthesis technique may not be possible or suitable for all chemical reactions [Bockris, 1972].

The basic setup of an electrochemical cell for oxide oxidation is shown in Fig. 2.1. The potential change of the working electrode is monitored by a nonpolarizable standard reference electrode because what we are interested in is the electrode potential change at the electrode/electrolyte interface. The direct potential difference between the working and counter electrodes involves double layers and is more difficult to interpret [Bockris, 1972]. Commonly used nonpolarizable reference electrodes include Hg/Hg_2Cl_2 saturated calomel electrode (SCE), Hg/HgO and Ag/AgCl electrodes.

In searching for oxide materials which show low overpotential for use as a reversible oxygen electrode in aqueous alkaline solutions,

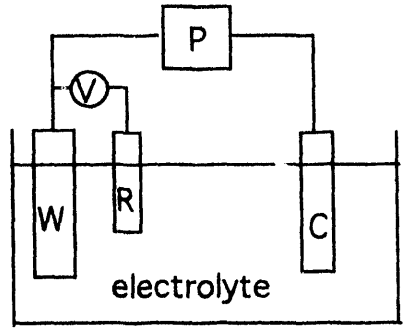

Fig. 2.1 The basic setup of an electrochemical cell for oxide oxidation. W = working electrode. P = power supply. C = counter electrode. R = reference electrode. V = voltmeter.

perovskite-related oxides have proved to be useful, particularly with regard to understanding the mechanism for oxygen evolution [Wattiaux, 1987]. Oxygen nonstoichiometry has been found to play an important role with regard to this electrocatalytic activity. In 1990, Wattiaux et al. first successfully produced superconducting $La_2CuO_{4+\delta}$ by electrochemical oxidation of a La_2CuO_4 working electrode.[Wattiaux, 1990]

2.2.2. Oxidation mechanism of La_2CuO_4

Cyclic voltammetry (CV), a controlled potential scan of the current-voltage (I-V) curve of an electrode, is commonly used to study the oxidation and reduction mechanism of surface species. There are three regions of interest on the CV plot as shown in Fig. 2.2: the oxidation plateau O1 corresponds to oxidation of a surface species, the steep slope O2 corresponds to oxygen evolution, and the peak R1 along the reduction route corresponds to the reduction of surface species. Based on the CV plot, we can oxidize the sample using either a fixed electrode potential at the surface species' oxidation level for a long time or apply a constant current, low enough not to cause the potential to exceed the oxygen evolution level, until the electrode potential reaches the oxidation level. In 1990, Wattiaux et al successfully produced superconducting $La_2CuO_{4+\delta}$ using this electrochemical oxidation technique [Wattiaux, 1990]. They applied an anodic constant potential of 450 mV (vs Hg/HgO) to a La_2CuO_4 sample electrode for 9 hours and reached an excess oxygen content up to $\delta \sim 0.09$. Rudolf et al.

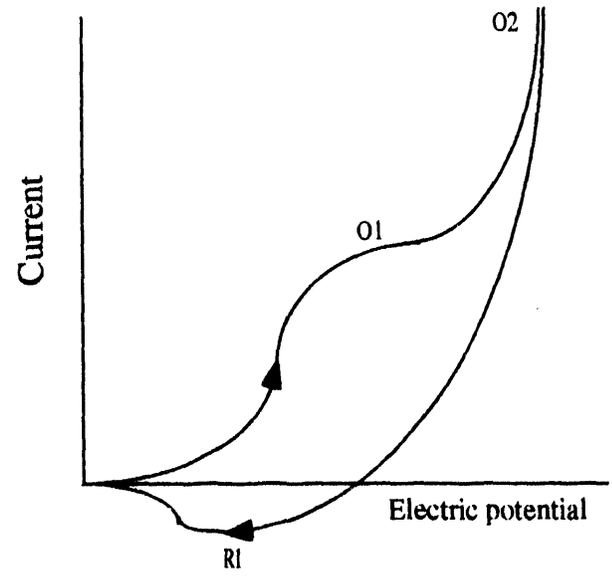

Fig. 2.2 A schematic cyclic voltammogram using La_2CuO_4 as a working electrode. Adapted from [Grenier, 1992].

used constant current to charge the sample until a charge transfer level of 0.14 electron/formula unit is reached and achieved the same results.[Rudolf, 1991] Even though the overall reaction of the oxidation of La_2CuO_4 is commonly accepted as [Grenier, 1991]

$$La_2CuO_4 + 2\delta\ OH^- \text{---> } La_2CuO_{4+\delta} + \delta\ H_2O + 2\delta\ e^-, \quad (2.1)$$

questions remain on the details of the oxidation mechanism especially at the electrode/electrolyte interface. In order to answer this question we have to examine the electrified oxide/electrolyte interface closely. Electrosorption of OH^- occurs as a sample electrode is anodically polarized. The hydroxide ions face two possible routes to oxidize the sample. The first is the direct in-diffusion and surface redox process of OH^- according to

$$La_2CuO_4 + \delta\ OH^- \text{---> } La_2CuO_4(OH)_\delta + \delta\ e^-.$$

But this possibility is overruled by the absence of a hydrogen signal from NMR as well as no OH^- band observed from IR spectra [Grenier, 1992]. The more likely second oxidation mechanism may be separated into several steps. We propose an oxidation process following the confirmed Pt surface oxidation steps [Angerstein-Kozlowska, 1973]. The reversible electrosorbed OH^- needs to construct a rearranged surface phase with lower free energy first. An electron/proton

transfer reaction occurs after the completion of rearranged surface layer as [Rudolf, 1991]

$$(OH)_\delta(La_2CuO_4)_{surf} \rightarrow (La_2CuO_{4+\delta})_{surf} + \delta H^+ + \delta e^-,$$

and then the intercalated oxygen ions diffuse from the surface into the bulk. The working electrode (anode) half-cell reactions can be summarized as shown in Fig. 2.3 following

Stage I : electrosorption of OH^-, $(La_2CuO_4)_{surf} - \delta(OH^-)$

Stage II: surface restructuring, $(OH)_\delta(La_2CuO_4)_{surf} + \delta e^-$

Stage III: electron/proton transfer reaction,

$$(OH)_\delta(La_2CuO_4)_{surf} \rightarrow (La_2CuO_{4+\delta})_{surf} + \delta H^+ + \delta e^-$$

Stage IV: O^{2-} diffusion, $(La_2CuO_{4+\delta})_{bulk}$.

We believe the oxygen diffusion process (stage IV) is the rate determining step. The estimated oxygen diffusion coefficient at 300 K is around $1.5 \pm 0.5 * 10^{-8}$ cm^2/s [Rudolf, 1991], which is the same order of the pre exponential value of oxygen diffusion in $La_{1.85}Sr_{0.15}CuO_4$ with an activation energy about 10^5 K [Smedskjaer, 1987]. This diffusion coefficient value is even three orders higher than the $3*10^{-11}$ cm^2/s at 400 °C for $YBa_2Cu_3O_7$ [Growacki, 1988]. Due to the high oxygen concentration gradient maintained at the surface layers and the diffusion channels formed by La_2O_2 interstitial sites (see below), synthesis of homogeneous bulk $La_2CuO_{4+\delta}$ can be achieved electrochemically even at

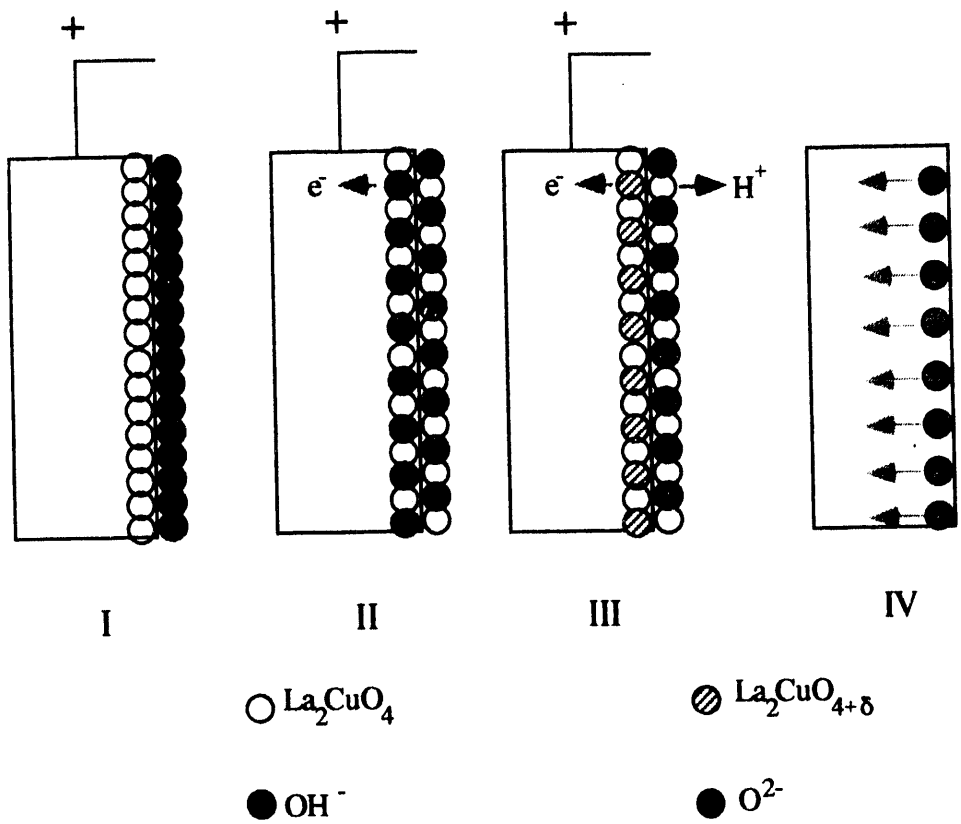

Fig. 2.3 The proposed working electrode (anode) half-cell reactions:
Stage I : electrosorption of OH^-, $(La_2CuO_4)surf - \delta(OH^-)$
Stage II: surface restructuring, $(OH)\delta(La_2CuO_4)surf + \delta e^-$
Stage III: electron/proton transfer reaction,
$(OH)\delta(La_2CuO_4)surf \rightarrow (La_2CuO_{4+\delta})surf + \delta H^+ + \delta e^-$
Stage IV: O^{2-} diffusion, $(La_2CuO_{4+\delta})bulk$.

room temperature. This electrochemical oxidation contrasts to the direct high-oxygen-pressure oxidation of La_2CuO_4, which needs to operate at high temperature around 600 °C. The high oxygen pressure annealing can only obtain limited intercalated oxygen ($\delta \approx 0.03$), a composition in which macroscopic phase separation occurs below ~ 300 K [Schirber, 1988][Jorgensen, 1988].

2.2.3. Band model of solid/solution interface

A chronopotential scan gives important information about the surface composition change of the sample electrode. Fig. 2.4 shows a plot of equilibrium open circuit potential versus electron transfer level for the La_2CuO_4 electrode, where the equilibrium is defined as being 500 seconds after a desired charge is delivered from a constant applied current. A potential level is reached after the sample is converted to $La_2CuO_{4+\delta}$ ($\delta \geq 0.08$). Since the open circuit potential corresponds to the relative Fermi level of the material, a change of the equilibrium potential is expected after a sample is electrochemically oxidized.

Morrison has proposed a band model of solid/solution interface for semiconductors as shown in Fig. 2.5. The sample electrode potential reading V_m is defined as [Morrison, 1980]

$$V_m = -[E_F - E_F(ref)] / q$$

where q is the electron charge and the measured qV_m at sample electrode is the sample electrode Fermi energy relative to the

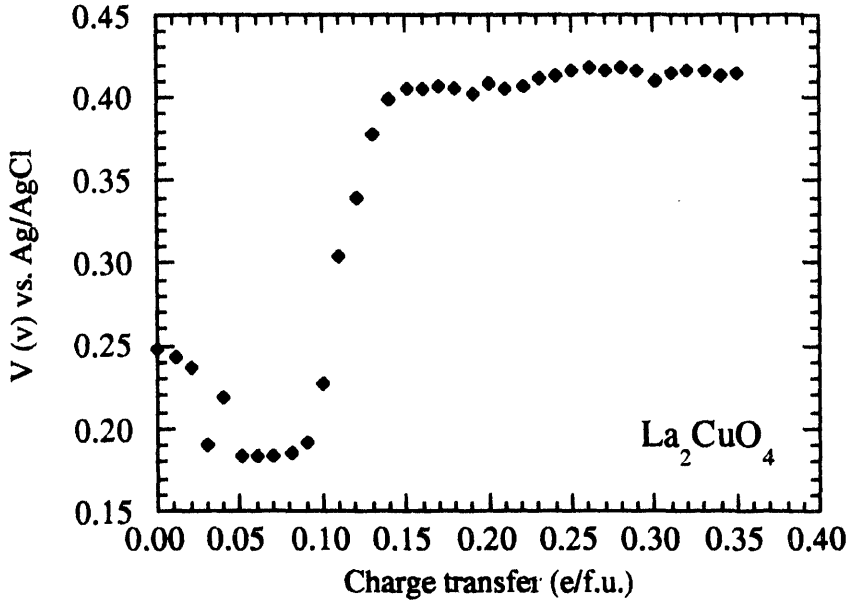

Fig. 2.4 Equilibrium open circuit potential versus electron transfer level for the La_2CuO_4 electrode.

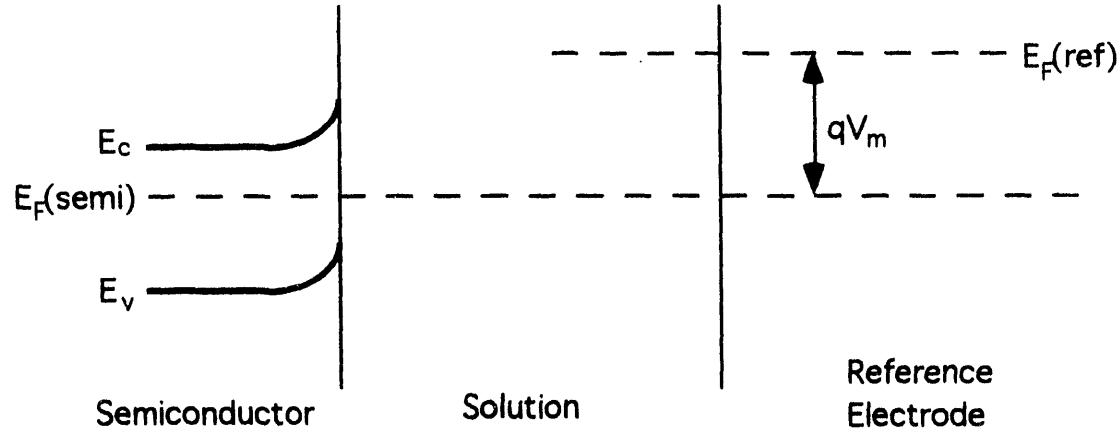

Fig. 2.5 Band model of solid/solution interface for semiconductors. Here V_m is the measured voltage.

reference electrode Fermi energy [Morrison, 1990]. If V_m is changed from its equilibrium value, a net current will flow.

2.3 Experimental Details

2.3.1. Sample preparation

The $La_{2-x}Sr_xCuO_4$ ($0 \leq x \leq 0.33$) starting materials were prepared in air from high purity La_2O_3 (99.99%), $SrCO_3$ (99.999%) and CuO (99.999%). The La_2O_3 powder was dried in air at 1050 °C for 12 hours prior to use. The mixed powders were calcined at 925 °C overnight and then sintered at 1050 °C in air for 2 days with frequent grinding, until the products were free of impurity phases according to x-ray diffraction measurements. The working electrode is prepared with ~200 mg $La_{2-x}Sr_xCuO_4$ powder, which is compressed into a 6.1 mm diameter × 2 mm thick pellet form and is annealed in 925 °C for 12 hours. Alternatively, samples in powder form were cold pressed to ≈70% theoretical density with a Pt wire embedded in the powder.

A two-chamber electrochemical cell was set up as [La_2CuO_4 / 1N NaOH / Pt], where the chambers containing the Pt counter electrode and the La_2CuO_4 working electrode were separated using a glass frit. A Ag/AgCl reference electrode was used, placed in the sample compartment. The counter electrode was a Pt wire of 0.15 mm diameter by 5 cm long. Electrical contact to the sample was made using Pt wire. The Pt wire was attached to a sintered pellet sample electrode with silver paint and then covered with silicone rubber.

A nominal anodic current density of ~100 $\mu A/cm^2$ was applied to the La_2CuO_4 working electrode. The charge Q passing through the cell was calculated from the product of current and time. The overall electrochemical oxidation reaction proposed by Grenier et al. is shown in Eq. (2.1) [Grenier, 1992]. One may identify the charge Q with 2δ provided that there are no electrochemical side reactions occurring. The charge Q over-estimates 2δ whenever the electrode potential is above the oxygen evolution potential (0.61 V vs. Ag/AgCl) of the reaction

$$2\ OH^- \text{---> } H_2O + 1/2\ O_2 + 2\ e^- \ , \qquad (2.2)$$

which competes with the desired sample oxidation process. During sample oxidation, we kept the cell potential low enough to avoid this oxygen evolution reaction. To reach a single phase sample with $\delta >$ 0.08, one needs to apply a constant current and monitor the sample electrode potential until it becomes independent of time. A single phase $La_2CuO_{4+\delta}$ with $\delta \approx 0.07$ and $T_c = 32$ K is prepared differently, using a constant potential of 0.6 V applied to the sample for 6 days without stirring the electrolyte [Radaelli, 1993], to avoid excessive 45 K phase surface nucleation when charging rate is too high. The electrochemically oxidized samples were washed with distilled water and absolute alcohol, then dried in vacuum (~ 10^{-3} torr) at room temperature for more than 9 hours. Similar electrochemical oxidation

was performed on samples of $La_{2-x}Sr_xCuO_4$ (x= 0.01, 0.02, 0.03, 0.04, 0.08, 0.15, 0.25, 0.33).

2.3.2. Electrode characterization

The oxygen content of a sample was calculated from the weight loss after hydrogen reduction at 550 °C or helium reduction up to 700 °C in a thermogravimetric analyzer (TGA, Perkin-Elmer Thermal Analysis 7). The copper oxidation state of a sample was determined from iodometric titration measurements using the procedure of Harris et al. [1987] Crystal structures were examined by powder x-ray diffraction (Rigaku diffractometer, Cu Kα radiation). Superconducting and normal state magnetic properties were measured using a SQUID magnetometer (Quantum Design Inc.); demagnetization factor corrections were not applied. The pressure dependence of T_c was performed in Sandia National Laboratory [Schirber, 1993]. Pressures to ~ 6 kbar were generated in gaseous He and in solid He depending upon the pressure and temperature involved; the superconducting transition temperatures were measured using a rf technique in which the specimen is placed in a custom wound coil. Neutron powder diffraction data were collected at room temperature and 10K, using the Special Environment Powder Diffractometer (SEPD) at Intense Pulsed Neutron Source (IPNS) at Argonne National Laboratory [Radaelli, 1993].

2.3.3. Iodometric titration method

Iodometric titration method was used to determine the hole concentration p [Harris, 1987]. About 30 mg of a sample was dissolved in 1N HCl and then reacted with I^- to liberate I_2. The liberated iodine can be titrated with standard thiosulfate using starch as an indicator. The amount of I_2 released is proportional to the oxidizing power of Cu ion and can be used as an indication of the quantities of Cu^{+2} and Cu^{+3}. Experiments are separated into two parts. Experiment A measures the quantity of both Cu^{+3} and Cu^{+2} in terms of I_2, and experiment B measures the quantity of total Cu^{+2} in terms of I_2 after all Cu^{+3} is converted into Cu^{+2} with steam heating. The fraction of Cu in the trivalent state, i.e. hole concentration p, can thus be calculated from the I_2 obtained in experiments A and B as (A-B)/B. Following Shafer et al. [1987], the hole concentration p is referred as originating from a $[Cu\text{-}O]^{+p}$ complex rather than Cu^{+2+p} or O^{-2+p}. The complete process is:

$$\text{Exp. A: } [Cu\text{-}O]^{+p} + (2+p)\, I^- \longrightarrow CuI + \mathbf{(p+1)/2}\ I_2,$$

$$\text{Exp. B: } [Cu\text{-}O]^{+p} \longrightarrow [Cu\text{-}O] + 2I^- \longrightarrow CuI + \mathbf{1/2}\ I_2.$$

Experiments were repeated two to three times for each sample to ensure agreement of p in the ±0.02 range.

For samples with doped holes from the intercalated oxygen, the calculated δ's from δ = p/2 are usually lower than those obtained from TGA direct decomposition. Both high oxygen pressure prepared $Sr_2CuO_{4-\delta}$ [Lobo, 1990] and $La_2CuO_{4+\delta}$ [Schirber, 1988] have shown serious disagreement on oxygen contents obtained respectively from TGA and titration. The possible source of complication could be the polyoxide anions such as O_2^- or $(O_2)^{2-}$ exist in a sample, where the formal valence of the excess oxygen ions are not -2 totally. The discrete O_2^- and $(O_2)^{2-}$ liberated from sample upon dissolution can also oxidize the I^- at slower reaction rates. However, the existence of peroxide in the solution of $La_2CuO_{4+\delta}$ and $La_2NiO_{4+\delta}$ could not be verified [Harris, 1989].

2.4. **Results and Discussion**

2.4.1. Electrochemically intercalated species

We prepared a series of superconducting $La_2CuO_{4+\delta}$ samples with controlled charge transfer Q. A weight gain (after drying) was always observed after electrochemical oxidation. We have addressed the question of the nature of the intercalated species by comparison of the electrochemical charge transfer Q and the sample weight loss (after drying) upon decomposition in hydrogen in the TGA. If the intercalated species is assumed to be oxygen, then the oxygen content of an oxidized sample can be calculated from the weight loss, following the equation

$$La_2CuO_{4+\delta} + H_2 \text{ ---> } La_2O_3 + Cu + H_2O\ (g)\ . \qquad (2.3)$$

The δ values can be calculated from the TGA weight losses using Eq. (2.3). We verified that $\delta = Q/2$ [Chou, 1992], which strongly supports the oxidation reaction that follows Eq. (2.1) and thus the intercalated species is assumed to be oxygen.

2.4.2. Oxidation states from Iodometric titration

Our titration results on several oxidized samples are shown in Table 2.1. Surprisingly, the maximum total hole concentration provided by excess oxygen and/or Sr doping (see below) in these samples was the same for each sample, $p = 0.15 \pm 0.02$ holes/f.u., which is near the optimum Sr doping level for superconductivity in $La_{2-x}Sr_xCuO_4$ [Torrance, 1989]. Additional titration on an as prepared $La_{1.85}Sr_{0.15}CuO_4$ is shown in the table also to demonstrate the validity of the present iodometric titration method [Harris, 1987]. We noticed that the oxygen contents calculated from p with O^{2-} species assumed are roughly half of that from TGA reduction. A similar, but smaller, disagreement between TGA and titration results for electrochemically oxidized La_2CuO_4 has been observed by Grenier et al. for $La_2CuO_{4.09}$ also [Grenier, 1991], where iodometric titration yielded $p = 0.14$ holes/f.u. The titration results in Table 2.1 suggest that the formal oxidation state of the doped oxygen species is close to -1, rather than -2. This suggests that an internal redox reaction occurs after the doped oxygen diffuses into the sample, producing a polyoxide anion

Table 2.1. Electrochemical oxygen doping level (δ) and hole concentrations (p) of $La_{2-x}Sr_xCuO_{4+\delta}$. The δ values are estimated from hydrogen reduction measurements in the TGA and p values are obtained by iodometric titration determinations.

Sample No.	δ ($\pm$0.01)	p (holes/f.u.) ($\pm$0.02)
#4129 $La_2CuO_{4+\delta}$	0.12	0.156
#4096 $La_{1.99}Sr_{0.01}CuO_{4+\delta}$	0.13	0.163
#4083 $La_{1.92}Sr_{0.08}CuO_{4+\delta}$	0.07	0.146
#5064 $La_2CuO_{4+\delta}$	0.07	0.08
#5039 $La_2CuO_{4+\delta}$	0.11	0.14
#3138 $La_{1.85}Sr_{0.15}CuO_4$	0	0.14

species. Similar results and conclusions were obtained for $La_2CuO_{4+\delta}$ samples synthesized by subjecting La_2CuO_4 to high pressure oxygen.[Schirber, 1988]

2.4.3. Thermal gravimetric analyses (TGA)

Fig. 2.6 shows TGA scans of two single phase samples of $La_2CuO_{4+\delta}$ in He gas. The excess oxygen is lost in two steps for samples of T_c = 42 K (42K phase), δ_1 at 180-250 °C and δ_2 at 250-400 °C. But the samples with T_c = 32 K (32K phase) and $\delta \leq 0.07$ lost oxygen and δ_2 values obtained from several TGA scans in He gas. The results imply that transformation

in one step which corresponds to δ_2 with the stronger bonding. Table 2.2 summarizes the δ_1 from a 32K phase to a 42K phase accompanies a redistribution of excess oxygen into portions δ_1 and δ_2 of different bonding strength. From the lattice parameters of 42K phase, we infer there is a preferred excess oxygen ordering along a axis.(see Sec. 2.4.5) The weaker bonded excess oxygen δ_1 in 42K phase may be related to such

Table 2.2. TGA analysis of $La_2CuO_{4+\delta}$ in He gas. The δ_1 and δ_2 values are obtained from the oxygen losses as described in Fig. 2.6.

T_c (K)	$\delta_1(\pm 0.01)$	$\delta_2(\pm 0.01)$	$\delta=\delta 1+\delta 2$
42	0.060	0.039	0.099
42	0.071	0.039	0.110
42	0.057	0.036	0.093
32	0	0.065	0.065

an additional interstitial oxygen ordering, which serves as a mechanism to stabilize the structure when excess oxygens beyond 0.07.

Additional TGA He gas scan results for four samples with $0 \leq x \leq 0.08$ are shown in Table 2.3. These samples were fully charged using a constant potential of 0.6 V (vs. Ag/AgCl) for 3.5 days. The maximum excess oxygen content δ_{max} decreases as the Sr doping level x increases and correlated as $2\delta_{max} + x \approx 0.20$. Suppose we assume that

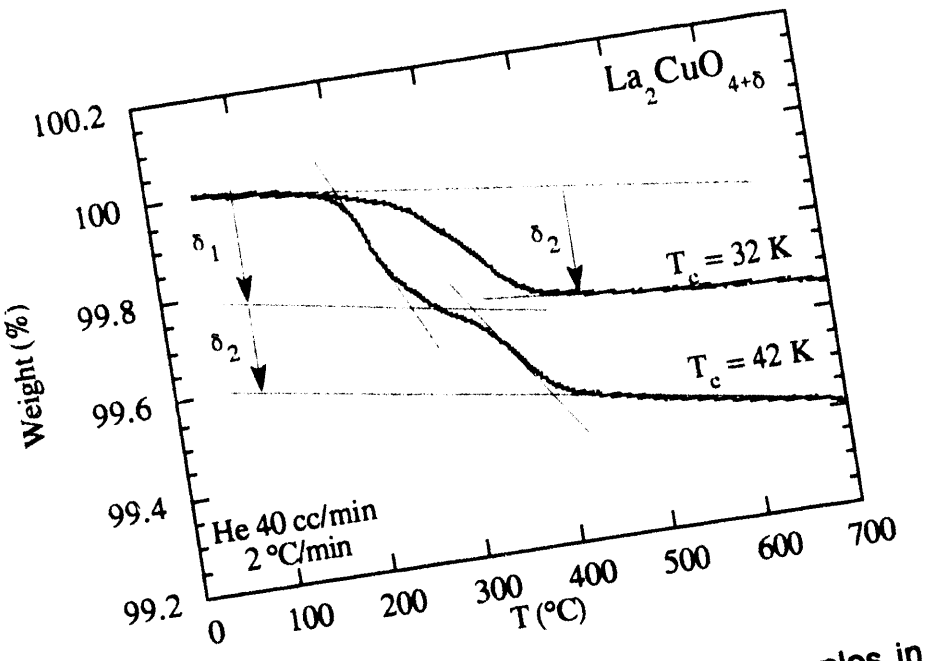

Fig. 2.6 TGA scans of two single phase $La_2CuO_{4+\delta}$ samples in He gas. Note that oxygen is lost in two steps for the sample with T_c = 42 K, but in one step for the sample with T_c = 32 K.

the stronger bonded δ_2 participate in O-O molecular bonding and have a formal valence -1, then the calculated hole concentration under this assumption is $p = 2\delta_1 + \delta_2 + x$ as shown in the table. These results do not agree with the titration results ($p_{max} \approx 0.16$ as shown in Table 2.1) except for the sample without Sr doping. We believe the Sr may have affected the near neighbor apical oxygen bonding as proposed by Tan et al. from the x-ray absorption measurement results.[Tan, 1990]

Table 2.3 TGA analysis of $La_{2-x}Sr_xCuO_{4+\delta}$ in He gas. The δ_1 and δ_2 values are analyzed by the method described in Fig. 2.6.

x	δ_1 (±0.01)	δ_2 (±0.01)	$\delta_{max}=\delta_1+\delta_2$	T_c (K)	$p=2\delta_1+\delta_2+x$
0	0.060	0.039	0.099	42	0.16
0.03	0.057	0.025	0.082	39	0.17
0.05	0.059	0.011	0.070	39	0.18
0.08	0.048	0.011	0.059	40	0.19

2.4.4. Superconducting properties of $La_2CuO_{4+\delta}$

We found that a two phase (T_c = 32 K and 42 K) sample may be produced after Q ~ 0.14 e/f.u. is applied at a charging rate of ~ 100 $\mu A/cm^2$ as shown in Fig. 2.7(a) [Chou, 1992]. The low field $\chi(T)$ data show a deflection at about 32 K and become zero above ~ 44 K, which suggests there are two superconducting phases with T_c's of 32 K and 44 K respectively. A single phase sample with T_c = 42-45 K can be prepared by charging a sample beyond Q ~ 0.16 e/f.u. The additional charging beyond Q ~ 0.16 e/f.u. does not change the lattice parameters, which suggests

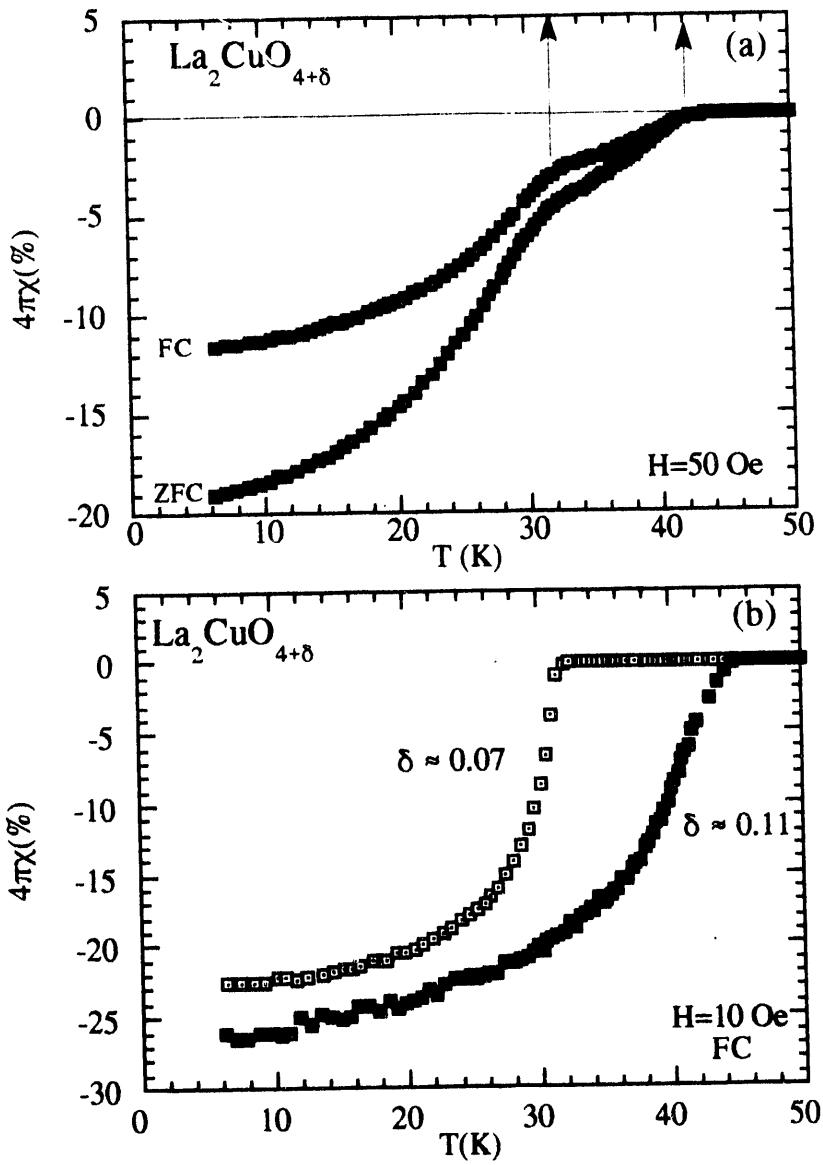

Fig. 2.7 (a) A two phase (T_C = 32 K and 42 K) sample is produced after Q ~ 0.14 e/f.u. is applied at a charging rate of ~ 100 $\mu A/cm^2$. (b) The low field susceptibilities of two single phase $La_2CuO_{4+\delta}$ with different oxygen contents $\delta \approx 0.07$ and 0.11.

that side reactions other than bulk property conversion occurred. A single phase sample with T_c = 32 K is difficult to prepare due to the formation of the 45 K phase from the surface when the charging rate is much higher than the oxygen in-diffusion rate. We prepared a sample with excess oxygen content about $\delta \sim 0.07$ differently as described in the sample preparation section. The low field susceptibilities of two single phase samples with different oxygen contents are shown in Fig. 2.7(b). The single-phase nature of the sample with $\delta \sim 0.07$ has been verified from the absence of a 250 K Néel peak in the normal state magnetic susceptibility (see Sec. 2.4.6. below), which indicates that no La_2CuO_4 remains within the sample and that phase separation does not occur. The fact of more than 20 % of ideal flux repulsion (without geometric factor correction) indicates there are two distinct superconducting phases of bulk superconducting nature with T_c = 32 K and 44 K of bulk superconducting nature.

2.4.5. X-ray diffraction analysis

Crystal structure analyses of our samples of $La_2CuO_{4+\delta}$ were performed using powder x-ray diffraction at room temperature. As shown in Table 2.4, the c-axis increases monotonically from 13.154 to 13.214 Å with increasing oxygen content. This c-axis elongation is consistent with that of high pressure oxygenated $La_2CuO_{4+\delta}$ [Jorgensen, 1988], in which $\delta \approx 0.03$ and the oxygen is believed to be inserted into an interstitial site in the La_2O_2 layer block [Chaillout, 1989]. There is a significant orthorhombicity variation as the oxidation level becomes

higher. The highly oxidized sample with $T_c \approx 45$ K has a higher orthorhombic strain than in La_2CuO_4, as originally reported [Grenier, 1991]. On the other hand, the lightly oxidized sample ($\delta \approx 0.03$) with $T_c \approx 32$ K has a smaller orthorhombic distortion than the La_2CuO_4 starting material. These results are in qualitative agreement with those obtained from in situ neutron diffraction experiments [Rudolf, 1991], where a significant orthorhombicity minimum occurred when Q ~ 0.05 e/f.u. transferred into the sample, and where the orthorhombicity increased again at larger values of Q.

Using an ionic model, the tolerance factor t is a good indicator to predict orthorhombic distortions from the tetragonal K_2NiF_4 structure [Goodenough, 1990][Bringley, 1990], where t for La_2CuO_4 is defined as t

Table 2.4 Room temperature lattice parameters a, b, c, unit cell volume V, and orthorhombicity 2(a-b)/(a+b) for starting and electrochemically oxidized La_2CuO_4.

Samples	a (Å)	b (Å)	c (Å)	V (Å^3)	2(a-b)/(a+b)
La_2CuO_4†	5.3572(6)	5.4011(7)	13.1542(12)	380.61(6)	0.80%
$La_2CuO_{4.03}$	5.3609(5)	5.3827(5)	13.1841(11)	380.44(5)	0.40%
$La_2CuO_{4.11}$	5.3408(6)	5.4043(6)	13.2188(13)	381.54(5)	1.18%
$La_2CuO_{4.18}$	5.3394(15)	5.4093(15)	13.2136(68)	381.64(17)	1.30%

† as-prepared sample before oxidation.

= (La-O)/(Cu-O)$\sqrt{2}$ and La-O and Cu-O are the respective bond lengths. For ideal matching of the La_2O_2 and CuO_2 layers, t should equal 1. Since t = 0.868 at room temperature for bond lengths estimated from ionic radii [Shannon, 1976], the observed orthorhombic distortion due to tilting of the CuO_6 octahedra [Thurston, 1989] is a mechanism that relieves the compressive stress in a CuO_2 layer generated from layer mismatch. Fig. 2.8 shows a tetragonal unit cell of La_2CuO_4 with an interstitial oxygen site at {1/4, 1/4, 1/4}, located at the center of a La tetrahedron. If excess oxygen goes into this La_2O_2-layer interstitial site as proposed by Chaillout et al. [1989], oxygen insertion will lengthen the average La-O distance and the doped holes in the CuO_2 plane will shorten the Cu-O distance due to removal of antibonding electrons, with both effects tending to relieve the compressive stress in the CuO_2 layer. Thus, a less orthorhombic structure is expected as hole doping is provided by interstitial oxygen through charge transfer. Both high-oxygen-pressure-annealed $La_2CuO_{4+\delta}$ and electrochemically oxidized $La_2CuO_{4+\delta}$ with $T_c \approx 32$ K satisfy this picture at room temperature. From a neutron diffraction study on $La_2CuO_{4+\delta}$ synthesized under high pressure oxygen [Jorgensen, 1988], below the phase separation temperature ($\approx$ 320 K) the oxygen-rich phase $La_2CuO_{4.08}$ indeed shows a smaller orthorhombic distortion than the stoichiometric La_2CuO_4 phase.

On the other hand, the electrochemically oxidized $La_2CuO_{4+\delta}$ phase with $T_c \approx 45$ K has a larger orthorhombicity than La_2CuO_4, contrary to the above arguments. We suggest that the explanation for this enhanced

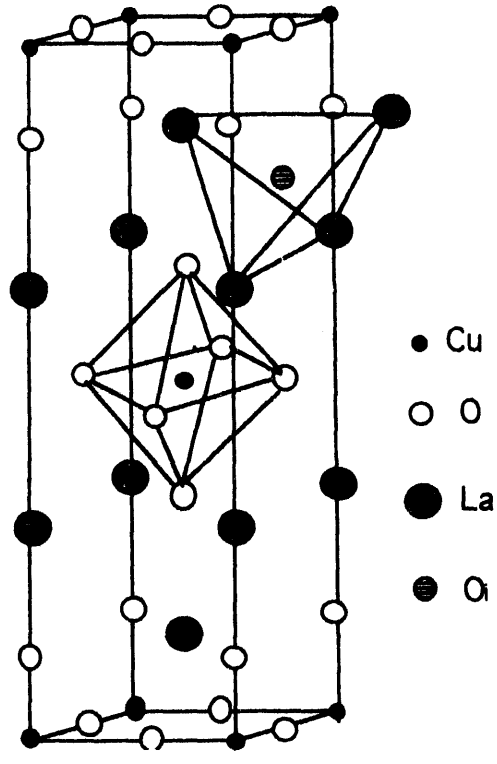

Fig. 2.8 Tetragonal structure of La_2CuO_4 with an interstitial oxygen O_i shown at position {1/4, 1/4, 1/4}. This interstitial oxygen O_i is at the center of a tetrahedron formed by four La atoms.

orthorhombicity is that for $\delta \geq 0.08$, the interstitial oxygen may become ordered along one of the plane-axis directions within the La_2O_2-layer blocks to form interstitial oxygen chains. Indeed, Loktev et al. have shown theoretically that a stable two-dimensional ordered superstructure should be present in $La_2CuO_{4.125}$ and $La_2CuO_{4.25}$ [Loktev, 1991]. Enhanced superconducting transition temperatures are associated with formation of CuO_3 chains in superconducting orthorhombic $YBa_2Cu_3O_7$ [Cava, 1987], which contrasts with the absence of ordered Cu-O chains in nonsuperconducting tetragonal $YBa_2Cu_3O_{6.4}$. Similarly, Takagi et al. [1992] found that superconductivity is depressed upon traversing the orthorhombic to tetragonal phase boundary at $x = 0.22$ in the $La_{2-x}Sr_xCuO_4$ system. Thus, our hypothesis is consistent with this empirical correlation between oxygen ordering, orthorhombic symmetry and enhanced superconductivity.

2.4.6. Normal state magnetic properties

The normal state magnetic susceptibilities $\chi(T)$ of $La_2CuO_{4.11}$ with $T_c \approx 42$ K, $La_2CuO_{4.07}$ with $T_c \approx 32$ K and conventionally prepared $La_{1.92}Sr_{0.08}CuO_4$ and $La_{1.85}Sr_{0.15}CuO_4$ are compared in Fig. 2.9. There is no T_N peak anomaly near 250 K associated with the antiferromagnetic ordering transition exists in the $\chi(T)$ data for $La_2CuO_{4+\delta}$, which suggests that no near-stoichiometric unreacted sample left nor occurrence of phase separation above 250 K. This demonstrates that the electrochemical oxidation process occurs throughout the volume of a sample, and suggests

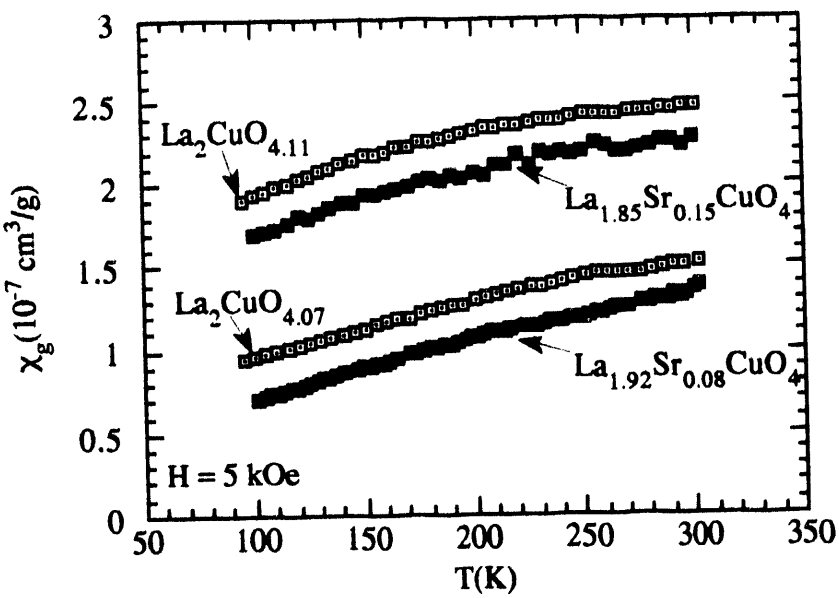

Fig. 2.9 The normal state magnetic susceptibilities $\chi(T)$ of $La_2CuO_{4.11}$ with $T_c \approx 42$ K, $La_2CuO_{4.07}$ with $T_c \approx 32$K and conventionally prepared $La_{1.92}Sr_{0.08}CuO_4$ and $La_{1.85}Sr_{0.15}CuO_4$ are compared.

that the electrochemical doping is homogeneous. The temperature dependence of χ(100-300 K) data for all four samples are seen to be nearly identical except for a constant difference. The significant enhancement of χ(T) can be assigned purely to the Pauli paramagnetic contribution in agreement with the analysis of χ(T) from $La_{2-x}Sr_xCuO_4$ [Johnston, 1989]. Judging from the hole concentrations p obtained by titration as shown in Table. 2.1, the $La_2CuO_{4.11}$ and $La_2CuO_{4.07}$ have the same p (within ± 0.02) as $La_{1.85}Sr_{0.15}CuO_4$ and $La_{1.92}Sr_{0.08}CuO_4$ respectively. Additional support for this observation is that the $\Delta\chi$(100-300K) between δ = 0.11 and δ = 0.07 is about the same as that of x = 0.08 and 0.15, which indicates the $\Delta\delta$ ~ 0.04 oxygen difference corresponds to Δp ~ 0.07, i.e. the excess oxygen has a valence -2 in this region. These results again support the model proposed in Sec. 2.4.4., where the stronger bonded interstitial oxygen (δ_2) below ~ 0.07 has formal valence -1 but the weakly bonded oxygen (δ_1) has valence -2. The T_c differences between x = 0.08 (~ 28 K) and $\delta \approx 0.07$ (32 K) as well as x = 0.15 (~ 39 K) and $\delta \approx 0.11$ (42 K) remain a puzzle, although the superoxygen ordering induced orthorhombicity change may be responsible as discussed in the previous section.

2.4.7. Neutron diffraction structural analysis of $La_2CuO_{4+\delta}$

Two powder samples with excess oxygen contents $\delta \approx 0.08$ and 0.12 (±0.01) were studied by high-resolution neutron diffraction and analyzed with the Rietveld technique. There is no anomaly in the lineshapes at room temperature or at 10 K. Thus both samples were

concluded to be single phase and to exhibit no phase separation [Radaelli, 1993]. Stoichiometric La_2CuO_4 has space group symmetry Bmab below 530 K. For the oxygen rich samples ($\delta \approx 0.08$ and 0.12), all diffraction peaks that should present in Bmab and extinct in Fmmm are absent for these two samples, from which we conclude that the structure is Fmmm. This result is in agreement with the two phase refinement of high pressure oxygen annealed $La_2CuO_{4.03}$ before, where the oxygen rich phase $La_2CuO_{4.08}$ has the Fmmm symmetry [Jorgensen, 1988].

The diffraction patterns of both powder samples show evidence of broad low intensity peaks, which can be indexed using an F-centered 10a*10b*c supercell. However, electron diffraction analysis for similar samples have shown there exists simultaneous presence of more than one set of superlattice reflections [Grenier, 1992]. The defect structure from the introduction of interstitial oxygens is very complicated. The superstructure ordering may create a network of short O-O bonds as proposed by Chaillout et al. [1989] Such short O-O bonds may be responsible for the discrepancy between TGA and iodometric titration as discussed in Sec. 2.3.3.

The lattice parameters of $La_2CuO_{4+\delta}$ for $\delta = 0.00$, 0.08 and 0.12 at 10 and 300 K (RT) are plotted in Fig. 2.10. Both the average in-plane lattice parameter and the orthorhombic strain are minimum for the 0.08 sample and this behavior has been explained in Sec. 2.4.5. with an ionic model of layer mismatch. The orthorhombic strain becomes larger at 10 K with a decrease of c-axes, which evidently arises due to a larger thermal

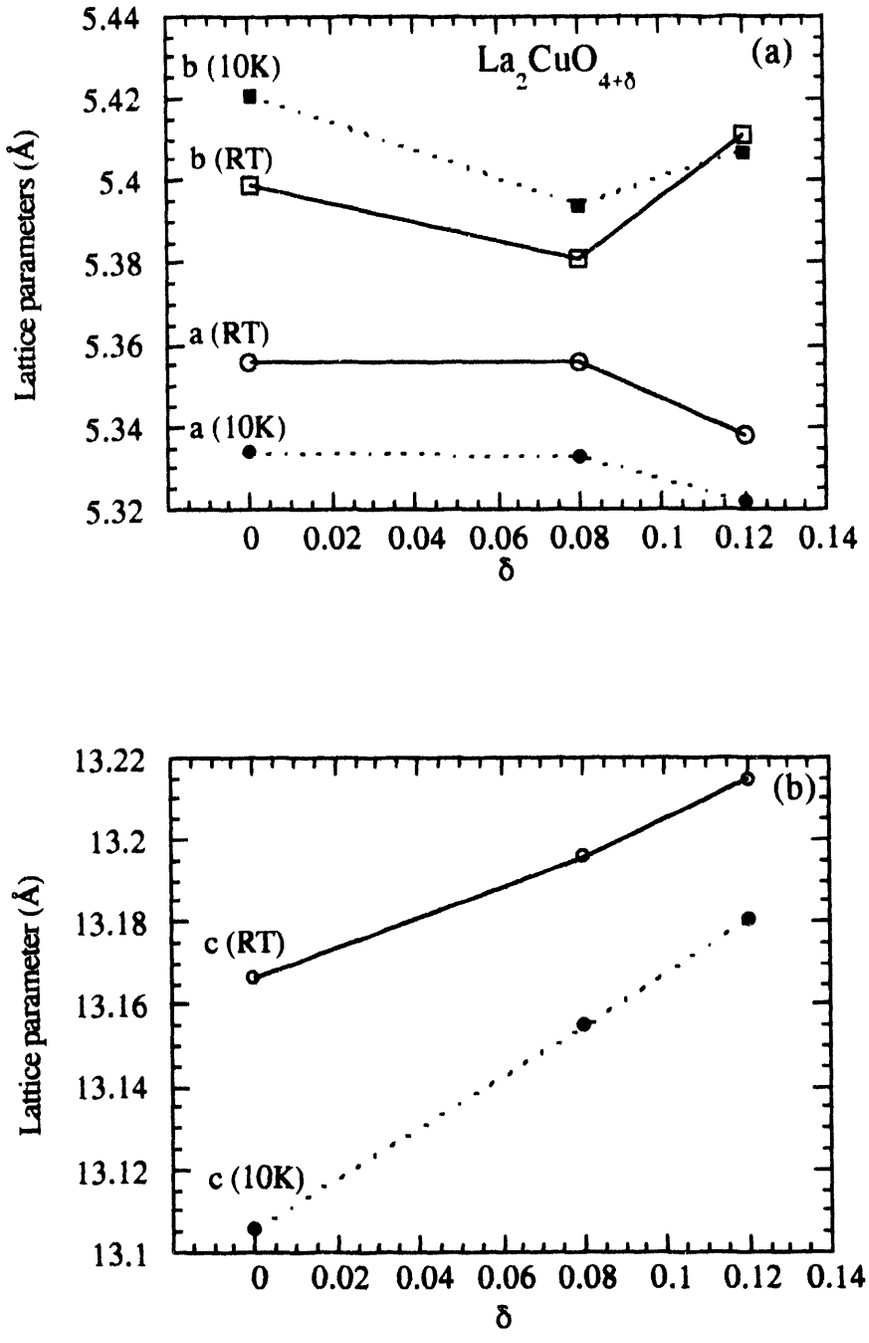

Fig. 2.10 The lattice parameters of $La_2CuO_{4+\delta}$ for δ = 0.00, 0.08 and 0.12 at 10 and 300 K, obtained by neutron diffraction.

contraction of the La-O distance relative to that of the Cu-O distance may be responsible for the additional CuO_6 tilt required by the matching layers. The change of orthorhombic strain from RT to 10 K for $\delta \approx 0.12$ is different from that of the $\delta \approx 0$ and 0.08 samples as shown in Fig. 2.10(a), where the a-axis elongates but the b-axis remains about the same. This behavior supports the assumption that the excess oxygen ordering is responsible for the larger orthorhombicity for $\delta \approx 0.12$.

2.4.8. Pressure dependence of T_c

The pressure derivatives of T_c of two electrochemically oxidized $La_2CuO_{4+\delta}$ samples above ($\delta \approx 0.08$ and 0.12) are shown in Table. 2.5. The pressure was changed either at room temperature (RT) or below 60 K. The optimally doped $La_{1.85}Sr_{0.15}CuO_4$ has $dT_c/dp \sim 0.2$-0.3 K/kbar [Griessen, 1988]. The sample with $T_c = 32$ K has a large positive derivative similar to $La_{1.85}Sr_{0.15}CuO_4$ which is independent of the temperature of pressure application. On the other hand, the sample with $T_c = 43$ K shows that T_c is nearly independent of pressure when pressure is applied at room temperature and has a small positive pressure derivative when the pressure is changed at low temperature.

Intrinsic dT_c/dp reflects the changes in the basic properties like carrier density, inter atomic distance and the density of states at Fermi level. However, there are two major pressure effects which may apply to the current oxygen doped system, the suppression of CuO_6 octahedra tilt and the movement of interstitial oxygens. In the study

Table. 2.5 Pressure derivatives of electrochemically oxidized $La_2CuO_{4+\delta}$. The pressure was changed either at room temperature (RT) or below 60 K (<60K).

T_C (K)	δ (±0.01)	dT_C/dp (K/kbar)(RT)	dT_C/dp (K/kbar)(<60K)
43	0.12	0.0 (±0.1)	0.12(±0.1)
32	0.08	0.25(±0.1)	0.2(±0.1)

of pressure dependence of T_C on a series of $La_{2-x}Sr_xCuO_4$ ($0.15 \leq x \leq 0.22$), Yamada et al. demonstrated that the positive dT_C/dp for the orthorhombic phase is due to the depression of the CuO_6 octahedra tilt under high pressure [Yamada, 1992]. They found that T_C is almost independent of pressure above p_C, where p_C is defined as the critical pressure above which the high temperature tetragonal phase can be stabilized down to below 20 K without low temperature orthorhombic phase transformation. On the other hand, variation of dT_C/dp due to mobility of the excess oxygen is observed and the ubiquitous positive pressure derivative is only seen in $Tl_2Ba_2CuO_{6+\delta}$ when $\delta = 0$ [Sieburger, 1991]. Our sample with $\delta = 0.12$ and $T_C = 43$ K shows a more orthorhombic structure than for $\delta = 0$ at room temperature but this higher orthorhombicity is believed coming from superoxygen ordering instead of the tilt of CuO_6 octahedra [Radaelli, 1993]. The almost zero dT_C/dp of the sample with $T_C = 43$ K indicates either a decrease under pressure of the CuO_6 octahedra tilt angle or a negative pressure effect on T_C due to oxygen movement canceling the positive dT_C/dp intrinsic

to the CuO2 layers. As for the slight positive dT_c/dp for the sample with T_c = 43 K when pressure is applied at low temperature, one reasonable explanation is related to the less effective pressure induced oxygen movement at low temperature.

2.4.9. Superconducting and magnetic properties of $La_{2-x}Sr_xCuO_4$ ($0 < x \leq 0.33$)

We applied the electrochemical oxidation method to different Sr doping regions of conventionally prepared $La_{2-x}Sr_xCuO_4$ ($0 < x \leq 0.33$). Three major regions in the T-x phase diagram of $La_{2-x}Sr_xCuO_{4+\delta}$ were examined. The as-prepared samples of $La_{2-x}Sr_xCuO_4$ ($0 < x \leq 0.02$), which show antiferromagnetic ordering and trace amounts of superconductivity, are converted into bulk superconductors with T_c up to 40 K after oxidation. Additionally, the as-prepared nonsuperconducting $La_{2-x}Sr_xCuO_4$ ($0.02 < x < 0.05$) and superconducting ($0.05 \leq x \leq 0.15$) compounds can also be converted into bulk superconductors, or T_c enhanced, with T_c up to 40 K after oxygen insertion, respectively. However, electrochemical oxidation could not improve the superconducting properties of $La_{1.75}Sr_{0.25}CuO_4$ or $La_{1.67}Sr_{0.33}CuO_4$. These results suggest that combined with Sr-doping, electrochemical oxidation doping by oxygen can only dope the CuO_2 planes to hole concentrations up to the optimum value for T_c, ~ 0.15 holes/f.u., for $x \leq 0.15$. If the optimum (or greater) hole doping is fully provided by Sr doping, the excess oxygen may be inserted as $(O_2)^{2-}$ in the La_2O_2 layer, as chemisorbed O_2 on the grain boundaries or simply evolved as gaseous O_2 following Eq. 2.2.

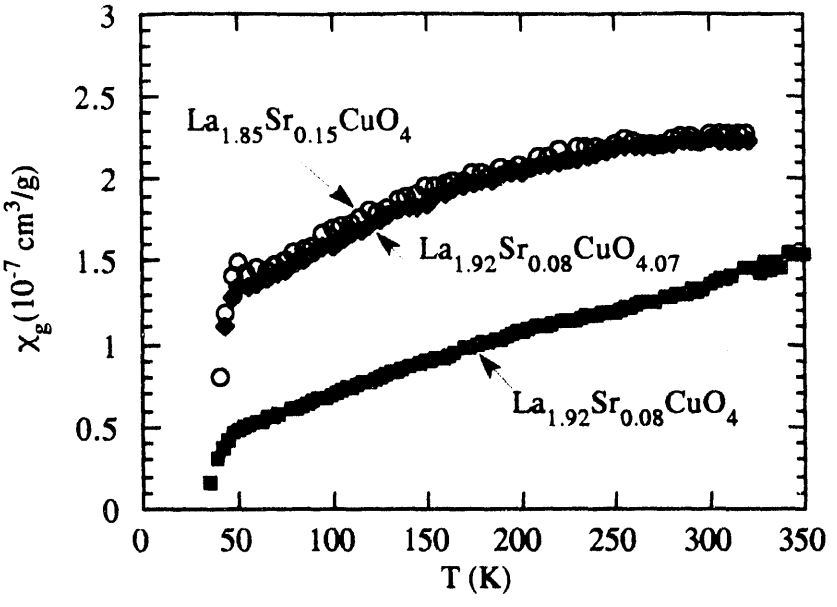

Fig. 2.11 Normal state magnetic susceptibilities χ_g vs. temperature T in an applied magnetic field H = 5 kOe of conventionally prepared $La_{1.92}Sr_{0.08}CuO_4$ and $La_{1.92}Sr_{0.08}CuO_{4.07}$ (after electrochemical oxidation). The $\chi_g(T)$ of the conventionally prepared $La_{1.85}Sr_{0.15}CuO_4$ is displayed for comparison.

The normal state $\chi(T)$ data for $La_{1.92}Sr_{0.08}CuO_4$ before and after electrochemical oxidation are compared with those of conventionally prepared $La_{1.85}Sr_{0.15}CuO_4$ in Fig. 2.11. The $\chi(T)$ of $La_{1.92}Sr_{0.08}CuO_{4.07}$ is nearly identical with that of $La_{1.85}Sr_{0.15}CuO_4$, indicating that the hole concentrations in the CuO_2 layers are about the same (~0.15) in the two compounds, in agreement with the iodometric titration results. The fact that 0.07 excess oxygen corresponds to 0.07 holes/f.u. is indicative that the excess oxygen has a formal valence of -1.

2.4.10. Chronopotentiometry studies on electrode reactions

Typical chronopotential scans of La_2CuO_4 and $La_{1.92}Sr_{0.08}CuO_4$ with nominal current density ≈100 $\mu A/cm^2$ are shown in Fig. 2.12. A chronopotential scan is performed by monitoring the potential change relative to the Ag/AgCl reference electrode verses time after a constant anodic current is applied to the sample electrode. For La_2CuO_4, the potential reaches a plateau when Q ≈ 0.16 e/f.u. A similar scan on $La_{1.92}Sr_{0.08}CuO_4$ shows that a charge of only ~ 0.07 e/f.u. is needed to reach a similar potential plateau, which indicates that the higher potential is a signature of the maximum oxidation level of about 0.16 holes/f.u. in the CuO_2 planes.

The plateau region corresponds to two-phases with thermodynamical consideration [Schollhorn, 1980]. The observed low potential plain region may correspond to a two phase region at room temperature [Dabrowski, 1989], where phases with δ ~ 0.08 and δ ~ 0.01 have been observed below phase separation temperature and will be discussed in Sec. 2.4.11. The

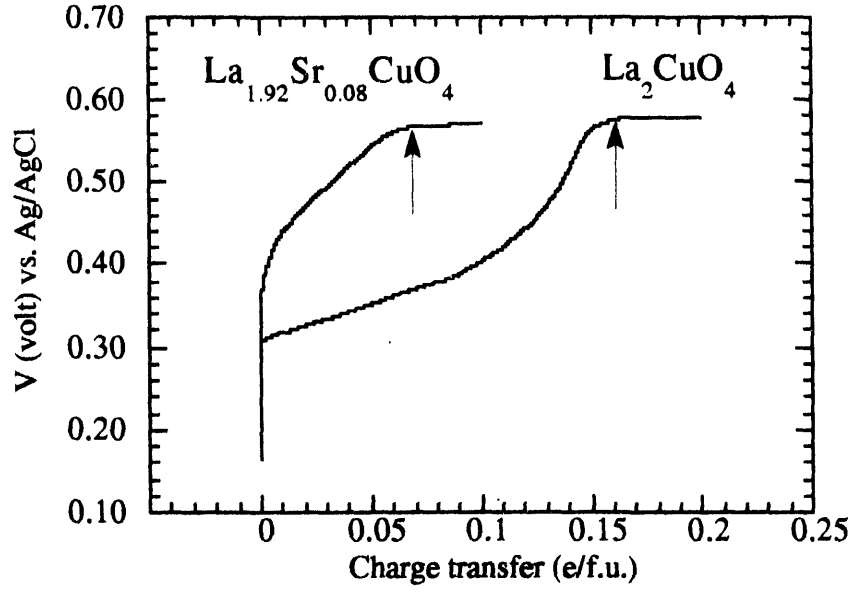

Fig. 2.12 Electrode potential (relative to Ag/AgCl reference electrode) vs. oxidative charge transfer through the electrochemical cell for La_2CuO_4 and $La_{1.92}Sr_{0.08}CuO_4$ working electrodes. Charge transfer levels of 0.07 and 0.16 e/f.u. are pointed out by arrows.

high potential plateau may have oxygen evolution reaction at the interface due to the bulk physical property change and/or other oxygen species formed at the surface.

We have monitored the open circuit potentials for different current densities on La_2CuO_4 microelectrodes (mass ≈ 1 - 5 mg). The sample electrodes were immersed in electrolyte for at least 9 hours prior to passing current through the cell. A steep increase in sample potential usually occurs at Q = 0.14-0.16 e/f.u. if the current density is low enough, as in Fig. 2.12 above. However, it has been observed that a potential jump can occur at higher charge transfer levels up to Q ≈ 0.23 and 0.31 e/f.u. when higher current densities 2.18 μA/mg and 2.74 μA/mg are applied, respectively. Since the electrode potentials are kept below the oxygen evolution potential and no anodic oxygen evolution is observed, we suggest that this phenomenon results from a slower oxygen diffusion rate than surface O^{2-} generating rate which is controlled by the anodic current at the sample/electrolyte interface. Accumulation of O^{2-} at the surface may form species like $(O_2)^{2-}$, $(O_2)^-$ or even chemisorbed O_2.

An irreversible oxidation-reduction behavior is observed in open circuit potential versus charge transfer measurements, as shown in Fig. 2.13. The potential is recorded 500 seconds after each specified charge is reached in 0.01 e/f.u. steps up to 0.35 e/f.u. For the charging current density of 1.54 μA/mg, relevant to Fig. 2.13, the potential increases sharply at Q ~0.10-0.15 e/f.u. under anodic current. When the current is reversed after Q = 0.35 e/f.u. is reached, the potential drops immediately

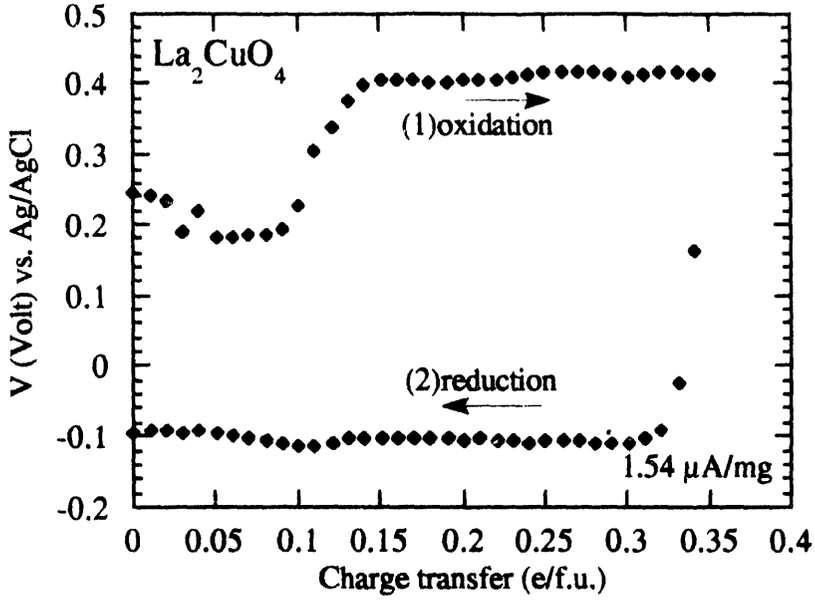

Fig. 2.13 Open circuit potential (relative to Ag/AgCl reference electrode) vs. oxidative charge transfer for La_2CuO_4 at a current density 1.54 μA/mg. All potential readings were taken 500 seconds after every 0.01 e/f.u. charging was completed. The reduction process was started immediately after 0.35 e/f.u. oxidative charge transfer was achieved.

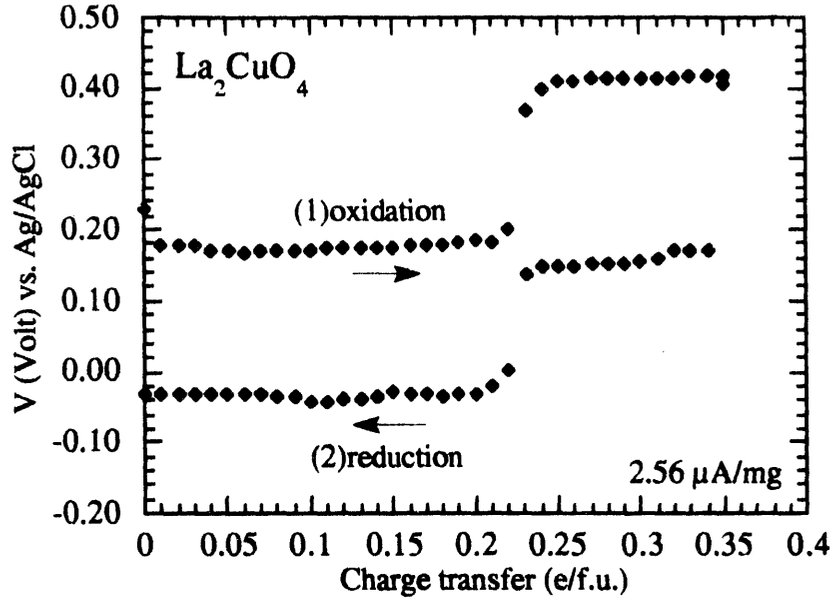

Fig. 2.14 Open circuit potential (relative to Ag/AgCl reference electrode) vs. oxidative and reductive charge transfer for La_2CuO_4 at a current density 2.56 μA/mg, taken by the same method as described in Fig. 2.13.

to a negative value of ~-100 mV. Only a small feature around Q ≈ 0.1 e/f.u. is observed in the reduction part of the cycle. Fig. 2.14 shows another open circuit potential versus charge transfer measurement on a fresh sample with a nominal current density of 2.56 μA/mg. This experiment displays a rapid increase in potential at Q ~ 0.22 e/f.u. under anodic oxidation. The potential of the subsequent reduction cycle immediately goes back to the original potential level, and then a sharp drop occurs at Q ~ 0.22 e/f.u. to a negative constant. The potential in the reduction cycles is a non-equilibrium measure of the surface state, which is a measure of an oxygen deficient state because of low oxygen out-diffusion from the bulk. We may interpret the difference in reduction cycles shown in Fig. 2.13 and 2.14 coming from different oxygen out-diffusion processes of different bulk properties. It seems the two electrodes shown in Fig. 2.13 and 2.14 have different bulk properties due to the different charging rate, the former may reached the 32 K phase only but the latter has converted to a sample with Tc = 44 K. We have introduced a model of weakly and strongly bonded interstitial oxygen for the phase with T_C = 44 K in Sec. 2.4.3. The reduction of 44 K sample above Q ~ 0.22 e/f.u. may have the weakly bonded oxygen (δ_1) to supply the out-diffusion process easily, which is why the potential goes back to the stoichiometric level (V ~ 0.15 v) first as shown in Fig. 2.14. The out-diffusion of strongly bonded δ_2 is too slow to compensate the surface oxygen deficiencies within the equilibrium time (500 seconds) and we see the potential falls to the oxygen deficient potential level as shown in Fig. 2.13 and 2.14. Due to

the difficulty in characterization of micro-electrodes, this scenario is not confirmed yet. Similar puzzling charging results have been found in high oxygen pressure annealed samples, where "identical" preparation conditions may produce either a phase with T_C ~30 K or a phase with T_C ~ 40 K [Schirber, 1993]. The difficulty in preparing a single phase with T_C = 32 K electrochemically suggests that specific current density or stringent interfacial conditions must be met during synthesis.

2.4.11. Phase separation in $La_2CuO_{4+\delta}$

The phase separation of high oxygen pressure annealed $La_2CuO_{4.03}$ has been observed from neutron diffraction two phase refinement analysis [Jorgensen, 1988] and from single crystal NQR/NMR experiments also [Hammel, 1993]. Direct observation of electrochemically oxidized $La_2CuO_{4+\delta}$ (δ = 0.03) macroscopic phase separation for $\delta < 0.07$ from $\chi_g(T)$ measurements is demonstrated in Fig. 2.15 (a), where the normal state magnetic susceptibility of $La_2CuO_{4+\delta}$ (δ = 0.03) can be simulated by contributions from two phases of $\delta \approx 0.02$ and $\delta \approx 0.07$. A correct order of magnitude for $\chi_g(\delta \approx 0.03) \approx$ (70%) $\chi_g(\delta \approx 0.02)$ + (30%) $\chi_g(\delta \approx 0.07)$ below 250K is obtained. The superconducting fraction of $La_2CuO_{4.03}$ is about 30% of that of $La_2CuO_{4.07}$ also as shown in Fig. 2.15 (b). All these results suggest that the composition of δ = 0.03 is composed of near stoichiometric phase ($\delta \approx 0.02$) of T_N ~ 250 K and superconducting phase (δ = 0.07) with T_C = 32 K, which is consistent with the results of NMR/NQR results and

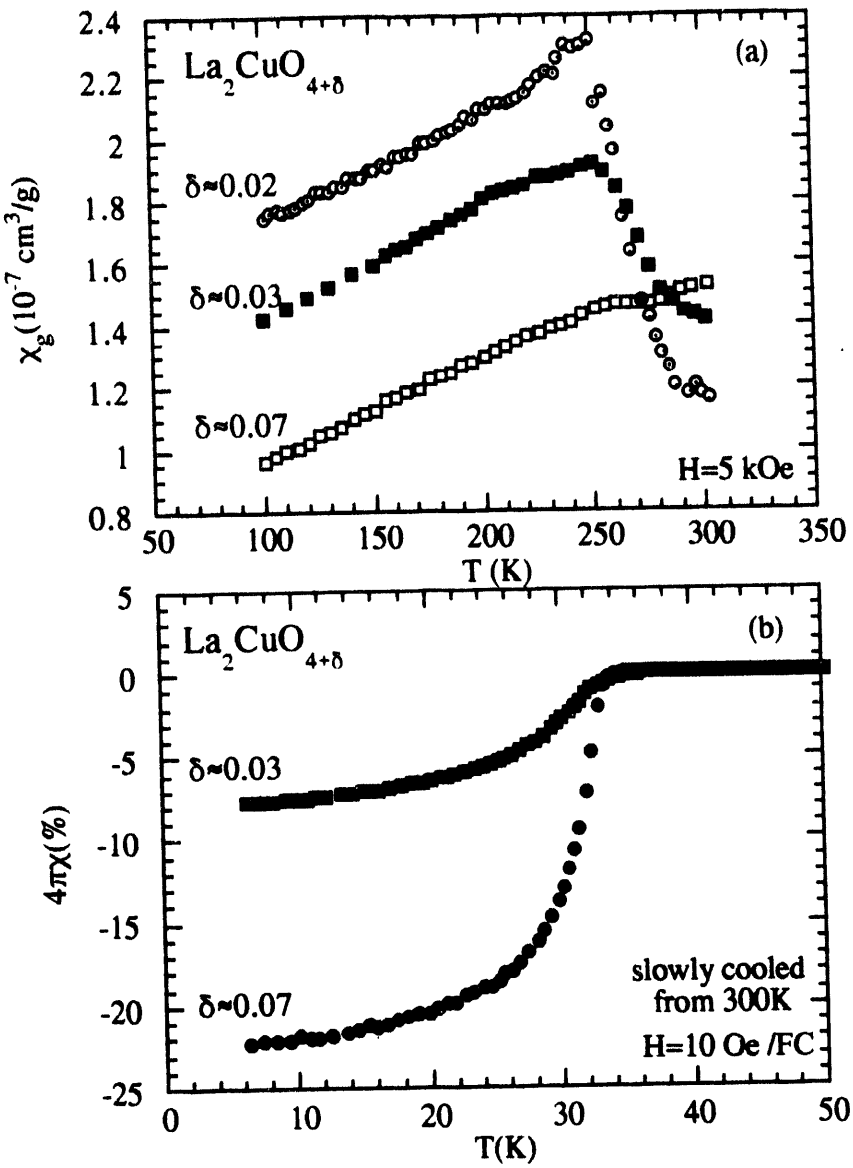

Fig. 2.15 (a) Magnetic susceptibility $\chi_g(T)$ for $La_2CuO_{4+\delta}$. Phase separation for $La_2CuO_{4+\delta}$ with $\delta \approx 0.03$ into phases of $\delta \approx 0.02$ and $\delta \approx 0.07$ is realized from $\chi_g(\delta \approx 0.03) \approx (70\%)\ \chi_g(\delta \approx 0.02) + (30\%)\ \chi_g(\delta \approx 0.07)$ below 250K. (b) Meissner fraction for $La_2CuO_{4+\delta}$ samples, the fraction at H = 10 Oe of $La_2CuO_{4.03}$ is about 30% of that of $La_2CuO_{4.07}$.

neutron diffraction analysis of high oxygen pressure annealed $La_2CuO_{4.03}$ [Jorgensen, 1988][Hammel, 1993].

2.4.12. Thermal history dependence of magnetic and superconducting properties

Fig. 2.16 compares $\chi_g(T)$ of $La_2CuO_{4.03}$ obtained from two different cooling sequences, (a) slowly field cooled (FC) from 300K and (b) zero field quenched to 6K then slowly warmed (ZFCW). Hysteresis appears below about 210K. It has been shown that the superconducting fraction can be enhanced through a slow cooling process from T > 250 K for lightly oxygen doped La_2CuO_4 [Kremer, 1992]. NQR spin-lattice relaxation rate study of lightly oxygen doped La_2CuO_4 has revealed that the oxygen freezes below around ~ 200K [Ziolo, 1988]. Macroscopic phase separation starting from ~ 280 K has been verified for similarly prepared $La_2CuO_{4.04}$ by neutron diffraction study [Radaelli, 1993]. The difference of $\chi(T)$ between FC and ZFCW processes below 210K can be explained from the oxygen disordering of ZFCW process after quenching. The disordered oxygen is frozen below ~ 210 K but begins the phase separation process as soon as it unfreezes above ~ 210 K. Similar thermal hysteresis has been observed from resistivity measurements also, with the same onset temperature of deviation [Grenier, 1992]. Ryder et al. have demonstrated that the interstitial oxygen is mobile down to ~200 K as inferred from the observed resistivity hysteresis [Ryder, 1991]. The overlap of the two $\chi(T)$ data sets immediately above ~ 210 K suggests that the phase separation mechanism is of activation type from oxygen hopping. Hammel et al. have shown that the phase separation process is discontinuous (first-order) at

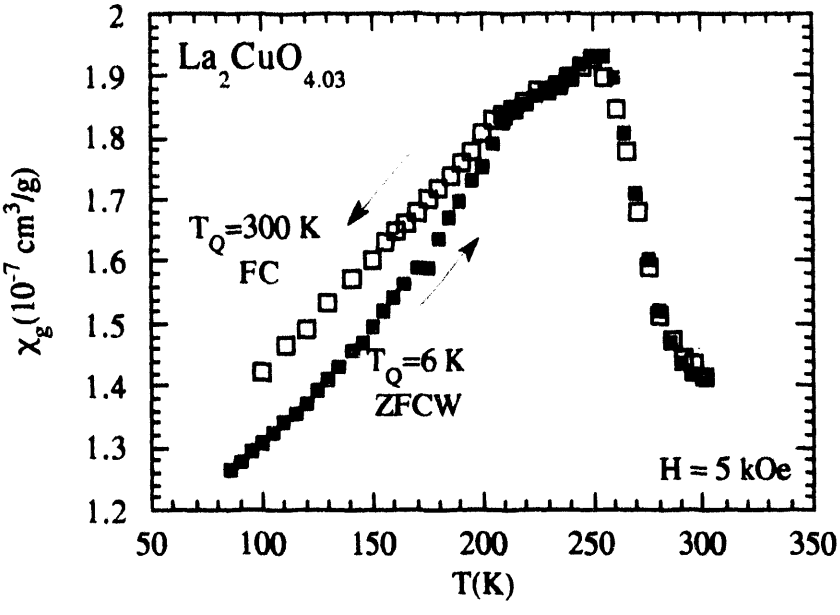

Fig. 2.16 Magnetic susceptibility $\chi_g(T)$ of $La_2CuO_{4.03}$ obtained from two different cooling sequences, (a) slowly cooled in the field H = 5 kOe (FC) from 300 K and (b) quenched from room temperature in zero field to 6K then slowly warmed (ZFCW).

phase separation temperature T_{ps} from a NQR/NMR study of high oxygen pressure prepared $La_2CuO_{4+\delta}$ [Hammel, 1993]. Our observation, on the phase separation process immediately above oxygen freezing temperature, is an additional support to the spontaneous nature of phase separation.

Fig. 2.17 shows that T_c is enhanced to 34K for samples slowly cooled from 300K for $\delta \leq 0.07$, compared to T_c for samples quenched to 6 K from 300 K. The enhanced superconducting fraction suggests that more and/or larger superconducting domains are formed due to phase separation and the higher T_c may be related to an oxygen ordering effect. The results for the $La_2CuO_{4.03}$ sample show that both the superconducting fraction and the T_c increase upon slow-cooling, which can be explained due to the phase separation process. On the other hand, the $La_2CuO_{4.07}$ sample, which shows no phase separation by neutron diffraction, shows only the T_c increase without the increase of superconducting fraction. A reasonable explanation is that oxygen ordering, and hence T_c is enhanced by slow cooling. However, a similar slow-cooling process does not enhance T_c for samples with T_c = 42 K, which suggests that the oxygen ordering is optimized already when higher oxygen content $\delta > 0.08$ is intercalated. The enhanced orthorhombicity of $La_2CuO_{4+\delta}$ with $\delta > 0.08$ supports the assumption of superoxygen ordering also.

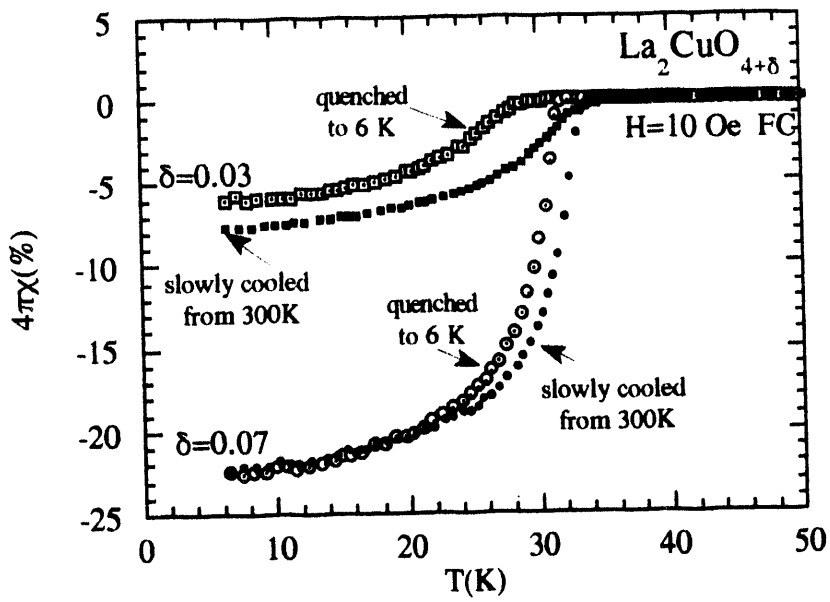

Fig. 2.17 Low field magnetic susceptibilities of $La_2CuO_{4+\delta}$ with $\delta \approx 0.03$ and 0.07. T_c's are enhanced to 34K as samples slowly cooled from 300K.

2.4.13. Bonding and ordering of excess oxygen in $La_2CuO_{4+\delta}$

Based on the analyzed results of oxygen contents and T_C's we conclude that there are two single superconducting phases in $La_2CuO_{4+\delta}$ with δ ~ 0.07 and 0.12 (± 0.01). Grenier et al. have proposed that based on the electron microscopy study of $La_2NiO_{4+\delta}$ excess oxygen ordering, one may have $\delta = 1/16 \approx 0.0625$ with T_C = 32 K and $\delta = 1/8 \approx 0.125$ with T_C = 44 K [Grenier, 1992]. Our experimental results agree with these two compositions very well.

Zhang and Sato recently found a universal relationship between normalized T_C and hole concentration per CuO_2 sheet [Zhang, 1993], where superconductivity begins at a hole concentration per CuO_2 sheet p_{sh} ~ 0.06, reaches the maximum T_C plateau at p_{sh} ~ 0.12-0.25, and is then lost by p_{sh} ~ 0.31. Since the 44 K and 32 K samples are close to the ideal δ = 1/8 and 1/16 respectively, there may be a direct connection between the doped oxygen and strontium concentrations. One can simulate Zhang's proposed hole arrangement of p = 1/16 (= 0.0625), 1/8 (= 0.125) and 1/4 (= 0.25), by the corresponding superoxygen orderings for δ = 1/16, δ = 1/8 and δ = 1/4 as shown in Fig. 2.18. An intercalated oxygen may occupy the interstitial site in a La_2O_2 layer as suggested by Chaillout et al. [1989] For simplicity we plot the oxygen at the Cu position. The proposed δ = 1/16 and 1/8 have 2D ordering of 4a and $2\sqrt{2}$a superstructure lattice constants respectively. Since the $\delta \approx 1/16$ samples have formal valence closer to -1, the extension from Sr doping to the excess oxygen doping is natural. On the other hand, the $\delta \approx 1/8$ samples may fall in between the δ= 1/8 and δ= 1/4 arrangements as suggested by their hole concentration ~

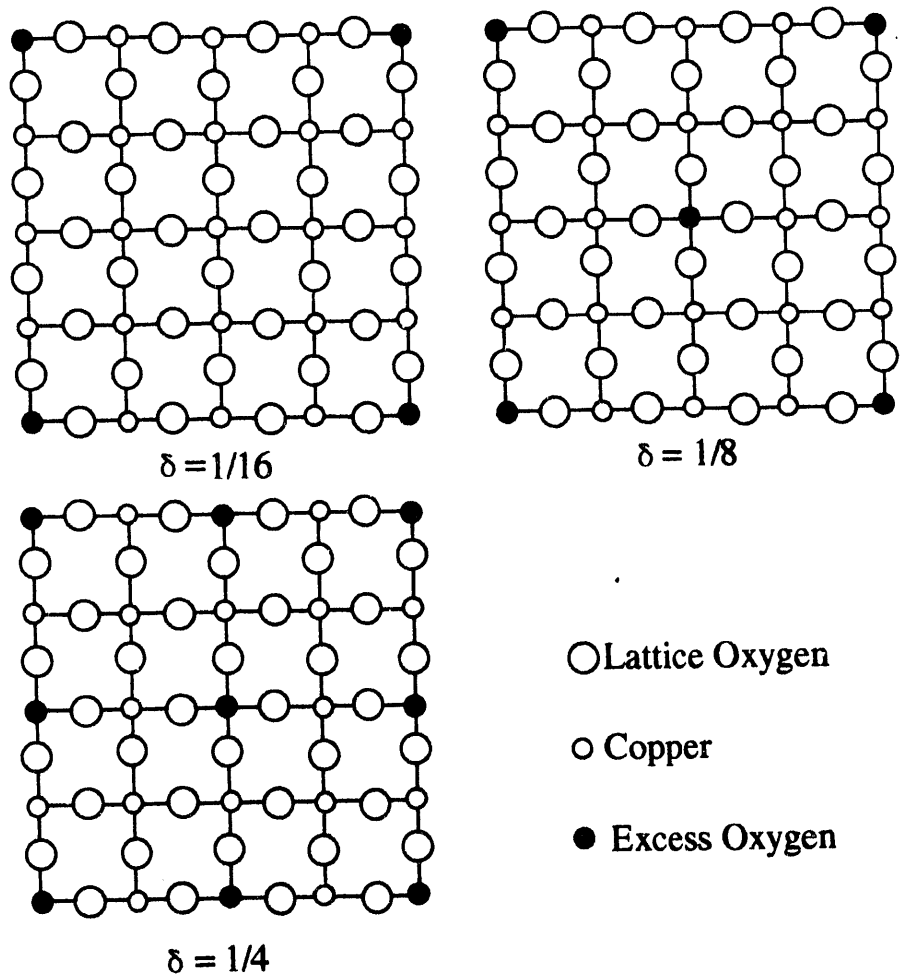

Fig. 2.18 A proposed 2D ordering model for the excess oxygen in samples with δ = 1/16 = 0.0625, δ = 1/8 = 0.125 and δ = 1/4 = 0.25.

0.16, if only 2D ordering is considered. Following the tolerance factor analysis as discussed in Sec. 2.4.5. and 2.5.6, the minimum orthorhombic strain observed for $\delta \approx 1/16$ samples suggests that the doped oxygen (holes) may distribute homogeneously in 2D as the above proposed model. On the other hand, the enhanced orthorhombicity for samples with $\delta \approx 1/8$ is indicative of a deviation from the homogeneous 2D arrangement shown in Fig. 2.18. Additional 3D ordering along the c-direction is suggested by the preliminary neutron and electron diffraction results. (see Sec. 2.4.7) The superlattice deduced from neutron diffraction (10a*10b*6c) clearly does consistent with the amount of excess oxygen in the lattice. The actual excess oxygen ordering may be more complicated than a 2D description in Fig. 2.18, especially for $\delta \approx 1/8$.

2.4.14. T-δ phase diagram of $La_2CuO_{4+\delta}$

Fig. 2.19 shows a tentative T-δ phase diagram for $La_2CuO_{4+\delta}$ based on current experimental results. A miscibility gap is observed between $\delta \sim 0.015$-0.07, which separates the near stoichiometric AF phase of Bmab symmetry and the oxygen rich PM phase of Fmmm symmetry. The phase with $\delta \sim 0.07$ becomes superconducting at low temperature with a $T_C = 32$ K. The phase boundaries are vertical below ~ 200 K due to oxygen freezing. The $T_{O/T}$ decreases with increasing δ up to ~ 0.07, which is inferred from the observed reduction of orthorhombicity. All samples with $\delta \approx 0.07$ and $\delta \approx 0.09$-0.12 show Fmmm symmetry, although the latter have enhanced orthorhombic distortion which may come from an additional excess oxygen ordering. The phase with $\delta = 0.09$-0.12 becomes

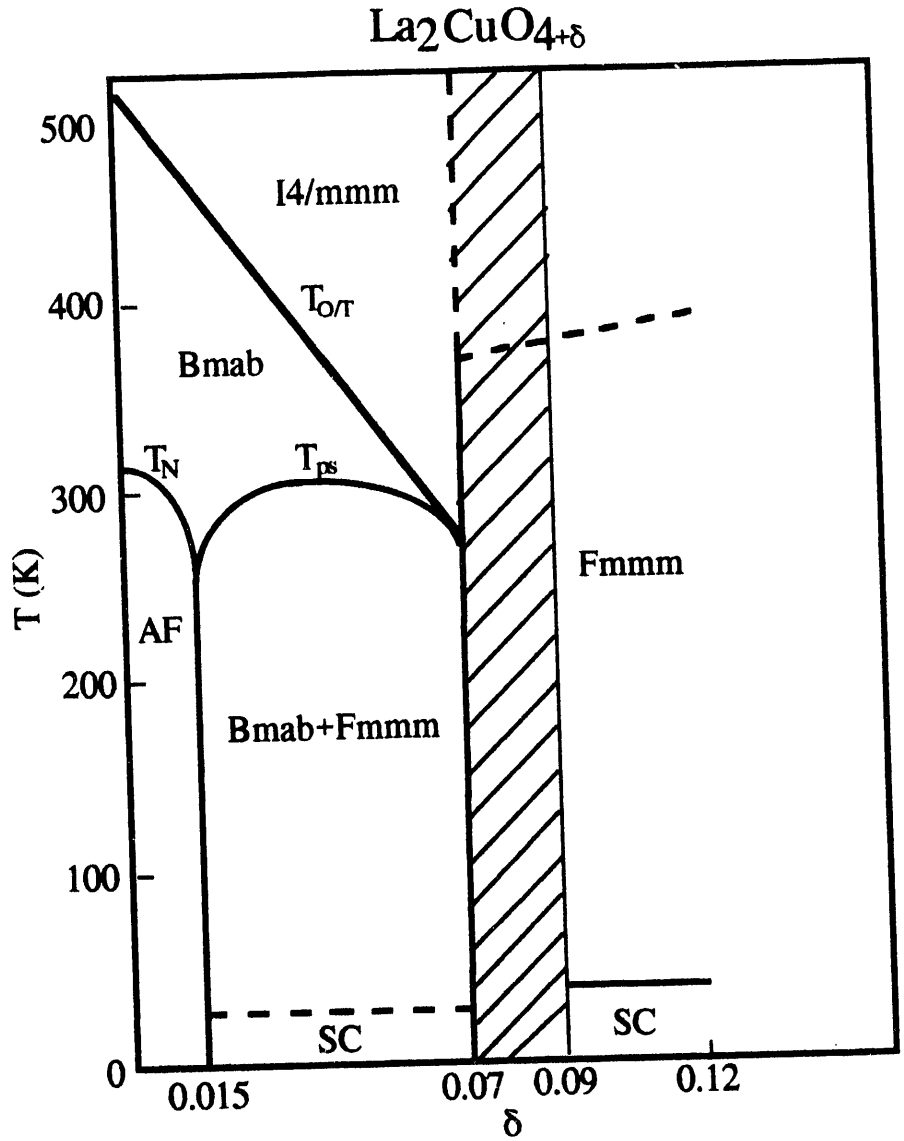

Fig. 2.19 A tentative T-δ phase diagram for $La_2CuO_{4+\delta}$ based on current experimental results. T_N is the antiferromagnetic (AF) transition temperature. T_{ps} is the phase separation temperature. $T_{O/T}$ is the orthorhombic to tetragonal transition temperature. SC = superconducting phase.

superconducting at low temperature with a T_C = 42-45 K. Preliminary differential scanning calorimetry (DSC) measurements indicate that there is an irreversible first order transition occurs at 370-390 K for samples with $\delta \geq 0.07$, which is suggestive of an excess oxygen order-disorder transition [Chou, 1993]. However, the high temperature characterizations usually have oxygen inhomogeneity problem due to oxygen disordering and/or oxygen loss.

2.5. **Summary**

From a comparison of oxygen content determinations, obtained from thermogravimetric analyses of the dried products in H_2 gas, with the measured charge passed through the electrochemical cell, we conclude that the electrochemical reaction oxygen-dopes La_2CuO_4 to form $La_2CuO_{4+\delta}$. From magnetization measurements in a low applied field, clear evidence is found for two distinct bulk superconducting phases at $\delta \approx 0.07$ ($T_C \approx 32$ K) and $\delta > 0.08$ ($T_C \approx 42$-45 K) at low temperatures. Phase separation occurs for $0.01 \leq \delta \leq 0.07$ into a nearly stoichiometric AF phase ($T_N \approx 250$ K) with $\delta \approx 0.02$ and the paramagnetic phase with $\delta \approx 0.07$, the latter becomes superconducting below $T_C \approx 32$ K. The $\delta \approx 0.07$ ($T_C \approx 32$ K) phase shows a smaller orthorhombic distortion than the La_2CuO_4 starting material, whereas the $\delta > 0.08$ ($T_C \approx 45$ K) phase shows a larger one. We propose that the latter higher distortion arises from ordering of the intercalated oxygen within the La_2O_2 layer blocks.

Sr-doped compounds $La_{2-x}Sr_xCuO_{4+\delta}$ were similarly synthesized by electrochemical oxidation of conventionally prepared $La_{2-x}Sr_xCuO_4$. Bulk superconductivity is found with onset $T_c \approx 40$ K for the whole range $0.01 \leq x \leq 0.15$; for $x = 0.25$ and 0.33, the electrochemical oxidation did not improve the superconducting properties. Normal state magnetic susceptibility $\chi(T)$ measurements indicate that the oxidation is homogeneous. The $\chi(T = 50\text{-}320$ K) data for $La_2CuO_{4.11}$ and $La_{1.92}Sr_{0.08}CuO_{4.07}$ are nearly identical with those of conventionally prepared $La_{1.85}Sr_{0.15}CuO_4$, indicating that the hole doping level (p) in the CuO_2 planes of the three compounds is nearly the same. Iodometric titration experiments confirmed that the maximum doped-hole concentration in the CuO_2 planes that can be achieved from combined Sr-doping and electrochemical oxygen doping for $0 \leq x \leq 0.15$ is $p \approx 0.16$ holes/formula unit.

Additional evidence of phase separation for $La_2CuO_{4+\delta}$ with $0.01 < \delta < 0.07$ is obtained from the correct ratio of near stoichiometric phase (with $T_N \sim 250$ K) and superconducting phase (with $T_c \sim 32$ K) from magnetic susceptibility measurements. A single superconducting phase of $T_c \sim 42\text{-}45$ K is found with $\delta \approx 0.09\text{-}0.12$. The intercalated oxygen may form polyoxide species in combination with the lattice oxygen and have formal valence close to -1 for $\delta \leq 0.07$. The additional excess oxygen beyond ~ 0.07 may have formal valence -2. The details of the superlattice ordering of the excess oxygen, as revealed by preliminary electron and neutron diffraction measurements, remain to be clarified.

CHAPTER 3. PREPARATION AND CHARACTERIZATION OF ELECTROCHEMICALLY OXIDIZED SINGLE CRYSTAL $La_2CuO_{4+\delta}$

3.1 Introduction

Following the discovery of the electrochemical oxidation technique for producing polycrystalline $La_2CuO_{4+\delta}$ [Wattiaux, 1990], intensive studies on superconductivity, magnetic properties [Grenier, 1991][Chou, 1992], transport properties [Grenier, 1992] and structural investigation [Rudolf, 1991][Radaelli, 1993] have been carried out on these materials [Wattiaux, 1990]. In order to investigate this type of highly anisotropic material, single crystal studies are desirable. Due to the difficulties (see below) with preparation, there are no single crystal studies reported up to now. Herein we report the preparation method and physical properties of the first electrochemically oxidized single crystals of $La_2CuO_{4+\delta}$ with T_c ~ 40 K.

3.2 Experimental Details

3.2.1. Sample preparation

La_2CuO_4 single crystals were grown using a flux method as described in Ref. [Cheong, 1988]. Two single crystals, crystal A with mass 36.35 mg (~4.5 × 2 × 1 mm^3) and crystal B with mass 72.80 mg (~4 × 3 × 1 mm^3), were subjected to electrochemical oxidation. The electrochemical cell is set up as

La_2CuO_4 / 1N NaOH / Pt,

where the working electrode is a single crystal of La_2CuO_4 and the counter electrode is a platinum wire. A platinum wire was attached to one side of the single crystal using silver paint. The silver paint was then fully covered with silicone rubber. Initially we tried to verify if the electrochemical oxidation process works for single crystal La_2CuO_4 just like that for pellet or powder La_2CuO_4, as described in our previous report [Chou, 1992]. An anodic current of 100 μA was applied to the crystal A working electrode yielding Q ~0.33 e/f.u.. A superconducting phase is expected at this Q for polycrystalline samples, but no superconductivity was observed for the crystal above 6 K from SQUID magnetometer measurement results. Additional oxidation at a current of 100 μA for 4 days (Q ~ 4 e/f.u.) led to only a trace of superconductivity. Bulk superconductivity and homogeneous oxidation were achieved (see below) after additional charging with a 10μA current for more than one month. The measured 0.19 mg weight gain after oxidation for the crystal A yields $\delta = 0.13 \pm 0.02$.

Based on our experience with crystal A, we applied a constant 10 μA anodic current to crystal B and reached bulk superconductivity in 2 months. An almost constant electrical potential of about 0.6 V/Ag-AgCl was maintained during the whole charging process. But we could not estimate the excess oxygen content from the weight gain of crystal B due to some small pieces the crystal were lost during handling.

3.2.2. Characterization of $La_2CuO_{4+\delta}$ crystals

Magnetic susceptibilities were measured by a Quantum Design SQUID magnetometer. The magnet was quenched to eliminate the remnant field before any low field measurement. An isothermal magnetization vs. field (M-H) curve was obtained after zero-field-cooling (ZFC); the "no overshoot" mode magnetic field setting was used. A four centimeter scan was used as a compromise between maximum signal and minimum field inhomogeneity. The low field field-cooled (FC) data are not quantitatively reliable due to the distorted SQUID signal, which will be discussed below. This asymmetric signal was still fitted to a dipole moment response. We even observed a paramagnetic Meissner signal in some of the FC runs, which were not always reproducible due presumably to some subtle sample position or magnet condition change.

The four-probe dc method was used to measure the in-plane and inter-plane resistivity. Because the excess oxygen tends to deplete from samples above room temperature as reported earlier [Chou, 1992], obtaining a good electrical contact becomes a difficult task. As applied, silver paint gives poor electrical contact on a single crystal after several thermal cycles unless high temperature annealing is performed subsequent to applying the silver paint [Hidaka, 1987]. Spark-welding the electrode leads onto a crystal can cause severe oxygen deficiency at the contact points and need additional annealing also [Iye, 1988]. We found that the best and most stable electrical contacts, which need no additional high temperature annealing, are

made by rubbing Indium metal into the crystal surface cracks and then covering with silver paste. For these contacts, the contact resistance at 293 K obtained by the three-probe method is about 1.5 Ohms and the 4-lead resistance was checked to be ohmic. Thermal EMF's were canceled out by averaging measured resistance with the current flow in opposite directions. The trial run using the Montgomery method [Montgomery, 1971] gave an unreasonably high in-plane resistivity value and we think maybe it is due to lack of a well-defined geometry of the leads as required with this method. The ordinary four probe method was used to measure resistivity in both parallel and perpendicular directions. The four probes were chosen to have a configuration similar to that suggested by Iye et al. on a $YBa_2Cu_3O_7$ crystal [Iye, 1988].

3.3 Experimental Results

3.3.1. Superconductivity

The low field susceptibility for fully oxidized crystal B in a 2 Oe applied field perpendicular to the CuO_2 planes is shown in Fig. 3.1. The 225 and 123 % ZFC $4\pi\chi$(6K) values for H //c and H //ab, respectively, at 2 Oe suggest perfect diamagnetism without a demagnetization factor correction. A low Meissner fraction is found from the FC $4\pi\chi$ data in Fig. 3.1(a). Such a low Meissner fraction has been observed in most of the high T_c superconductor single crystals and may be explained due to the high pinning force from tiny precipitates, twin boundaries and/or cracks in

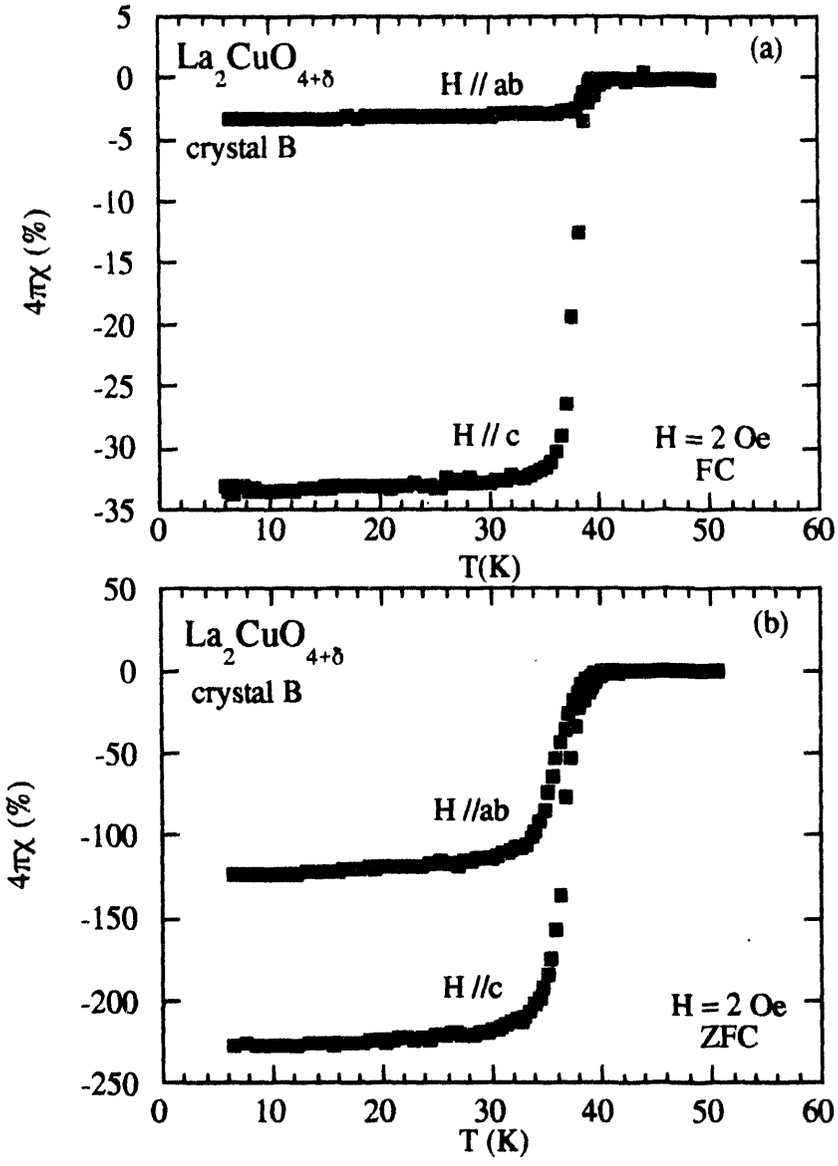

Fig. 3.1 Magnetic susceptibilities χ of crystal B vs. temperature T in an applied magnetic field H = 2 Oe, normalized to the value $1/4\pi$ without demagnetization effect correction. (a) Field cooled (FC) and (b) zero-field-cooled (ZFC) data are taken upon warming. H //c and H //ab represent the applied field is perpendicular and parallel to the CuO_2 planes.

the crystal. The demagnetization factors, n, estimated from low field ZFC measurements assuming perfect diamagnetism at 6 K, are around 0.56 and 0.19 for H //c and H //ab respectively, where $-4\pi\chi = 1/(1-n)$, which are reasonable values comparing with ellipsoid of shorter principal axes. The onset of T_c at 40 K with mid point around 37 K is comparable to those of the best Sr doped single crystals reported up to now [Kishio, 1992][Li, 1993][Terasaki, 1992], but lower than that of the corresponding polycrystalline samples (42-45 K) [Chou, 1992]. There are no additional inflections in the FC $\chi(T)$, which suggests a single superconducting phase is reached.

The FC $4\pi\chi(T)$ values for crystal A are shown in Fig. 3.2. The $4\pi\chi(6K)$ values are near 6 % (FC) and 200 % (ZFC) (not shown) under a magnetic field H = 10 Oe. The data exhibit a linear drop from ~ 38 K to 32 K, with the onset of superconductivity at ~ 40 K. We have found two distinct superconducting phases in polycrystalline $La_2CuO_{4+\delta}$ with T_c of ~ 32 K and ~ 42-45 K with $\delta \approx 0.07$ and ≥ 0.09 respectively [Chou, 1992]. The linear drop of $4\pi\chi(32\text{-}40\ K)$ indicates the proximity-effect coupling between two phases of T_c ~ 32 K and ~ 40 K.

3.3.2. Lower critical field H_{c1} and critical current density J_c

The anisotropic magnetization hysteresis at 5 K is shown in Fig. 3.3, where we have used the demagnetization factor obtained from 2 Oe ZFC data (Fig. 3.1(b)) to correct the magnetization values. The initial $d(4\pi M)/dH$ becomes -1 after the demagnetization effect correction, corresponding to perfect diamagnetism below H_{c1}. The field dependence

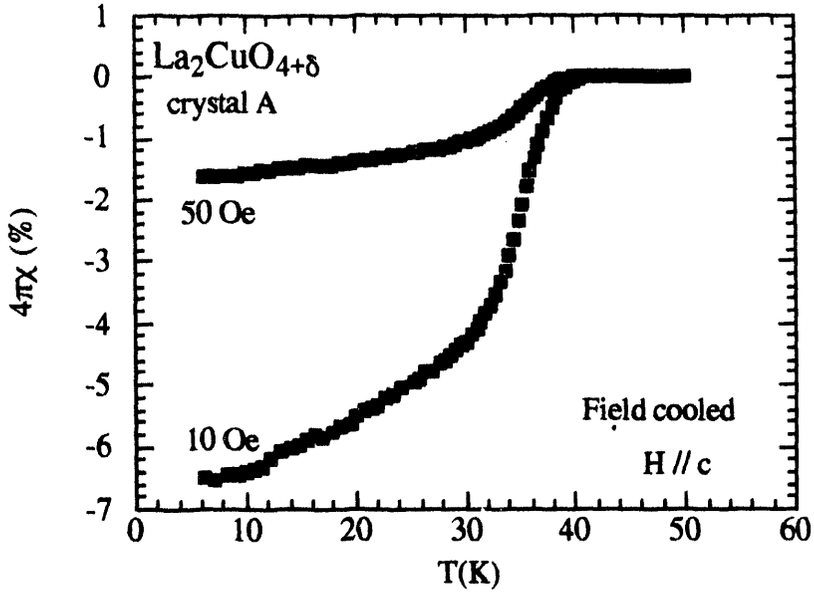

Fig. 3.2 Field cooled magnetic susceptibilities χ of crystal A vs. temperature T in an applied magnetic field H = 10 Oe and 50 Oe perpendicular to the CuO_2 planes; the data were taken on warming.

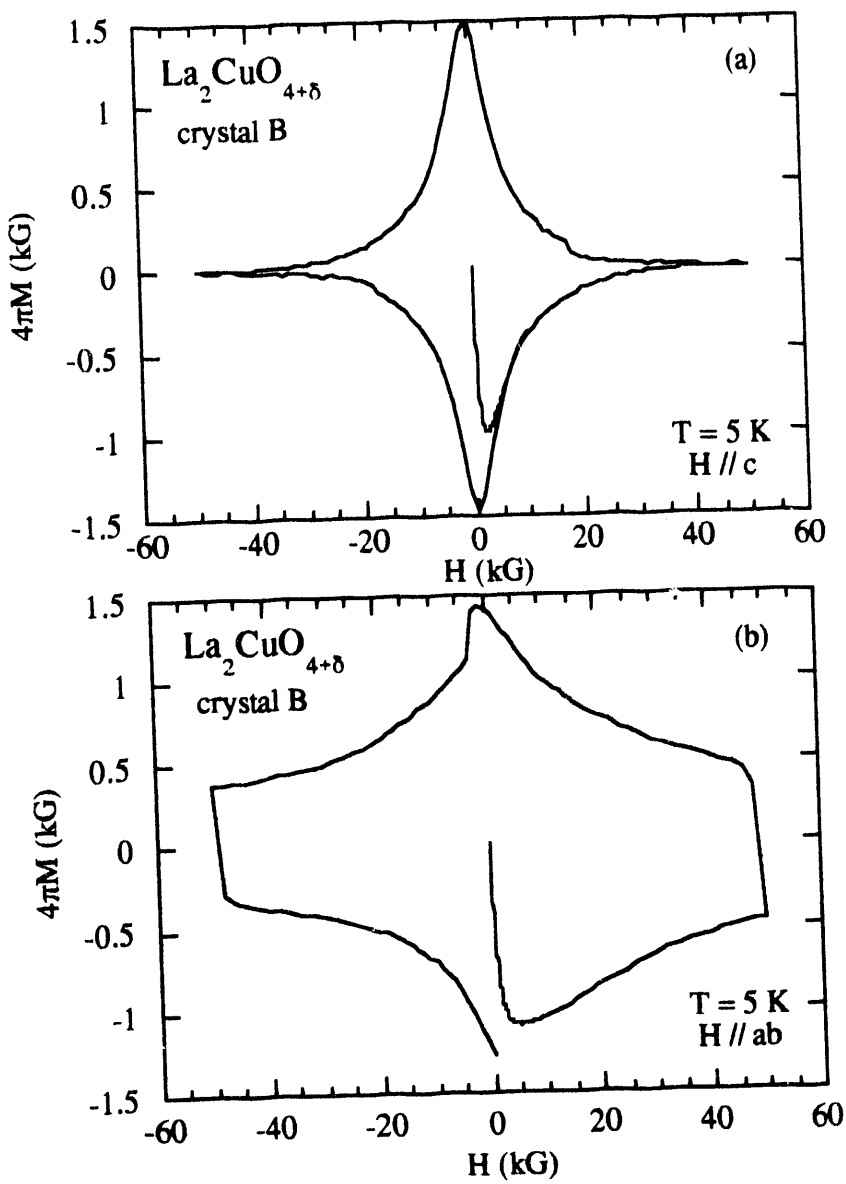

Fig. 3.3 Magnetization hysteresis loop for crystal B at T = 5 K after the sample is zero-field cooled from above T_c. The magnetic field is applied (a) perpendicular (H//c) and (b) parallel (H//ab) to the CuO_2 planes respectively.

at 5 K for H //c is similar to that for "under-doped" $La_{2-x}Sr_xCuO_4$ (x = 0.12) reported by Kimura et al. [1992] The H_{c1}'s were estimated from the M-H data which first deviate from the linear part of the ZFC magnetization curve. Due to the repulsive interactions betw vortices, the magnetization deviates very gradually from the diamagnetism and hence the current estimated H_{c1} should be viewed as the flux entry field,[de Gennes, 1966] the actual H_{c1}'s are lower than the values obtained from current method. The H_{c1} values are is about 660 ± 20 Oe for H //c and 380 ± 20 Oe for H // ab, which are comparable to 640 Oe estimated for a polycrystalline sample by Grenier et al. [1992].

The critical current density $J_c(H)$ for the two principal directions of H at T = 5 K are shown in Fig. 3.4. The irreversible pinning current density $J_c(H)$ is related to the width of the resis loop $\Delta M(H)$ according to Bean's critical state model as $J_c(H) = \Delta M(H)/2r$, where r is the effective crystal radius perpendicular to the applied field [Bean, 1964][Daeumling, 1990]. The observed J_c's at zero field are at least one order smaller than that of the Y123 and LaSr single crystals reported [Kishio, 1992][Kimura, 1992][Dinger, 1987], where more pinning centers in the latter are provided by the oxygen deficiencies [Dinger, 1987] or material inhomogeneities. There is an ideal exponential field dependence with a decay constant of 8 kOe for H //c as shown in Fig. 3.4. An exponential field dependence of J_c has been proposed theoretically [Kumar, 1989]. However, the existence of the reversible part of magnetization at fields below H_{c1}, which is due to a screening current near the specimen surface and associated with the

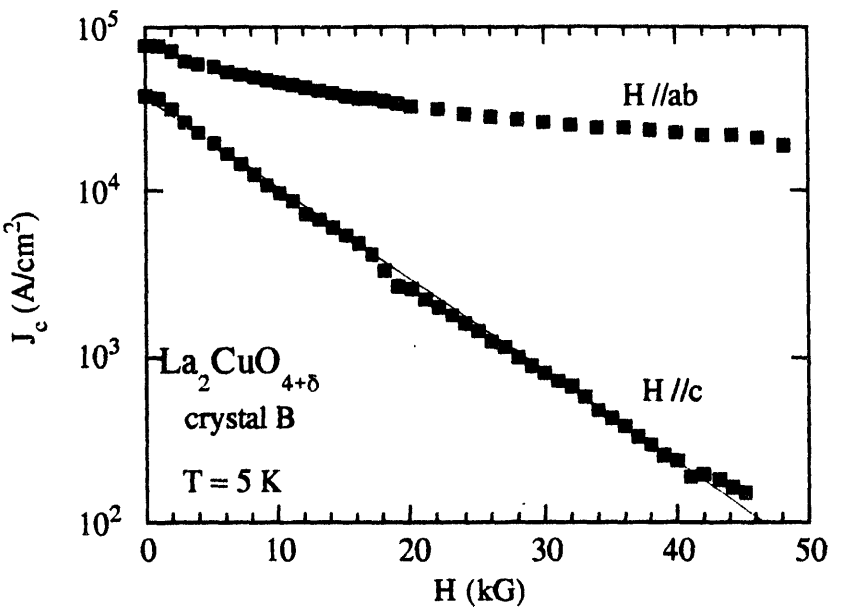

Fig. 3.4 Critical current density J_C vs. applied field H at T = 5 K on a semi-log scale. The straight line is a fitting of exponential field dependence.

expulsion of the magnetic field [Yang, 1993], forbids the direct observation of exponential dependence of $J_C(H)$. The low field reversible magnetization shifts the maximum of magnetization in M-H curve at H = 0 usually, which may cause underestimation of $J_C(H)$ at low fields [Chaddah, 1989]. We observed that extremely little low field reversible magnetization exists for H //c as shown in the hysteresis loop.(Fig. 3.3) This unique properties allows us to observe the direct $J_C(H)$ field dependence. A perfect exponential field dependence of J_C have been observed in both crystals for H //c, which imply that these properties are intrinsic to the electrochemically oxidized $La_2CuO_{4+\delta}$.

3.3.3. Normal state magnetic susceptibility

The normal state susceptibilities vs. temperature with applied magnetic fields of 1 T perpendicular (χ_c) and parallel (χ_{ab}) to the CuO_2 planes for crystal B are shown in Fig. 3.5(a). The as-prepared La_2CuO_4 or high oxygen pressure oxygenated $La_2CuO_{4+\delta}$ usually display an anomaly at T_N around 250-300 K due to the 3D antiferromagnetic (AF) ordering [Cheong, 1989][Miller, 1992]. The absence of a peak in both χ_c and χ_{ab} demonstrates that there is no unreacted original phase left and no 3D AF phase generated from phase separation either, which has been verified by neutron diffraction refinement analysis also [Radaelli, 1993]. The anisotropic susceptibilities resemble those observed in $La_{2-x}Sr_xCuO_4$ (x = 0.15) single crystals by Terasaki et al and are field independent up to 5T [Terasaki, 1992]. The temperature dependence of χ_c and χ_{ab} are similar except that χ_{ab} has a small Curie like behavior present below ~ 100 K.

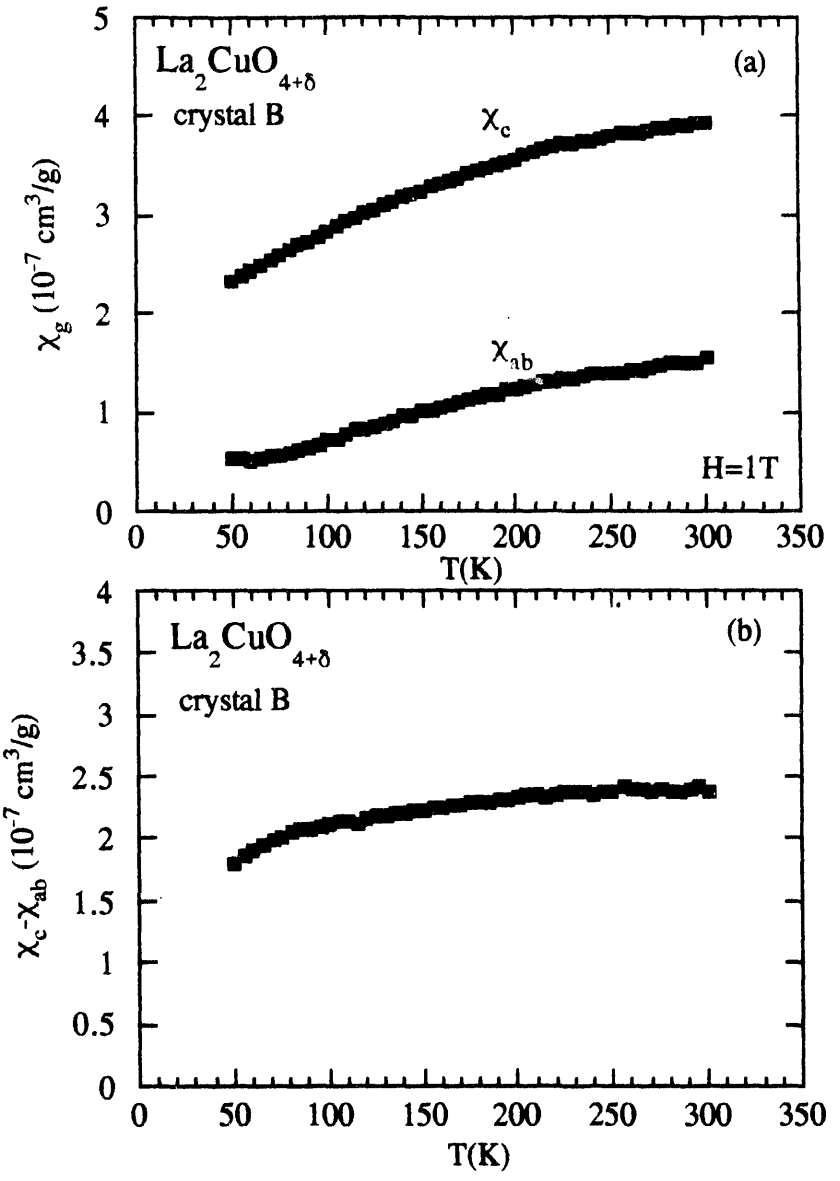

Fig. 3.5 (a) Magnetic susceptibility χ_g vs. temperature T for crystal B in an applied field H = 1 Tesla perpendicular (χ_c) and parallel (χ_{ab}) to the CuO_2 planes. (b) Magnetic susceptibility anisotropy $\Delta\chi = \chi_c - \chi_{ab}$ as computed from (a).

The weighted average 1/3 × χ_c+2/3 × χ_{ab} gives the predicted polycrystalline result fairly well below 150 K as shown by comparison with that of a $La_2CuO_{4.09}$ powder sample [Chou, 1993].

The magnetic susceptibility anisotropy $\Delta\chi = \chi_c - \chi_{ab}$ of crystal B is shown in Fig. 3.5(b). The anisotropy $\Delta\chi$(220-300K) = 9.7×10^{-5} cm^3/mole is significantly larger than reported for any other La_2CuO_4-type compounds [Terasaki, 1992][Johnston, 1992]. The enhanced anisotropy from tetragonal $YBa_2Cu_3O_{6.1}$ to orthorhombic $YBa_2Cu_3O_7$ has been observed by Yamaguchi before [Yamaguchi, 1989]. The orthorhombic structure due to the ordered interstitial oxygen [Radaelli, 1993] may have changed the electronic environment near the Cu sites significantly. The values $d\chi_c/dT \approx 12.2\times10^{-8}$ cm^3/mole-K and $d\chi_{ab}/dT \approx 10.9\times10$-8 cm^3/mole-K were obtained in the T range 220-300 K. These values are larger than reported for pure La_2CuO_4 by 2-3×10^{-8} cm^3/mole-K. The g_c/g_{ab} value, where $(g_c/g_{ab})^2 = (d\chi_c/dT)/(d\chi_{ab}/dT)$, is about 1.06 assuming that the temperature dependence is from the spin susceptibility and the anisotropy in $d\chi/dT$ is coming from the g-factor [Johnston, 1992]. This g_c/g_{ab} ratio is very close to that of the insulating La_2CuO_4 (1.11±0.05) but smaller than that of $La_{1.85}Sr_{0.15}CuO_4$ (1.24) [Terasaki, 1992].

3.3.4. Resistivity

The anisotropic resistivities perpendicular and parallel to the CuO_2 planes for crystal A are shown in Fig. 3.6. The in-plane ρ_{ab} shows a typical linear T dependence up to 300 K (with slope ~ 0.0069 mΩ-cm/K) as

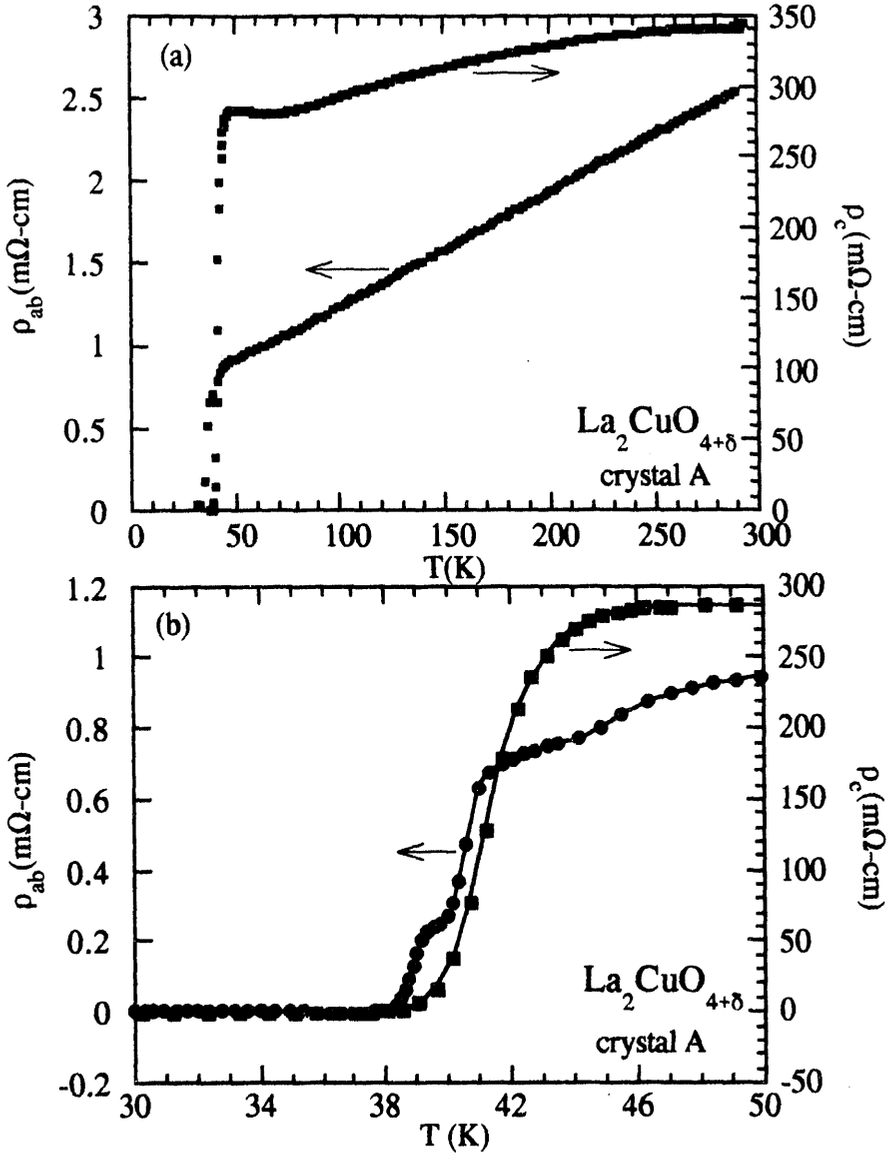

Fig. 3.6 (a) In-plane resistivity ρ_{ab} and inter-plane resistivity ρ_c vs. temperature T from 4.2 to 300 K for crystal A. (b) Resistivities vs. temperature T around T_c obtained while slowly warming.

often observed in high T_c superconductors [Takagi, 1992][Iye, 1989]. On the other hand, the magnitude of ρ_c displays a semiconductive behavior like that observed in $La_{2-x}Sr_xCuO_4$ (x = 0.144) single crystal [Kimura, 1992]. Iye et al. [1988] have found that ρ_c can be linear in T also for fully oxygenated $YBa_2Cu_3O_7$ single crystal. Fig. 3.6(b) shows a detailed look around T_c in a slow warming sequence. There are two steps for ρ_{ab} at around 44 and 40 K before the resistivity goes to zero at ~38 K. The value 44 K is the T_c often observed in polycrystalline samples and the value 40 K corresponds to the onset of diamagnetism in this crystal.

3.3.5. Intermediate states of $La_2CuO_{4+\delta}$

Fig. 3.7(a) shows the progressive change with oxygen doping level of normal state $\chi_g(T)$ from the undoped single crystal to a superconductor with T_c ~ 40 K with applied field 5T along the c-axis. The untreated La_2CuO_4 crystal shows a large anomaly between 110 - 260 K superimposed on an almost temperature independent background. The χ_g(110-260 K) anomaly is related to the field driven weak ferromagnetic (WFM) contribution due to the out of plane canting of Cu moments [Cheong, 1989]. The onset of the 3D AF transition occurs at ≈ 260 K, below which the canted AF spins between CuO_2 layers were driven to the same direction by a high field of 5T. However, the 5T field is lower than the critical field required to align the canted spins for temperature below ~ 110 K, where we see the sharp reduction in $\chi_g(T)$. As more oxygen is intercalated into the crystal, the WFM contribution becomes smaller, and the χ(260-300K) becomes larger. Eventually a single superconducting

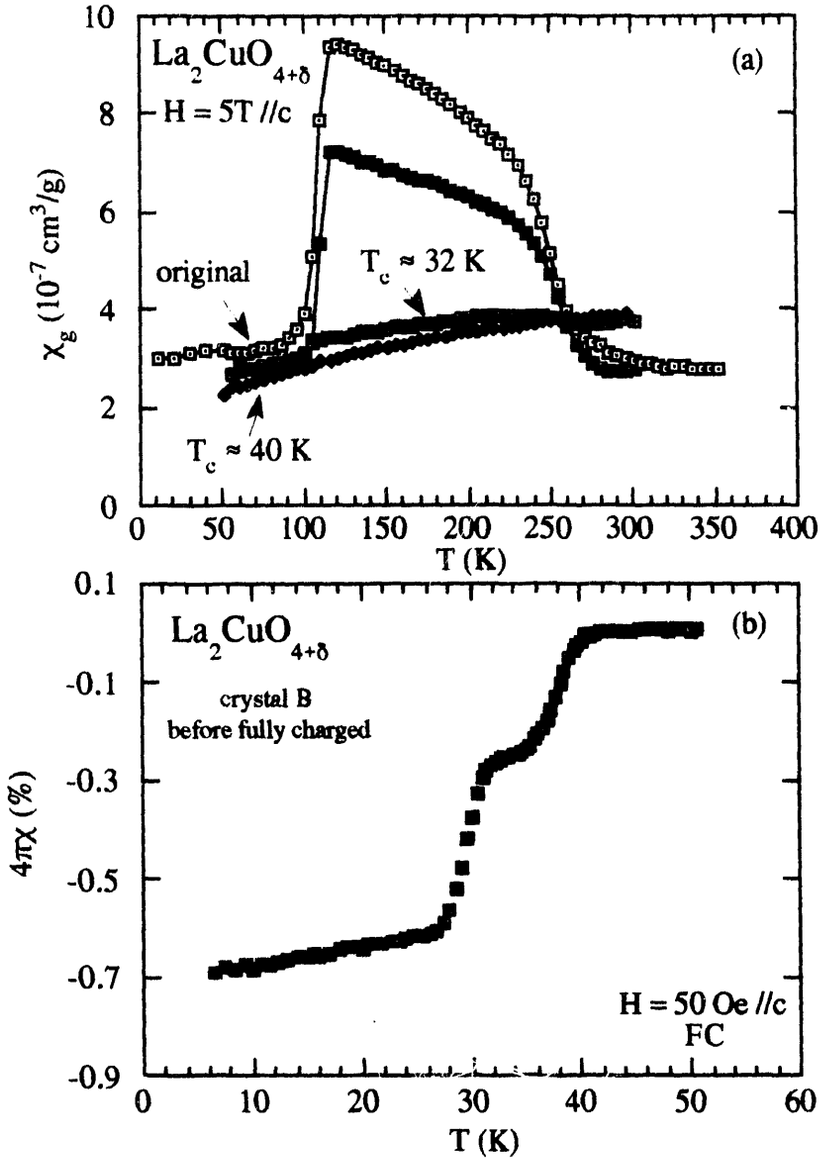

Fig. 3.7 The progressive change of normal state $\chi_g(T)$ from the undoped as prepared single crystal to a superconductor with Tc ~ 40 K along the c-axis direction (a) with applied field 5T. (b) Field-cooled $4\pi\chi$ vs. temperature T in an applied magnetic field of 50 Oe perpendicular to the CuO_2 planes; the data were taken on warming.

phase sample with T_C ~ 40 K can be reached without any WFM anomaly observed. This type of evolution indicates the progressive disappearance of the near-stoichiometric phase as oxygen is intercalated. Another observation is that just before the single phase with $T_C \approx$ 40 K is formed, a bulk superconductor of T_C ~ 32 K is formed first as shown by the $4\pi\chi$(5-50 K) of a low current (2 μA) charged single crystal.

Before a single phase with $T_C \approx$ 32 K for crystal B is reached, there are two superconducting phases with T_C ~ 32 and 40 K as shown in Fig. 3.7(b). This kind of two-phase feature usually shows up when the charging current density is too high as observed in polycrystalline samples, where the phase with $T_C \approx$ 42-45 K nucleates from the surface due to a charging rate higher than the bulk oxygen redistribution rate [Chou, 1992]. The phase with T_C ~ 40 K is lower than that T_C ~ 42-45 K observed in polycrystalline samples, even though the 32 K T_C of the lower T_C phase remains the same. From the above observation, the highest T_C ~ 45 K in polycrystalline $La_2CuO_{4+\delta}$ reported up to now is possibly related to surface superconductivity. Additional data which support this scenario are the observed broad transition temperature widths and the aging character in polycrystalline samples [Chou, 1993], where T_C decreases from 44 K to 42 K within 2 months.

3.4. Discussion

3.4.1. Micro cracks and charging rate

Initially we suspected that the existence of micro-cracks in the single crystal enables electrochemical oxidation as in polycrystalline samples. But additional experimentation on a small (2 × 2 × 0.7 mm) crystal without micro cracks, which was picked from the top of the flux, can also be charged by the same method, although it takes at least twice the time than the previously described crystals A and B above. The charging time for a single crystal to reach single phase is extremely slow compared to the polycrystalline samples. We believe the smaller specific surface area and long diffusion distance are responsible for the slow charging process in single crystals. Suppose the oxygen diffusion rate is fixed at room temperature and the same current per gram is applied to the single and polycrystalline samples. The single crystal has the smaller specific surface area to support the oxygen formation at the sample-electrolyte interface. On the other hand, if we apply a higher current on a single crystal in order to reach a comparable oxygen level like that on a polycrystalline sample surface, it usually causes the sample electrode potential to be above 0.62 V/Ag-AgCl and oxygen evolution occurs [Chou, 1992]. Our experience shows that the best choice of charging current is the one that can maintain the sample electrode at around a potential 0.6 V/Ag-AgCl. If a constant potential of about 0.6 V/Ag-AgCl is applied to the sample by a potentiostat, the electrolyte needs constant stirring

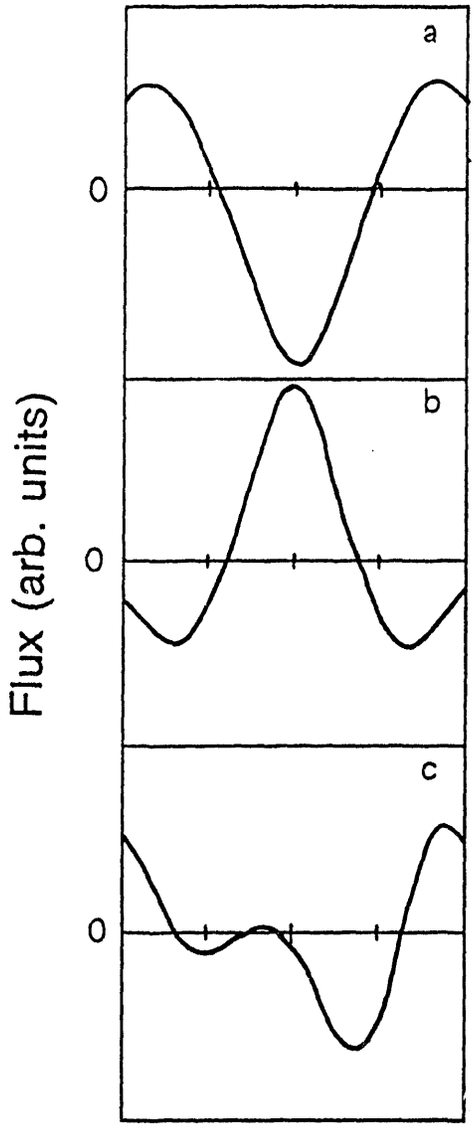

Fig. 3.8 Typical flux (in volts) profiles detected by the second derivative coil configuration of SQUID magnetometer at 6 K. The scan length is 4 cm. (a) Normal dipole moment diamagnetic response. (b)-(c) Distorted diamagnetic responses.

to maintain the concentration around the sample electrode.

3.4.2. Distorted dipolar signal and superconducting paramagnetism

Fig. 3.8 shows some typical flux (in volts) profiles detected at low field by the second derivative coil configuration of a SQUID magnetometer at 6 K. The ZFC response in Fig. 3.8(a) is a typical dipole moment response, but the FC signal in Fig. 3.8(b)-(c) has an asymmetric shape or even paramagnetic-like response, which cannot be assigned as coming from a pure dipole moment. Suenaga et al. [1992] have reported SQUID signal deformation usually occurs below irreversibility temperatures due to the irreversible motion of the flux lines. Grover et al. [1991] have explained the asymmetric SQUID response as arising from the pronounced higher multipole moment contributions due to the inhomogeneous mixed state of type II superconductors. Blunt et al. [1991] suggest that some reported paramagnetic-like signals may come from the trapped flux in an inhomogeneous field [Lee, 1990]. They conclude that a positive moment can be obtained in a commercial SQUID magnetometer if the sample is measured in a field which is lower than the field in which it was cooled. We observed paramagnetic-like SQUID responses only in low field (up to 10 Oe) FC measurements. But such paramagnetic-like signals are not always reproducible in different runs where favored conditions may have been altered. Asymmetric signals may dominate like that in Fig. 3.8(c) instead of the symmetric paramagnetic-like signals in Fig. 3.8(b), which cannot be explained simply by a para- or diamagnetic dipole moment only.

If we ignore the dipole signal distortion, it seems the paramagnetic-like signal shown in Fig. 3.8(b) represents a paramagnetic Meissner state as observed in $Bi_2Sr_2CaCu_2O_8$ polycrystalline samples [Braunisch, 1992]. However, the paramagnetic-like signal in Fig. 3.8(b) has a narrowed central peak which actually simulates a diamagnetic octupole moment response better as judged from the inverted shape plus narrowed central peak [Grover, 1991]. Due to its irreproducible nature, further detailed measurements using other types of magnetometers are necessary to further characterize the low-field FC behavior.

3.5. **Summary and Conclusions**

We have reported the details of the preparation method of electrochemically oxidized single crystal $La_2CuO_{4+\delta}$. The anisotropic superconducting, magnetic and transport properties are summarized and compared with the polycrystalline $La_2CuO_{4+\delta}$ as well as the $YBa_2Cu_3O_{7-\delta}$ (Y123) and $La_{2-x}Sr_xCuO_4$ (LaSr) single crystals. The single crystal $La_2CuO_{4+\delta}$ has a T_c ~ 40 K which is lower than that of the corresponding polycrystalline sample by 4-5 K. The magnetic anisotropy $\Delta\chi$ is significantly larger than all the La_2CuO_4-type compounds reported up to now. The H_{c1} is about 660 ± 20 Oe for H //c and 380 ± 20 Oe for H // ab. A strong exponential-like field dependence is observed for J_c at 5 K when the field is applied perpendicular to the

CuO_2 plane. Multipole moments due to the inhomogeneous flux distribution are observed from SQUID responses.

The oxygen can intercalate into the single crystal La_2CuO_4 through a slow electrochemical oxidation process. The required low current plus long time charging process reflect that oxygen intercalation in a single crystal is limited by its small specific surface area and long diffusion distance. The oxygen intercalated $La_2CuO_{4+\delta}$ is a bulk superconductor with T_c ~ 40 K, which is comparable to that of $La_{1.85}Sr_{0.15}CuO_4$ but lower than that (42-45 K) of the corresponding polycrystalline $La_2CuO_{4+\delta}$ samples. The critical current densities at 5 K extracted from the magnetization hysteresis are lower than those reported for Y123 and LaSr crystals, which reflects a lower pinning in the current system. There is a strong exponential-like field dependence directly observed in the $J_c(H)$ when the applied magnetic field is perpendicular to the CuO_2 plane. Analysis of the normal state susceptibility shows that the magnetic anisotropy $\Delta\chi$ is 9.7×10^{-5} cm^3/mole and the g-factor ratio g_c/g_{ab} is 1.06, the former being significantly larger than that of the original La_2CuO_4. The in-plane resistivity ρ_{ab} has a typical metallic magnitude and linear temperature dependence, but the ρ_c shows a semiconductive magnitude.

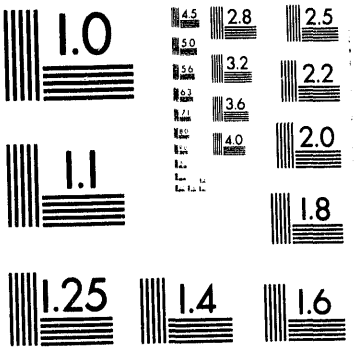
1.0
1.1
1.25
1.4
1.6
1.8
2.0
2.2
2.5
2.8
3.2
3.6
4.0
4.5
5.0
5.6

2 of 2

CHAPTER 4. MAGNETIC PHASE DIAGRAM OF LIGHTLY DOPED $La_{2-x}Sr_xCuO_4$ FROM ^{139}La NQR

4.1. Introduction

Since the discovery of superconductivity in $La_{2-x}Sr_xCuO_4$, it has been of great importance to clarify the role of magnetic interactions in the CuO_2 planes and of their modifications in the presence of holes introduced by Sr doping and/or by excess oxygen. The introduction of doped holes in the CuO_2 plane is known to reduce drastically the Néel temperature $T_N \approx 320$ K of the planar Heisenberg antiferromagnet (AF) La_2CuO_4, whereby T_N decreases to 0 K by $x \approx 0.02$ [Johnston, 1991]. Throughout the low doping regime, $x < 0.08$, a rich phenomenology is observed below ~ 20 K in ^{139}La NQR relaxation rate [Cho, 1992][Watanabe, 1990], μSR [Harshman, 1988], neutron scattering [Sternlieb, 1990] and magnetic susceptibility $\chi(T)$ measurements [Filipkowski, 1990], which have been attributed to a low temperature magnetic phase similar to a spin-glass. In the "spin-glass regime" $0.02 \leq x \leq 0.08$, Cho et al. have recently inferred from ^{139}La NQR data that this phase is an unconventional cluster-spin-glass [Cho, 1992]. In the AF regime $0 \leq x \leq 0.02$, on the other hand, the origin of these anomalies below T_N is obscure, although similarities in behavior to so-called re-entrant spin-glass systems have been noted [Harshman, 1988][Aharony, 1988].

4.2. Theoretical Background of ^{139}La NQR

4.2.1. Hamiltonian and energy levels

The Hamiltonian of a ^{139}La nucleus in La_2CuO_4 (I = 7/2) in the principal axes system can be written as [Abragam, 1961]

$$H = H_Q + H_M = \frac{e^2qQ}{4I(2I-1)}[3I_Z^2 - I(I+1) + \frac{1}{2}\eta(I_+^2 + I_-^2)] - \gamma(\frac{h}{2\pi})\,\mathbf{H}\cdot\mathbf{I}, \qquad (4.1)$$

where the first term describes the nucleus with a quadrupole moment in an electrostatic crystal field and the second term is Zeeman splitting due to a weak internal magnetic field. The nuclear gyromagnetic ratio for ^{139}La is $\gamma_N/2\pi$ = 601.44 Hz/Gauss and Q is the quadrupole moment of La. The asymmetry factor η and the electric field gradient V_{ij} along the principal axes X, Y, Z are defined as [Abragam, 1961]

$$\eta = \frac{V_{XX} - V_{YY}}{V_{ZZ}}, \quad eq = V_{ZZ},$$

where

$$|V_{ZZ}| \geq |V_{XX}| \geq |V_{YY}|.$$

A schematic energy level diagram obtained by diagonalizing the Hamiltonian is shown in Fig. 4.1 [Nishihara, 1987]. The allowed transition rule is $\Delta m = \pm 1$ but it is relaxed at $|\pm 3/2\rangle \leftrightarrow |\pm 1/2\rangle$ transitions

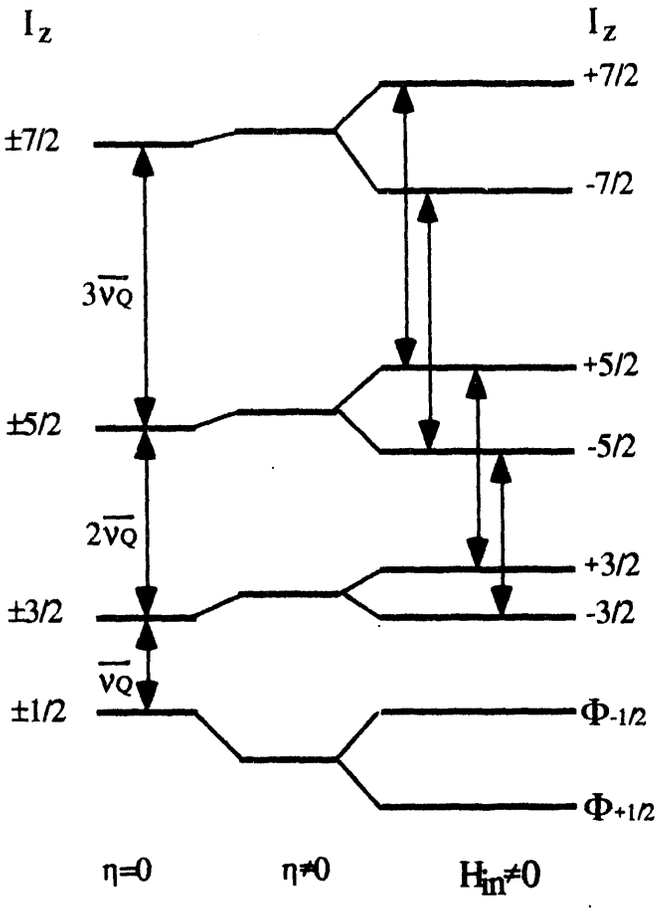

Fig. 4.1 A schematic energy level diagram obtained by diagonalizing the Hamiltonian shown in Eq. 4.1.[Nishihara, 1987]

due to the mixed states of $|\pm 1/2\rangle$, $\Phi_{\pm 1/2}$. The calculated NQR spectrum based on this energy level diagram agrees with the spin-echo spectrum of ^{139}La at 1.3 K very well, where the latter gives the fitted values [Nishihara, 1987]

$$\overline{\nu_Q} \equiv \frac{3e^2qQ}{2I(2I-1)h} = 6.38 \pm 0.02 \text{ (MHz)}$$

and

$$\eta = 0.01 \pm 0.01.$$

4.2.2. Internal magnetic field and its determination

The internal magnetic field can be estimated from a calculation of the dipole magnetic field generated at the ^{139}La site by neighboring Cu magnetic moments, which are antiferromagnetically ordered. Following the spin configuration [Vaknin, 1987] and the structure data obtained at 10 K from neutron diffraction [Jorgensen, 1987] and including the canted angle 0.17 ° out of the CuO_2 plane [Thio, 1988], the dipole field is calculated up to a radius 40 Å using La as the center. This calculation suggests the H_{dipole} is about ~ 2 ° out of the CuO_2 plane. A detailed calculation of the EFG tensor from Ref. [Doroshev, 1990][Nishihara, 1987] suggests that the principal axis Z (also X) is tilted from the b-axis by 7-9°. The complete angle correlation is shown in Fig. 4.2. The angle between the Z-axis and H_{dipole} is α ~ 79-81°. The calculated dipole sum

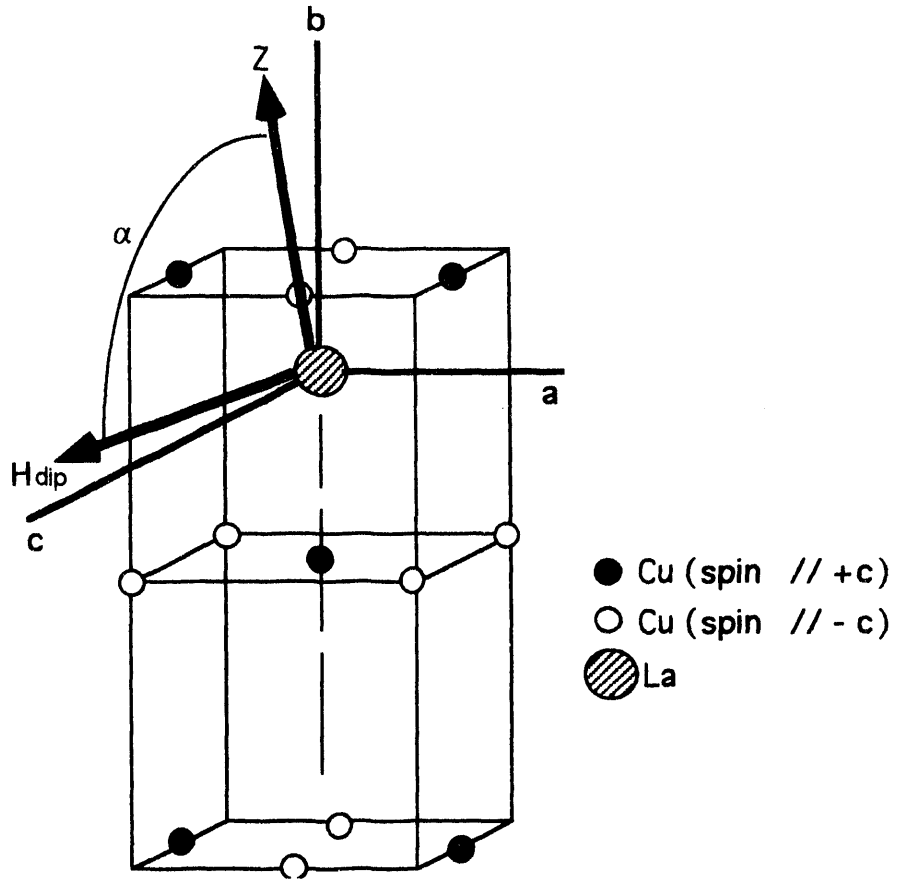

Fig. 4.2 Spin structure of La_2CuO_4 with orientations of dipole field H_{dipole}, principal axis Z and the orthorhombic structure axes.

within a distance of 40 Å leads to values

$$H_{dipole} = \sum_i \frac{3n_i(n_i \cdot m_i) - m_i}{r_i^3} = 0\ \mathbf{a} + 924\ \mathbf{c} + 38\ \mathbf{b}\ \text{(Gauss)},$$

where the orthorhombic b-axis is perpendicular to the CuO_2 plane. The calculated dipole field is ~925 Gauss when the Cu^{2+} moment is assumed to be 1 μ_B. However, the theoretical prediction of the copper magnetic moment in the quantum spin 1/2 2D Heisenburg model is about 0.62 μ_B [Johnston, 1991] and is about 0.5 μ_B at low temperature according to neutron diffraction results [Vaknin, 1987]. Thus the estimated H_{dipole} value can only account for about half of the observed internal field H_{int} ~ 1kG [Nishihara, 1987]. Superhyperfine interactions among La, Cu and O may generate hyperfine field at La site, which may contribute to the internal field also. [Takahashi, 1991].

The asymmetry term $\frac{1}{2}\eta\,(I_+^2+I_-^2)$ in the Hamiltonian is unable to lift the two-fold degeneracy of the eigenstates for half-integer spins [Abragam, 1961]. Meanwhile $m = I_z$ is still a good quantum number as long as η is small. The Zeeman term lifts the degeneracy, and the internal magnetic field parallel to the Z-axis of the EFG (H_Z) causes a split spectrum from two $\pm m \leftrightarrow \pm(m-1)$ transitions as

$$\Delta\nu = 2\,(\gamma_N/2\pi)\,H_Z. \qquad (4.2)$$

Note that the deduced H_Z is the Z component of H_{int}, where $H_Z = H_{int} \cos\alpha$. From the measured $\Delta\nu$ of a split spin-echo spectrum we can determine the internal magnetic field at the La site using equation 4.2.

4.2.3. Nuclear spin relaxation time and its determination

From a classical treatment, we can view the magnetic field, H_0, as causing a free spin to precess about the field at the Larmor frequency $\omega_0 = \gamma H_0$ as shown in Fig. 4.3(a), which depends on the quantized I_Z. We can use a small rf field H_1 perpendicular to H_0 such that in the Larmor rotating frame the magnetization will rotate about H_1 as shown in Fig. 4.3(b), which indicates an energy absorption. The application of rf H_1 can be viewed as a perturbation that induces transitions between energy levels. When the magnetization is not in thermal equilibrium, it will approach equilibrium in a relaxation process described by two time constants T_1 and T_2. T_1 describes spin-lattice relaxation that characterizes the flow of energy between the spin system and its surroundings (lattice) [Ailion, 1983]. T_2 describes spin-spin relaxation that does not involve net energy flow but an exchange of energy between different parts of the spin system. The combined effects of the rf H_1 and relaxation times T_1 and T_2 can be described by the Bloch equations, which are solved for the power absorption from the rf H_1 [Kittel, 1981].

When the rf H_1 is turned on for a time τ such that $\gamma H_1 \tau$ is 90°, we call this perturbation a $\pi/2$ pulse and similarly a π pulse for a 180° perturbation. There are two kinds of relaxation mechanism after a $\pi/2$

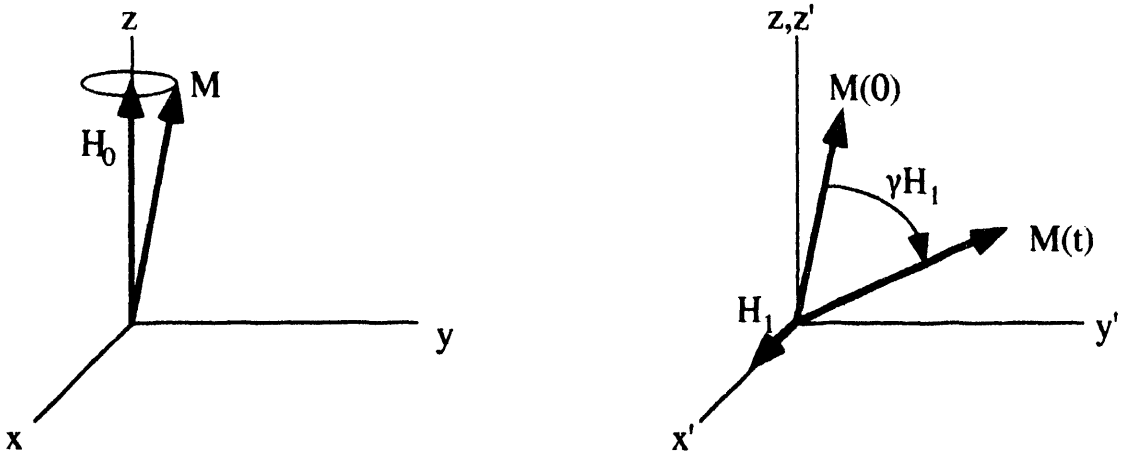

(a) Laboratory frame

(b) Larmor rotating frame

Fig. 4.3 (a) The magnetic field, H_0, causing a free spin to precess about the field at the Larmor frequency $\omega_0 = \gamma H_0$ (b) A small rf field H_1 perpendicular to H_0 such that in the Larmor rotating frame the magnetization will rotate about H_1

pulse is applied to the system in the rotating frame: the T_1 relaxation mechanism is the tendency for the magnetization vector to return to the z-axis from the x'-y' plane and the T_2 mechanism is a tendency for the vectors of the individual nuclei to dephase with one another in the x'-y' plane. In general, $T_1 \geq T_2$ in solids. The T_2^* effect, a sum of the transverse relaxation plus the field inhomogeneity effects of spins, produces a spin "pancake" in the rotating frame shortly after the spin isochromats have dephased first but the individual spin isochromats have not dephased yet [Fukushima, 1981]. Hahn designed a $\pi/2$ - π pulse sequence to produce spin echoes that enable us to measure the intrinsic T_1 and T_2 without any field inhomogeneity effect [Hahn, 1950]. As shown in Fig. 4.4, the spins start to dephase after a $\pi/2$ pulse is applied along the x' axis at time t=0. A π pulse is applied some time τ later about the x' axis and then these spins rephase into a coherent spin echo at another τ later. We can measure T_2 and T_1 by tracing the time dependence of the spin echo, and the magnetization vector M(t) is deduced from the spin echo amplitude vs. τ.

4.2.4. Nuclear spin-lattice relaxation mechanism in La_2CuO_4

There are two major relaxation mechanisms of quadrupole and magnetic origin respectively. The quadrupole relaxation mechanism is related to the interaction of the ^{139}La nuclear quadrupole moment with the fluctuating electric field gradients (EFGs). An estimate of T_1 can be obtained by considering the EFG modulation due to the Jahn-Teller optical mode in which a La atom vibrates against the five neighboring oxygen

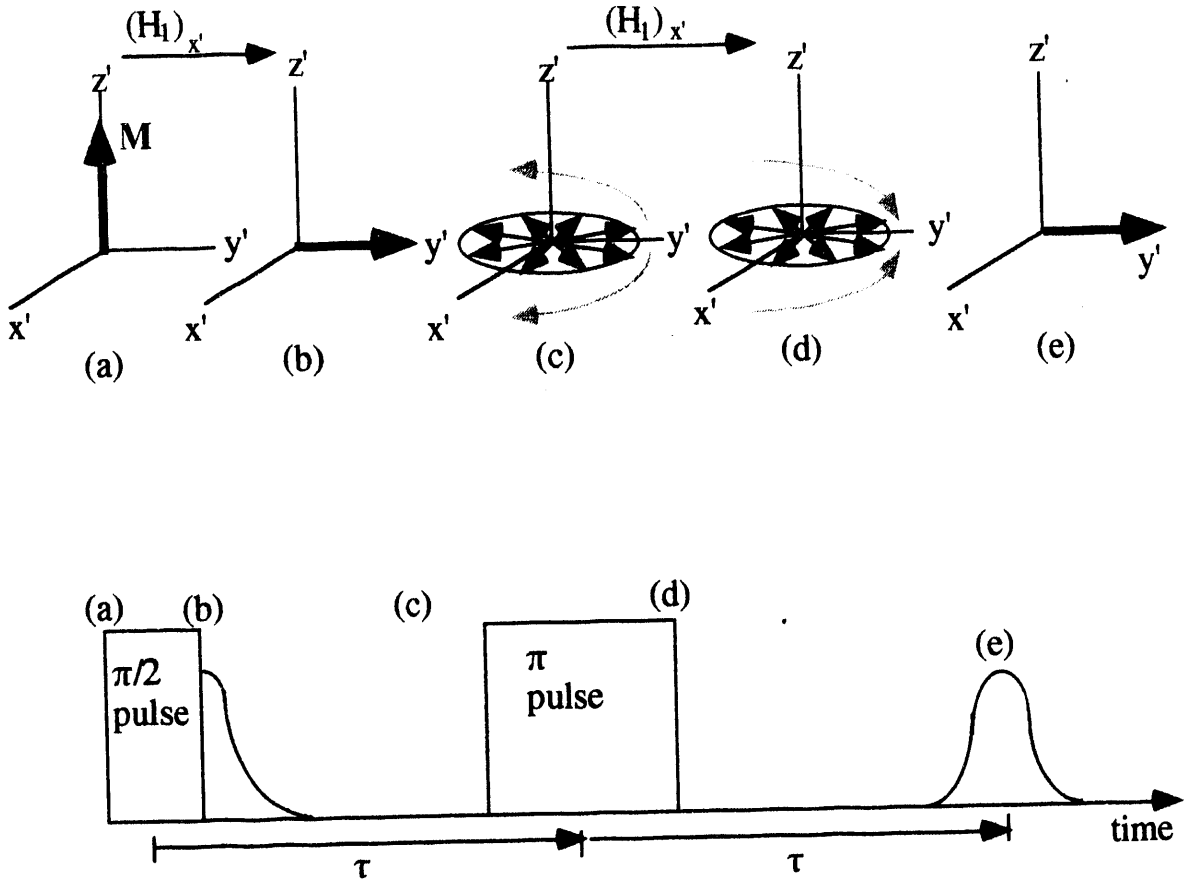

Fig. 4.4 A $\pi/2$ - π pulse sequence to produce spin echoes that enable us to measure the T_1 and T_2.

ions [Rigamonti, 1990]. One finds that the quadruple contribution to T_1^{-1} has T^2 temperature dependence and cannot be neglected for T > 200 K relative to the contribution to T_1 of magnetic origin [Borsa, 1989].

The magnetic contribution is due to the fluctuation in time of the local hyperfine field generated at the La site by the Cu^{2+} coupled localized magnetic moments [Borsa, 1989]. Below T_N, the Cu^{2+} spins are highly correlated and the hyperfine field comes from the antiferromagnetic ordering that dominates the relaxation process.

Other relaxation mechanisms have been proposed which may be dominant at different temperature regions and/or dopant concentrations. For example, the low temperature spin-lattice relaxation for $La_{2-x}Sr_xCuO_4$ ($0.02 \leq x \leq 0.08$) is proposed due to fluctuations of the staggered magnetization in locally ordered mesoscopic domains [Cho, 1992].

4.2.5. Nuclear spin-lattice relaxation rate and transition probability

The spin-lattice relaxation rate of ^{139}La is not a simple exponential form. Because the ^{139}La nucleus has angular momentum quantum number I = 7/2, this leads to unequally spaced energy levels as shown in Fig. 4.1. Since the unequally spaced energy levels inhibit the mutual spin flips necessary to establish a common spin temperature [Slichter, 1990], one has to solve the master equation to obtain a multiexponential recovery law. The master rate equation for ^{139}La is

$$\frac{dp_m}{dt} = \sum_{n=-7/2}^{7/2} (W_{mn}p_n - W_{nm}p_m),$$

where the p_m are defined to be the population of the energy level m and the W_{mn} are the transition probability per unit time [Abragam, 1961]. Based on the assumption that the magnetic relaxation mechanism is dominant, one can solve the master equation by taking into account the initial conditions from appropriate rf field disturbed populations. For the $3\nu_Q$ transitions ($\pm 7/2 \leftrightarrow \pm 5/2$) after a short ($\tau << R_1^{-1}$) saturating sequence, the solution of the master equation is

$$\frac{M(\infty)-M(t)}{M(\infty)} = \frac{11}{154}e^{-6W_M t} + \frac{115}{154}e^{-20W_M t} + \frac{28}{154}e^{-42W_M t}$$

where M(t) is the nuclear magnetization at time t after the saturating sequence and $M(\infty)$ is the magnetization after thermal equilibrium. If we use only the initial recovery, i.e. the tangent of $1-M(t)/M(\infty)$ at $t \rightarrow 0$, an effective single exponential $1/T_1 \approx 23W_M$ can be obtained. Similar calculation gives the effective $1/T_1 \approx 41W_M$ for the $2\nu_Q$ transition.[Rega, 1991]

4.3. **Experimental**

Sixteen samples of nominal composition $La_{2-x}Sr_xCuO_4$ were prepared by conventional solid state reaction at 1050° C using predried La_2O_3, $SrCO_3$, and CuO in x increments of 0.002 from x = 0 to 0.030.

For each x value, the sample was separated into two parts which were treated at 650° C for 5 h in 1 bar O_2 or N_2 respectively. The ^{139}La NQR measurements were performed at both the $3\nu_Q$ and $2\nu_Q$ transitions with a pulse Fourier Transform (FT) spectrometer ($\nu_Q \approx 6$ MHz). Line shapes and line widths were determined either by direct FT of half of the echo or by plotting the integrated echo intensity as a function of the resonance frequency. The nuclear spin-lattice relaxation rate (NSLR), R_1, was measured from the initial recovery of the nuclear magnetization M(t) after a short ($\tau << R_1^{-1}$) saturating sequence. For a magnetic relaxation mechanism described by a relaxation transition probability W, one has $R_1 \approx 23$ W for the $3\nu_Q$ line and $R_1 \approx 41$ W for the $2\nu_Q$ line [Borsa, 1989].

4.4 **Experimental Results and Data Analysis**

4.4.1. ^{139}La NQR spin-lattice and spin-spin relaxation rates

The spin-lattice relaxation rate (NSLR) R_1 of oxygen annealed $La_{2-x}Sr_xCuO_4$ (x = 0.014, 0.016, 0.018) have been measured in the temperature range from 4 to 250 K using the $3\nu_Q$ ($\pm$ 7/2 $\leftrightarrow$ $\pm$ 5/2) transitions as shown in Fig. 4.5. The resonance frequency is around ~19 MHz.

The NSLR (R_1) data exhibit a weak peak associated with the AF ordering at the same T_N as obtained from $\chi(T)$ results. Based on the T_N's obtained from $\chi(T)$ measurements [Cho, 1993], which are indicated by arrows in Fig. 4.5, the anomalies observed between 100 K to 200 K

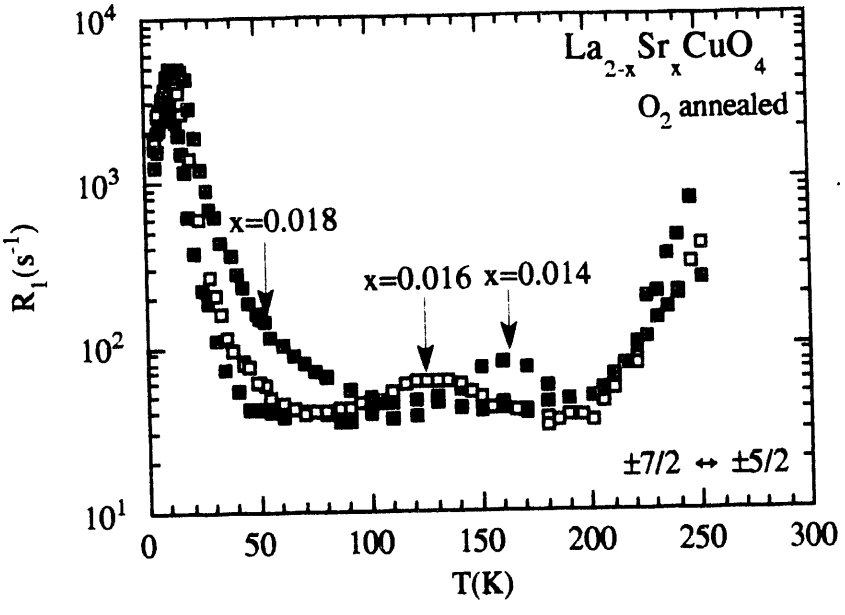

Fig. 4.5 The spin-lattice relaxation rate R_1 of oxygen annealed $La_{2-x}Sr_xCuO_4$ (x = 0.014, 0.016, 0.018) in the temperature range from 4 to 250 K using $3\nu_Q$ (± 7/2 ↔ ± 5/2) transitions.

for x=0.014 and x=0.016 must correspond to antiferromagnetic transitions. The clear difference of R_1 around 50 K between x=0.018 and the other two samples in Fig. 4.5 suggests that the peak expected at T_N ~ 53 K for x=0.018 is dominated by an additional higher relaxation rate. The spin-spin relaxation rate for x=0.016 is shown in Fig. 4.6. Basically the shorter T_2 shows similar behavior like that of T_1 except there is a step like anomaly at T_N. The M(t) of T_2 decays change from a Gaussian type at high temperature to a $\sqrt{t}$ exponential type decay below T ~ 35 K.

There is a drastic increase of relaxation rate above 200 K for all three oxygen annealed samples as shown in Fig. 4.5. The similar enhancement of $1/T_1$ in this region has been observed in La_2CuO_4 before and was assigned to originate from the mobility of excess oxygen [Ziolo, 1988]. In order to clarify the effect of excess oxygen on the relaxation mechanism in the range of T > 200 K, additional T_1 measurements on N_2 annealed $La_{1.984}Sr_{0.016}CuO_4$ was performed and the results are shown in Fig. 4.6. In contrast to the significant increase of R_1 above 200 K in the O_2 annealed sample, the N_2 annealed sample shows an almost temperature independent relaxation rate up to 300 K. The excess oxygen in O_2 annealed La_2CuO_4 is evidently responsible for the anomalous relaxation above 200 K.

A large enhancement of R_1 develops below ~ 70 K and reaches a maximum around 10 K for all $0.014 \leq x \leq 0.018$ as shown in Fig. 4.7. Similar relaxation behavior for $0.02 \leq x \leq 0.08$ in this temperature range has been observed before [Cho, 1992]. Instead of using the initial

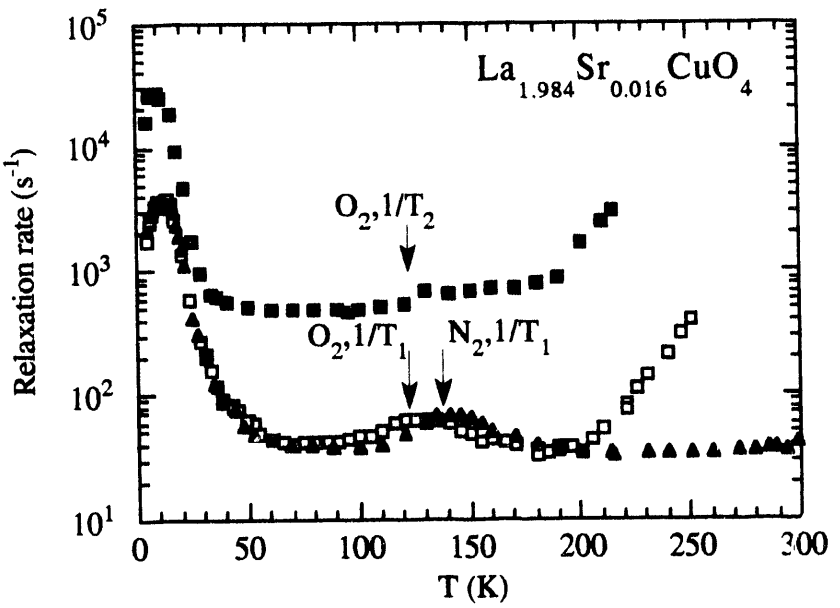

Fig. 4.6 Spin-spin relaxation rate ($1/T_2$) for O_2 annealed $La_{1.984}Sr_{0.016}CuO_4$ and $1/T_1$ for N_2 annealed $La_{1.984}Sr_{0.016}CuO_4$.

tangent of 1-M(t)/M(∞) as an approximation to R_1 from the multiexponential recovery, as for the data analyzed above ~35 K, we found that an $\exp[-(t/T_1)^{1/2}]$ time dependence for the recovery gives a better fit for the whole recovery process below ~ 35 K. Fig. 4.8 shows a typical recovery behavior for x=0.018 at 4.2 K, versus $\sqrt{t}$. A similar $\sqrt{t}$ type of recovery has been observed for the x=0.03 sample at low temperatures also.

4.4.2. Spin-echo frequency spectrum

The ^{139}La NQR frequency spectrum has been measured in the temperature range from T = 1.5 K to T > T_N using the $2\nu_Q$ ($\pm$ 5/2 $\leftrightarrow$ $\pm$ 3/2) transitions. A typical frequency spectrum for x = 0.008 at T = 1.5 K obtained with point by point integrated echo intensity is shown in Fig. 4.9. Each frequency spectrum is fitted with the sum of two Gaussian functions which allows the frequency splitting ($\Delta\nu$) and the full width at half maximum (FWHM) of each doublet to be extracted. The frequency splitting is proportional to the internal field at the La site as

$$\Delta\nu = 2\,(\gamma_N/2\pi)\,H_Z,$$

where $\gamma_N/2\pi$ = 0.60144 kHz/Oe and H_Z is the component of the internal field parallel to the principal Z axis of the electric field gradient (EFG). The spectrum shapes for samples with x $\geq$ 0.02 are broad and almost unresolved as shown in Fig. 4.10. Since nonzero internal field has been

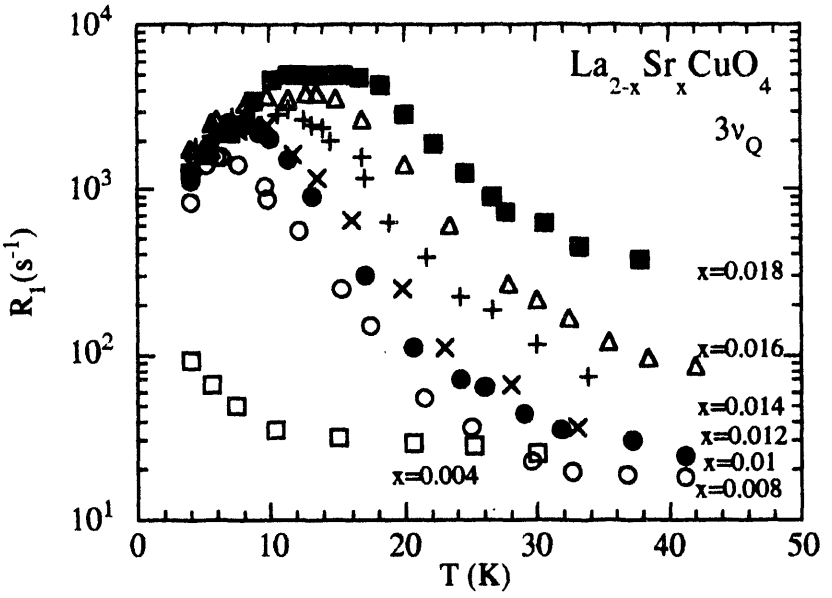

Fig. 4.7 NSLR for $La_{2-x}Sr_xCuO_4$ with $0.004 < x < 0.02$ at low temperature.

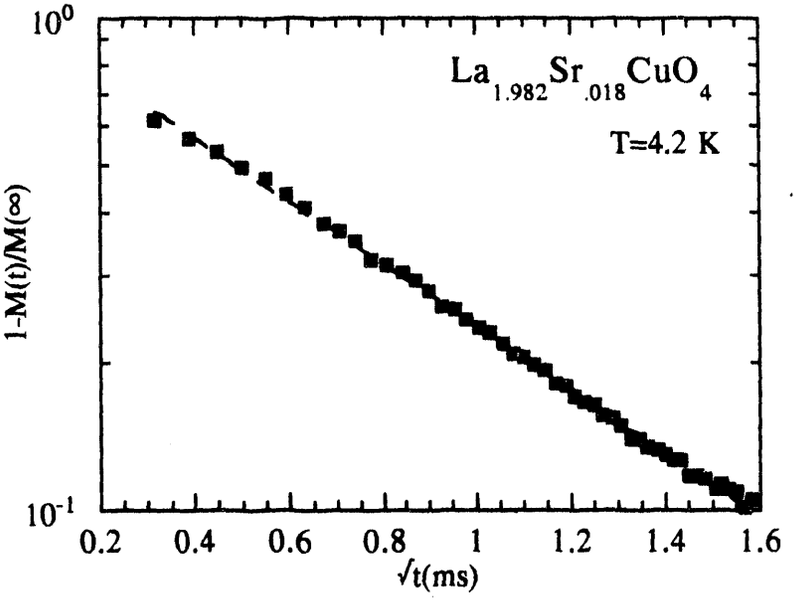

Fig. 4.8 A typical recovery behavior for x=0.018 at 4.2 K scaled in an $\exp[-(t/T_1)^{1/2}]$ form. T_1 = 0.46 ms

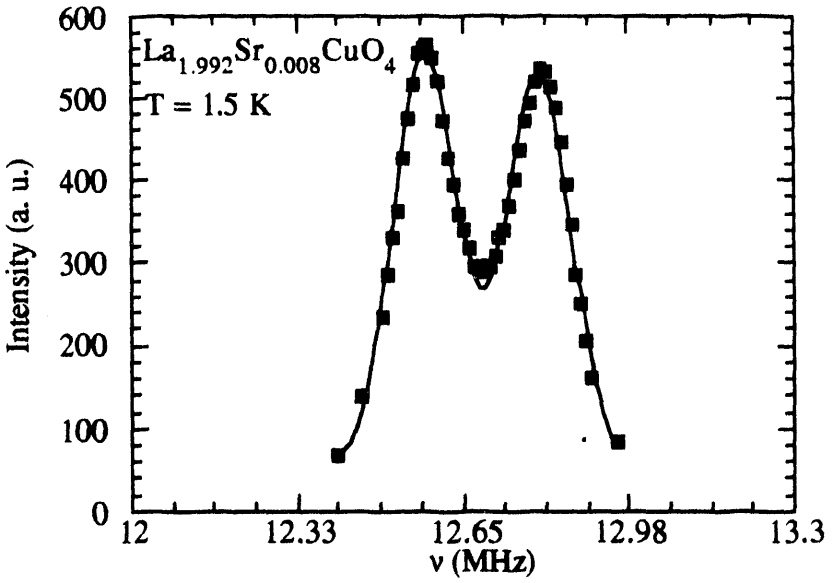

Fig. 4.9 A typical ± 5/2 ↔ ±3/2 transition (see Fig. 4.1) frequency spectrum of x = 0.008 at T = 1.5K obtained with point by point integrated echo intensity. The solid line is a two Gaussian fit with one common width.

observed for samples with x > 0.02 below SG transition temperatures [Rettori, 1993]. we may still fit the spectrum into two Gaussian functions for $T < T_g$.

The static NQR results for several of the $La_{2-x}Sr_xCuO_4$ samples are summarized in Fig. 4.11(a)-(d). From $\chi(T)$ data [Cho, 1993], T_N = 227, 209, 194, 164, 122 K for x = 0.008, 0.010, 0.012, 0.014, 0.016, respectively. Below T_N, the ^{139}La NQR splits into a doublet at frequencies ν_1 and ν_2 whose separation $\Delta\nu$ measures the component of the internal magnetic field parallel to the principal Z axis of the electric field gradient (EFG) tensor at the La site [Nishihara, 1987]. The $\nu_1+\nu_2$ corresponds to $4\nu_Q$ as a result of cancellation of the Zeeman term contributions. For x > 0 and T below ~ 30 K, the NQR resonance frequency shows an anomalous decrease and the NQR line width (FWHM) displays an anomalous increase. The line broadening is about 50 % more pronounced for the $3\nu_Q$ transition than for the $2\nu_Q$ transition, indicating a quadrupole rather then a magnetic broadening mechanism. There is a significant increase of $\Delta\nu$ below ~ 30 K for x > 0.00 as temperature decreases, which indicates an additional contribution to the internal field at the La site. Similar results on $La_{2-x}Ba_xCuO_4$ (x=0.012, 0.016) have been observed by Watanabe et al. [1990]. The solid lines shown in Fig. 4.11(d) are power law fits using the data above ~30 K, where $\Delta\nu(T)/\Delta\nu^{AF}(0) = (1-T/T_N)^{\beta}$ with $\beta = 0.41\pm0.02$, and the T_N values are from Ref. [Cho, 1993]. The details will be discussed in Sec. 4.5.6.

Figures 4.12 (a,b) show the line broadening (FWHM) and frequency splitting ($\Delta\nu$) for $0.00 \leq x \leq 0.03$ at T = 1.5K and 4.2K analyzed from the

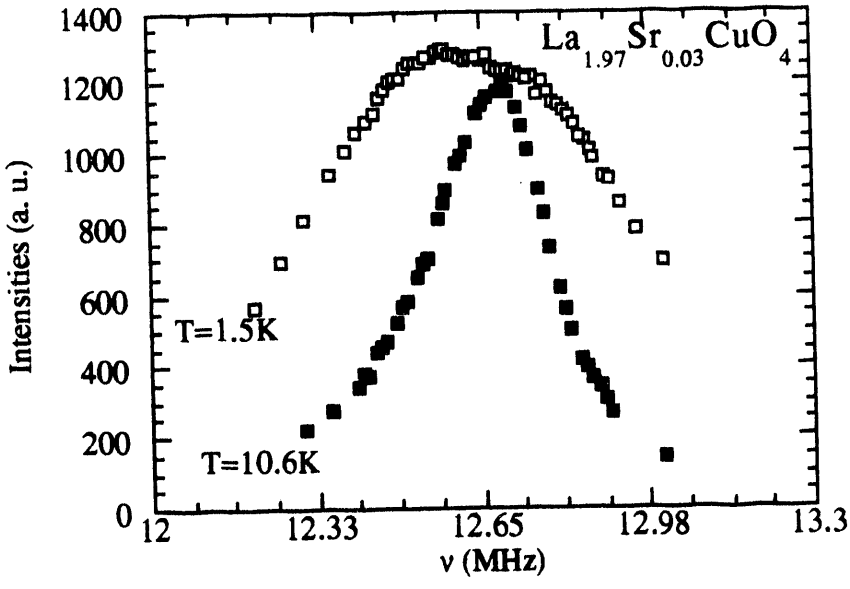

Fig. 4.10 The frequency spectrum for samples with x = 0.03. The T = 1.5 K data can be fitted with the sum of two Gaussians.

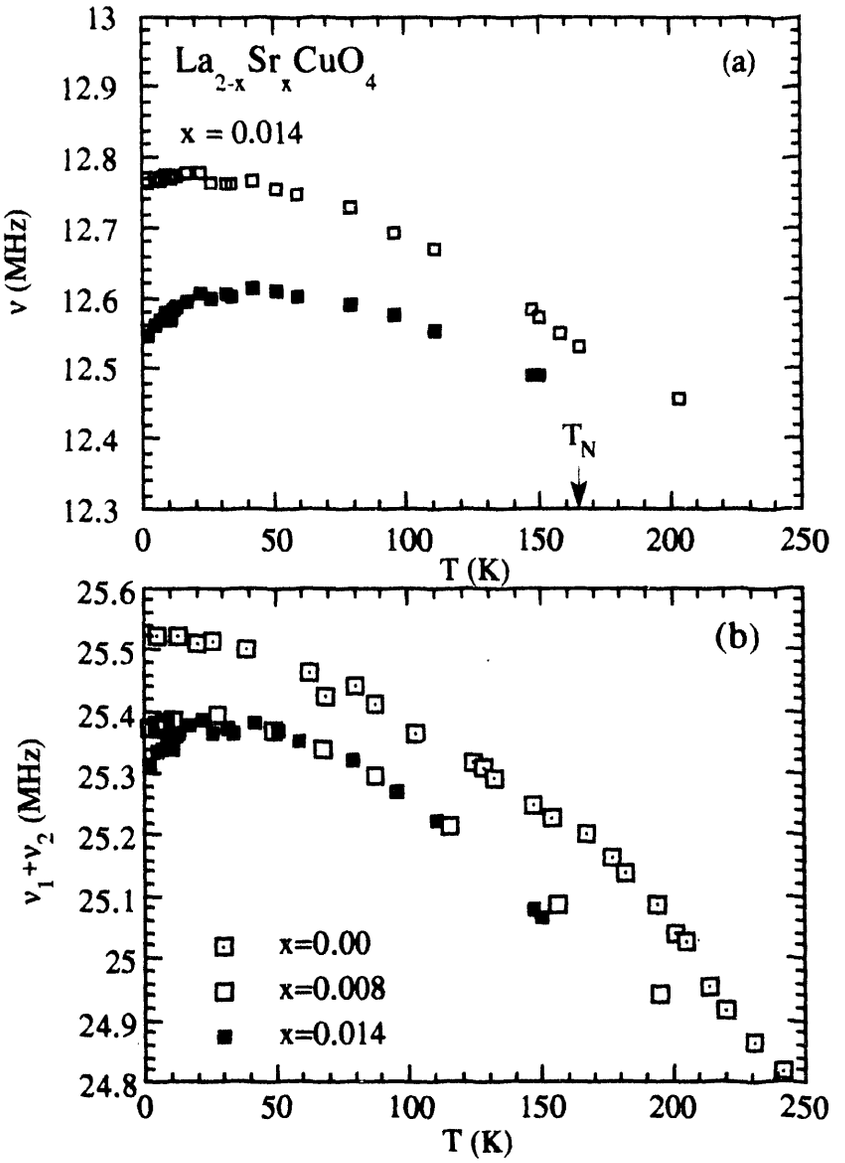

Fig. 4.11 The static NQR results for several of the $La_{2-x}Sr_xCuO_4$ samples, where (a) ν_1 and ν_2 are the peak frequencies analyzed from a two Gaussian fit like that in Fig. 4.9; (b) $\nu_1+\nu_2 \approx 4\nu_Q$.

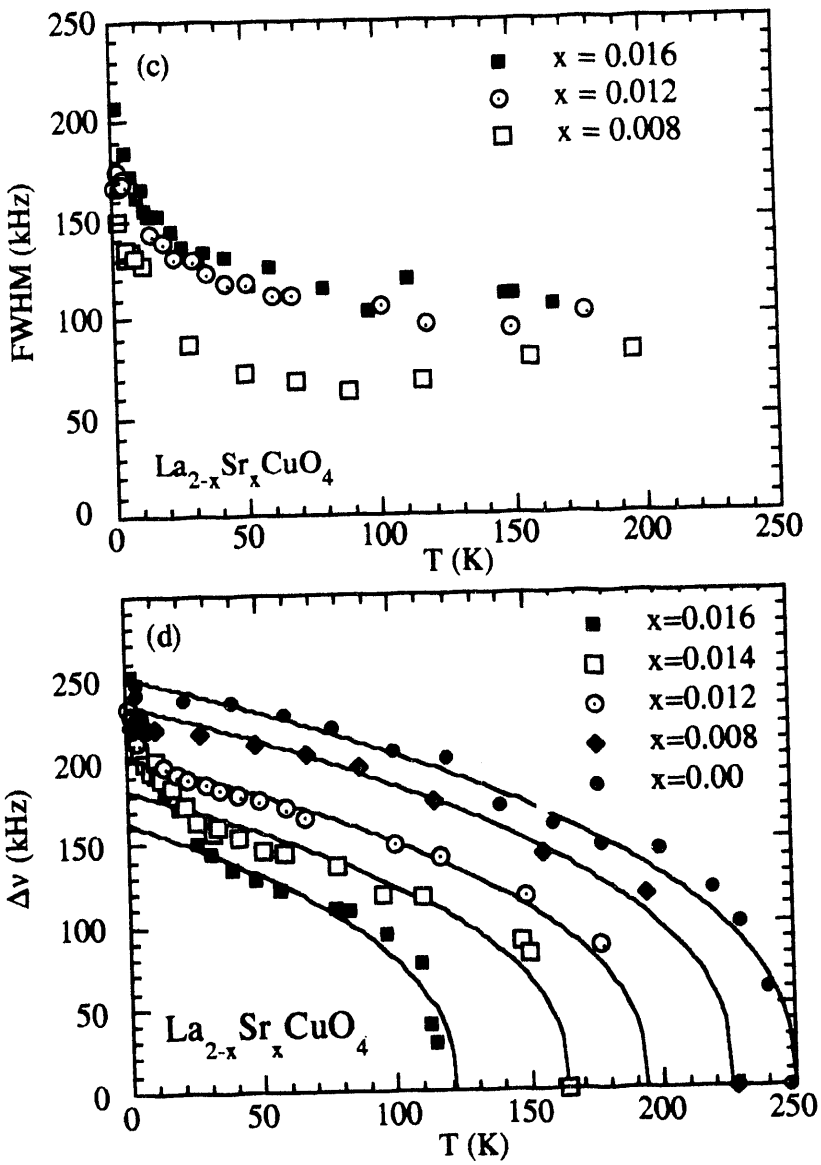

Fig. 4.11 (continued) where (c) FWHM is the peak width and (d) $\Delta\nu = \nu 2 - \nu 1$. The solid lines shown in (d) are power law fits of the expression $\Delta\nu(T)/\Delta\nu^{AF}(0) = (1-T/T_N)^{\beta}$ to the data, where $\beta = 0.41 \pm 0.02$ and only data above ~ 30 K were used in the fitting.

frequency spectra. There is a decreasing trend in $\Delta\nu$ as x increases from 0 to 0.014. Above x=0.016, a more significant increase in $\Delta\nu$ as x increases is observed at T = 1.5 K than at T = 4.2 K. On the other hand, the FWHM increases linearly with x all the way from x=0.00 to 0.03 at T = 1.5K. The linear dependence of FWHM can thus be identified as an inhomogeneous broadening of quadrupolar origin. If we interpret $\Delta\nu$ as the Z-axis (principal axis) component of the internal field at the La site, what we observed in $\Delta\nu(x)$ suggests two regions of different x dependence of internal field.

4.5. **Discussion**

4.5.1. Nuclear spin-lattice relaxation by Interstitial oxygen

The comparison of $1/T_1$ between O_2 and N_2 annealed $La_{1.984}Sr_{0.016}CuO_4$ shown in Fig. 4.7 revealed several oxygen related phenomena. The Néel temperature of the N_2 annealed sample is higher as expected and is consistent with the value obtained by $\chi(T)$, which is indicated by an arrow. The O_2 annealed sample shows a drastic increase of R_1 above ~ 200K, which is not seen in the N_2 annealed sample. The N_2 annealed sample is found to be very close to the stoichiometry ($\delta \approx 0$) and the O_2 annealed sample has only $\delta \approx 0.01$ excess oxygen per formula unit [Cho, 1993]. Macroscopic phase separation below ≈ 300 K due to the redistribution of excess oxygen is proposed in the O_2 annealed samples. It is conceivable that the mobile excess oxygen, as low as 0.01 per formula unit, provides a strong relaxation mechanism during macroscopic

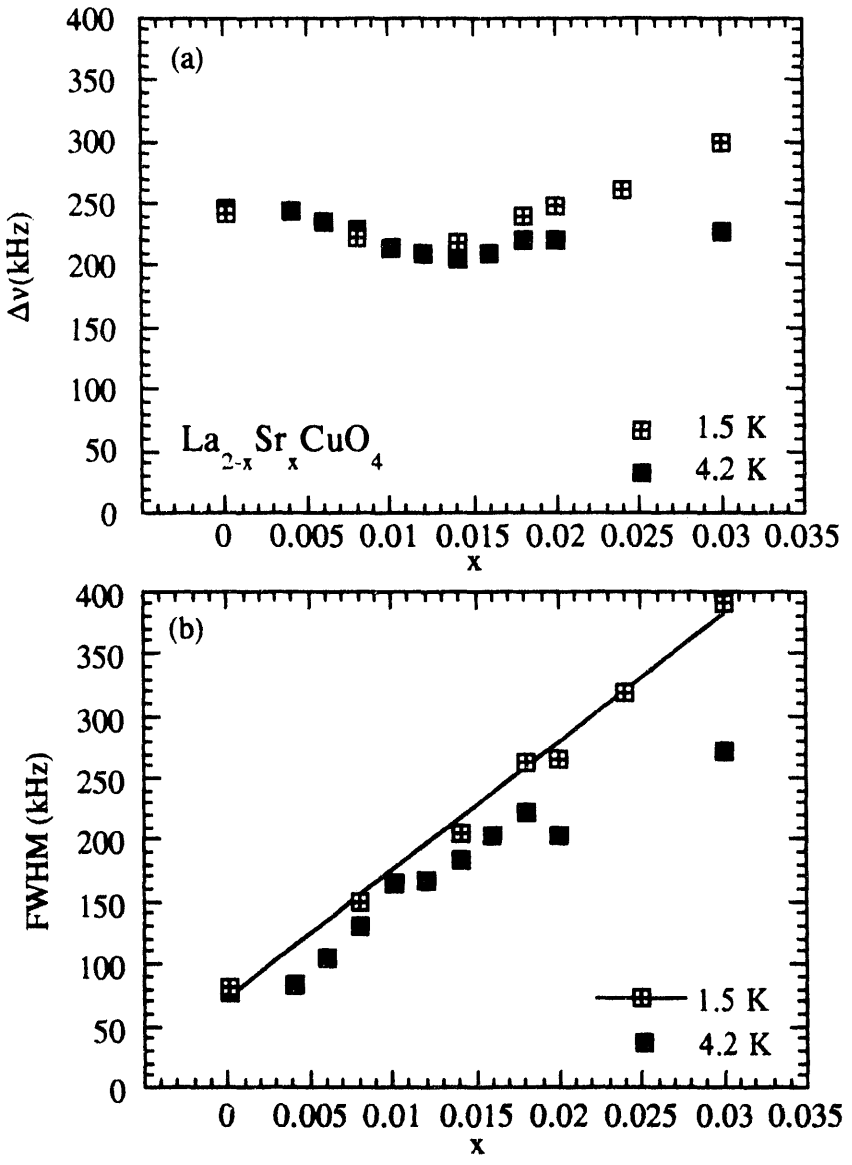

Fig. 4.12 (a) $\Delta\nu$ and (b) FWHM for samples with Sr doping level $0.00 \leq x \leq 0.03$ at T = 1.5K and 4.2K.

phase separation above 200 K. Ryder et al. have demonstrated that the interstitial oxygen is mobile down to 200 K as inferred from the resistivity hysteresis [Ryder, 1991]. On the other hand, the low temperature R_1 peak of these two samples are almost the same within our experiment resolution. The current observations suggest that the anomalous enhancement of R_1 at low T is related to the amount of Sr doping instead of the combined hole contribution from Sr and interstitial oxygen.

As $T \rightarrow T_N^+$, a divergent behavior corresponding to critical slowing down of the correlated spin dynamics is expected. Below T_N, the relaxation rate is expected to drop rapidly for magnetic ordering [Borsa, 1992]. The anomalies at T_N in Fig. 4.5 do not show such typical critical behavior as observed in the ^{35}Cl NMR of $Sr_2CuO_2Cl_2$ [Borsa, 1992], but are similar to that observed in pure La_2CuO_4 [Ziolo, 1988]. We believe the oxygen inhomogeneity and the finite size effect proposed by Cho et al. [1993] may be responsible for the smooth transformation at T_N without a critical behavior.

4.5.2. Anomalous ν_Q change at low T

The asymmetric decrease of the splitted ν_1 and ν_2 line below $T < 30$ K for $x=0.014$ as shown in Fig. 4.11(a) cannot be explained by pure internal field change or pure quadrupole frequency shift. We must explain the T dependence of the two NQR resonance frequencies in the doublet with both quadrupole frequency ν_Q down shift and an extra internal field contribution other than internal magnetic field of AF

origin. We can parametrize ν_1 and ν_2 as follows: $\nu_{1,2} = 2(\nu_Q - \Delta\nu_Q) \pm (\gamma_N/2\pi)(H + \Delta H)$, where the + and - signs refer to ν_1 and ν_2 respectively. $\gamma_N/2\pi$ = 601.44 Hz/Gauss is the nuclear gyromagnetic ratio, H is the Z component (EFG principal axis) of internal magnetic field at a La site due to AF ordering below T_N, and $\Delta\nu_Q$ and ΔH are respectively the changes in ν_Q and H below ~ 30K. The $\nu_1+\nu_2$ shown in Fig. 4.11(b) corresponds to $4\nu_Q$ and shows clearly that ν_Q decreases below ~ 30 K. On the other hand the $\nu_1-\nu_2 = \Delta\nu$ is proportional to H, which shows an increase of the internal field below ~ 30K as shown in Fig. 4.11(d).

The decrease of ν_Q occurs smoothly below about 30 K and is accompanied by an inhomogeneous quadrupole broadening of each of the two NQR lines in the doublet as shown in Fig. 4.11(b,c). Due to the effect of anharmonic lattice vibration on EFG, generally the resonance frequency decreases smoothly with increasing temperature [Borsa, 1975]. Perturbed-angular-correlation studies on undoped La_2CuO_4 have shown a smooth decrease of η with increasing temperature from 100 to 300 K [Saylor, 1989]. But the unusual decrease of ν_Q at temperature below ~ 30K with decreasing temperature cannot be assigned to the same origin. Similar behavior at low temperatures has been observed in Ba doped systems also [Kumagai, 1987]. Watanabe et al. have reported that for the lightly Ba doped sample, the η value decreases from ~ 0.04 at $T > T_N$ to ~ 0.01 at 1.3 K [Watanabe, 1990]. The reduction of η may be partially responsible for the ν_Q drop. However, the accompanying increase of FWHM in the same temperature region (see

Fig. 4.11(c)) cannot be simply explained by the η change only. We will address this issue in Sec. 4.5.4. further.

4.5.3. Chiral moment and effective spins

Herein we consider the enhancement of the internal magnetic field for x = 0.012-0.018 below ~ 30K. Clearly, the enhanced internal field of x = 0.012-0.018 below ~ 30 K must come from a magnetic ordering with a Z (principal axis) component magnetization. An anomalous increase of the internal field at low temperature has been observed in ferromagnetic AuFe (~ 16% at. Fe) from Mössbauer effect measurements [Lauer, 1982]. The authors interpreted that the anomalous increase of internal field comes from the development of a transverse spin component coexisting with the FM longitudinal magnetization. Similar enhancement of internal field for $La_{2-x}Sr_xCuO_4$ with x = 0.009 and 0.024 below ~ 20 K have been observed by EPR also [Rettori, 1993]. Gooding et al. have proposed that partially delocalized holes in the CuO_2 planes of AF ordered Cu spin system may form a novel spin state on the AF background, which can produce an effective spin out of the AF sublattice magnetization direction [Gooding, 1993]. Considering the effective spins of chiral moments, we can reasonably accept the observed anomalous increase of the internal field as chiral moment spins growing with more localized holes as T → 0 K. Preyer et al. have found that the magnetoresistance of $La_{1.98}Sr_{0.02}CuO_4$ is similar to that found in Kondo systems and spin

glasses, in which the conductance is limited by spin scattering, which supports the charge localization and its effective spins.[Preyer, 1991]

4.5.4. Charge localization

We propose that the decrease of ν_Q and the increase of $\Delta\nu$ and FWHM below ~ 30 K (see Fig. 4.11) can be explained consistently as a result of charge localization. We have estimated the change in the EFG associated with the localization of a hole on a plaquette comprising a square of four oxygen ions below the Sr^{2+} ion in a point charge approximation with 1/4 of a hole's charge per oxygen ion [Gooding, 1993]. The change, calculated for a ^{139}La nucleus next to the Sr^{2+} dopant, is found to be about 0.23% increase of V_{zz} when one takes average to the half inter dopant distance. This result cannot account for the down shift of ν_Q but could be responsible for the broadening of the NQR lines observed below 30 K as shown in Fig. 4.11(b-c) due to a distribution of EFG. The anomalous behaviors of the EFG and thus ν_Q reflected in Fig. 4.11(b-c) below ~ 30 K could arise from an onset below 30 K of a small incoherent or incommensurate (or long-range commensurate) modulation of the oxygen positions and/or from the localization [Chen, 1991] of the doped holes below this temperature. The only alternative explanation for the anomalous decrease of ν_Q at low temperature would be the occurrence of a structural phase transition, however no structural data support this assumption. In favor of charge localization is the gradual increase of the inhomogeneous quadrupole broadening at low T. The FWHM obtained at

1.5 and 4.2 K has a linear x dependence. Furthermore it is noted at T > 100 K, where the holes are not localized, FWHM depends little upon x. The resistivity of x = 0.02 has been observed to have a significant increase below ~ 50 K also.[Preyer, 1991]

The effect of charge localization on the internal field is shown in Fig. 4.11(d). The internal field of all doped samples approaches the value of undoped La_2CuO_4 as $T \rightarrow 0$ K as seen in Fig. 4.11(d). The internal field is reduced with increasing temperature from 0 to ~30 K, which may be interpreted by the delocalization of the holes with increasing temperature and thus lowering the effective spin of a chiral moment. These delocalized holes then aggregate into domain walls, a preferred microscopic phase separation at low doping [Cho, 1993], and then the sublattice magnetization $M_S(T)$ is determined by the thermal excitation of spin waves of AF ordering [Singh, 1990].

4.5.5. Spin freezing

We turn now to the experimental evidence for the freezing of the effective spin degree(s) of freedom of the doped holes. We emphasize that a study of the NQR line intensities vs. x and T showed that all or almost all of the La nuclei participate in the NSLR behaviors. The dependence $\ln[1-M(t)/M(\infty)] \propto \sqrt{t}$ observed below 30 K for both T_1 and T_2 implies a distribution of relaxation rates as expected in the presence of a distribution of localized relaxing centers with diffusionless relaxation of the ^{139}La nuclei to the impurities (no common spin temperature) [McHenry, 1972], where

$$M(\infty)-M(t) \propto \exp[-(t/T_1^*)^{1/2}] = \int_0^\infty \rho(T_1)\ \exp(-t/T_1)\ dT_1. \quad (4.3)$$

$T_1^* = \bar{T}_1/2$ and $R_1 = (T_1^*)^{-1}$ is the average NSLR and $\rho(T_1)$ is the distribution function of T_1 [Lindsey, 1980]. In order to relate $(T_1^*)^{-1}$ to the holes' concentration and spin dynamics, we follow the approach by McHenry et al. for NMR relaxation driven by dilute paramagnetic impurities [McHenry, 1972]. We assume that the relaxation transition probability W of a ^{139}La nucleus at a distance r from a localized hole's effective spin is given by the dipolar interaction: $23W(r) = (A/r^6)\ \tau$. Here, A is the dipolar coupling constant and τ is the autocorrelation time of the effective spin. For negligible nuclear-spin diffusion, the M(t) is an ensemble average over all possible hole spin configurations about a given nuclear site:

$$M(\infty) - M(t) \propto \langle \exp\{-t\ \textstyle\sum_j W(r_j)\}\rangle = \textstyle\prod_j \{(1-x) + x\ \exp[-t\ W(r_j)]\}, \quad (4.4)$$

where the contribution to the recovery is taken to be $\exp(-t\ W(r_j))$ if site r_j is occupied (with probability x) and unity if it is not occupied by a hole (probability 1-x). For $x << 1$ and $(A/r_o^6)\ \tau\ t >> 1$, where r_o is the minimum distance between a ^{139}La nucleus and a hole spin, one obtains a single exponential form from Eq. (4.4) as [McHenry, 1972]

$$M(\infty) - M(t) \propto \exp[-\sqrt{t}\ (4/3\ \pi^{3/2}\ N_o x\ \sqrt{(A\ \tau)}\ )], \quad (4.5)$$

where N_o is the number of available hole sites per unit volume. Comparing Eq.(4.3) and (4.5) one then finds

$$R_1 = (T_1^*)^{-1} \approx (4/3\ \pi^{3/2}\ N_o)^2 x^2\ A\ \tau. \qquad (4.6)$$

For $x << 1$, the correlation time τ, which depends on the interaction which couples the localized hole spins, scales as $\tau \propto x^{-1}$ [McHenry, 1972] and predicts $R_1 \propto x$ in Eq. (4.6). Indeed, the peak values of R_1 shown in Fig. 4.13 are linear in x.

In the presence of spin-freezing, one expects a slowing down of τ, leading to an enhancement of the NSLR at low temperature according to Eq. (4.6). Phase-transition theories predict $\tau \propto (T - T_f)^{-n}$, whereas non-equilibrium models predict an Arrhenius law, $\tau = \tau_o \exp(E/k_BT)$ [Chen, 1983]. The two predictions are compared with the data in Fig. 4.14. On the basis of the present data and fits in Fig. 4.14, where deviations from both behaviors occur when $T \rightarrow T_f^+$ as shown in both plots, we cannot distinguish whether a continuous freezing or a true phase transition occurs at T_f. In the Arrhenius case, the measured $T_f(x)$ could depend on the dynamical range of the probe used (MHz range for ^{139}La NQR), which would be consistent with the conclusions from μSR and neutron scattering results of Ref. [Sternlieb, 1990]. In either case, the phase transition or activated models for τ above, in order to account for the very fast NSLR at T_f, we infer that τ^{-1} reaches the MHz range. In the presence of a distribution of correlation times, one expects a broad and asymmetric maximum of $\ln(R_1)$ vs. $1/T$, as seen in Fig. 4.14, with the average

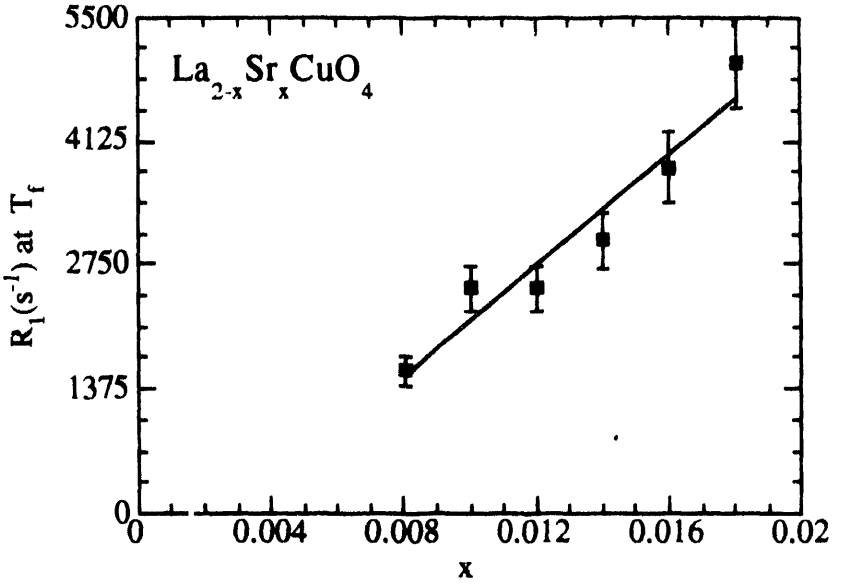

Fig. 4.13 The peak values of R_1 versus x for $La_{2-x}Sr_xCuO_4$ with $0.008 \leq x \leq 0.018$.. The solid line is a linear fitting.

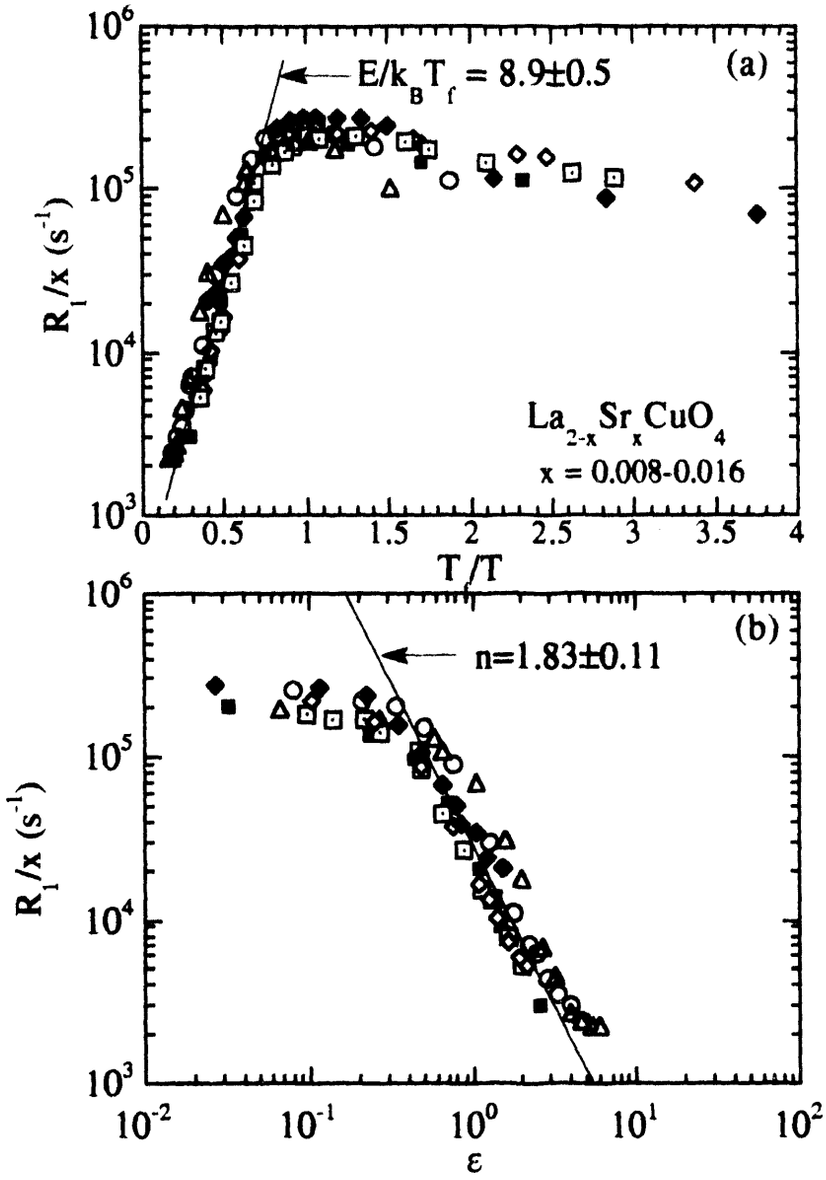

Fig. 4.14(a) A common behavior for R_1/x versus the inverse reduced temperature T_f/T, where T_f is the temperature of the R_1 peak for a given x. The straight line defines an activated behavior for τ with activation energy $E/k_BT_f = 8.9\pm0.5$. (b) The log-log plot is R_1/x vs. $\varepsilon = (T-T_f)/T_f$. The straight line corresponds to a critical behavior of τ with $n = 1.83\pm0.11$.

correlation time $\tau \approx \omega_Q^{-1}$ (ω_Q = nuclear quadrupole frequency) at the maximum [Chen, 1983]. This τ, the data in Fig. 4.5 and Eq. (4.6) yield $A \approx 10^{-31}$ $rad^2sec^{-2}cm^6$, which is of the order of magnitude expected for a dipolar interaction of a ^{139}La nucleus with a hole moment of about one Bohr magneton. This supports the validity of Eq. (4.6) and the assumptions leading to it, i.e. a dipolar fluctuation at the La site. Examination of Fig. 4.11(d) shows that this spin freezing has no clear influence on the effective internal magnetic field at the La site.

4.5.6. Internal field and sublattice magnetization

Samples with different T_N's show a similar $\Delta\nu(T)$ temperature dependence above ~ 30 K as shown in Fig. 4.11(d), . However, the samples with $x > 0.00$ display a gradual increase of $\Delta\nu$ with decreasing temperature below ~ 30 K which approach the same $T = 0$ value. Comparing with neutron diffraction results on single crystals of La_2CuO_4 with different T_N, the obtained sublattice moment $M_S(T)$ all show the same molecular mean field description of Brillouin function for spin 1/2 but no common $M_S(0)$ has been approached [Yamada, 1987]. For our samples of $0.008 < x < 0.02$, on the other hand, the $M_S(T)$ reduces almost linearly from a common saturated value at 0 K to ~ 10-35 K and then follow the same thermal contour like pure La_2CuO_4. We propose the initial decrease of H_{in} is from hole delocalization. When holes delocalize and move into the AF domain boundaries due to the microscopic phase separation mechanism [Cho, 1993], $M_S(T)$ restores to the thermal fluctuation of spin waves of AF ordering [Singh, 1990].

Although reentrant M_S was found according to the neutron diffraction study on a single crystal La_2CuO_4 with $T_N \approx 100$ K, that is, the diminution in M_S below 25 K is accompanied by the appearance of intense 2D $E \approx 0$ scattering, the reported crystal may have Li impurity of unknown effect [Endoh, 1988]. Besides, neutron scattering may face the cancellation effects from non uniformity of the spin order in the measured order parameter, which prevents the observation of reentrant behavior.

The temperature dependence of $M_S(T)$ for La_2CuO_4 has been interpreted in the context of thermal excitation of spin waves in a highly anisotropic antiferromagnet [Singh, 1990]. The solid lines in Fig. 4.11(d) are power law fits of $(1-T/T_N)^{\beta}$ for all samples with $\beta = 0.41\pm0.02$ with only data points above ~ 30 K used for the fitting. Using the extrapolated $\Delta\nu^{AF}(0)$ and T_N obtained from $\chi(T)$ measurement, a reduced form of sublattice magnetization verses temperature is shown in Fig. 4.15. It is clear that all samples collapse into one thermal contour for $T > 0.2\ T_N$ within our experimental error. We noticed also that the H_{in} decrease as $T \rightarrow T_N^-$ is drastic for samples with different T_N. MacLaughlin et al. [1993] have shown from NQR study that the AF transition for La_2CuO_4 is strongly discontinuous and indicative of a first-order transition.

Fig. 4.16 shows that the extrapolated $\Delta\nu^{AF}(0)$ values versus T_N, which are obtained from a power law fitting using data above ~ 30 K as described in Fig. 4.11(d). If we interpret the $\Delta\nu^{AF}(0)$ is proportional to the ordered moment $\langle\mu\rangle(0)$ in the AF state, the linear dependence $\langle\mu\rangle(0)$ verses

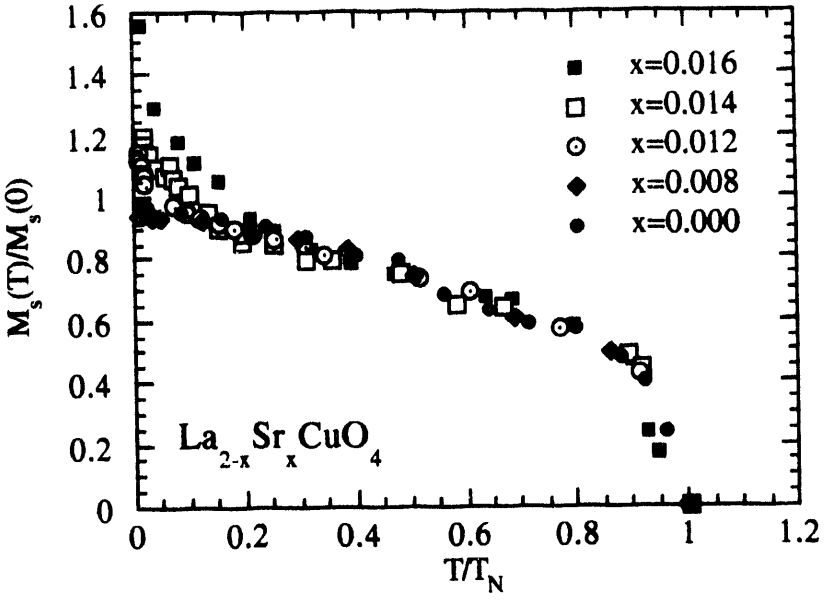

Fig. 4.15 A reduced form of sublattice magnetization verses temperature for $La_{2-x}Sr_xCuO_4$ with $0.00 \leq x \leq 0.016$, where $\Delta\nu^{AF}(0)$ are obtained from values in a power law fitting above ~ 30 K as described in Fig. 4.11(d).

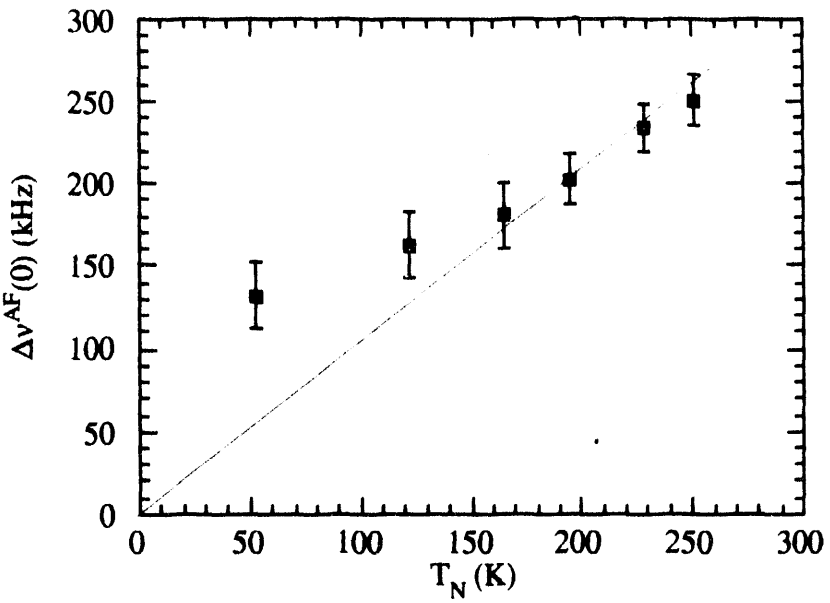

Fig. 4.16 The $\Delta\nu^{AF}(0)$, extrapolated from data above ~ 30 K as shown in Fig. 4.11(d), versus T_N.

T_N is good only above ~ 150 K but with larger deviation at lower T_N, which is consistent with the results obtained by neutron diffraction on a series of $La_2CuO_{4-\delta}$ with different T_N's [Yamada, 1987]. A scattered linear relation between $<\mu>(0)$ and T_N has been obtained by magnetic neutron diffraction [Johnston, 1991]. However, it was found that $<\mu>(0)$ is nearly independent of T_N for $La_2CuO_{4+\delta}$ for $100 \leq T_N \leq 250$ K from μSR measurement [Uemura, 1988], which is opposite to the neutron results [Yamada, 1987]. The difference can be resolved from the different probing character of neutron diffraction and μSR, the former is based on the volume average and the latter is a local probe. Since the NQR is also a local probe, our data shown in Fig. 4.11(d) and 4.16 suggests the detected long range ordered AF moment below ~ 30 K is masked by the contribution from ordered chiral moments due to charge localization. Therefore the NQR measured $<\mu>(0)$ is nearly independent of T_N as indicated in Fig. 4.11(d) but the extrapolated $<\mu>(0)$ from AF ordering is linearly dependent of T_N.

With the derived $<\mu>(0)$ and $T_N(x)$ correlations, we can also explain the gradual decrease of $\Delta\nu(x)$ at 1.5 K as shown in Fig. 4.12(a). If the role of Sr doping is changing from the AF state to the PM state background, the expected boundary should be around $x = 0.02$. However there is a broad minimum observed around $x \sim 0.01$-0.014 instead. Subtracting the fitted values of the expected $\Delta\nu^{AF}(0K)$ (see Fig. 4.11(d)) from the measured $\Delta\nu(1.5$ K)(see Fig. 4.12(a)), the approximate excess $\delta\nu(0K, x < 0.02)$ are obtained and shown in Fig. 4.17. It is clear that the excess $\delta\nu(0)$ is greatly enhanced above $x \sim 0.008$ and increases with x up to $x = 0.018$. Since the

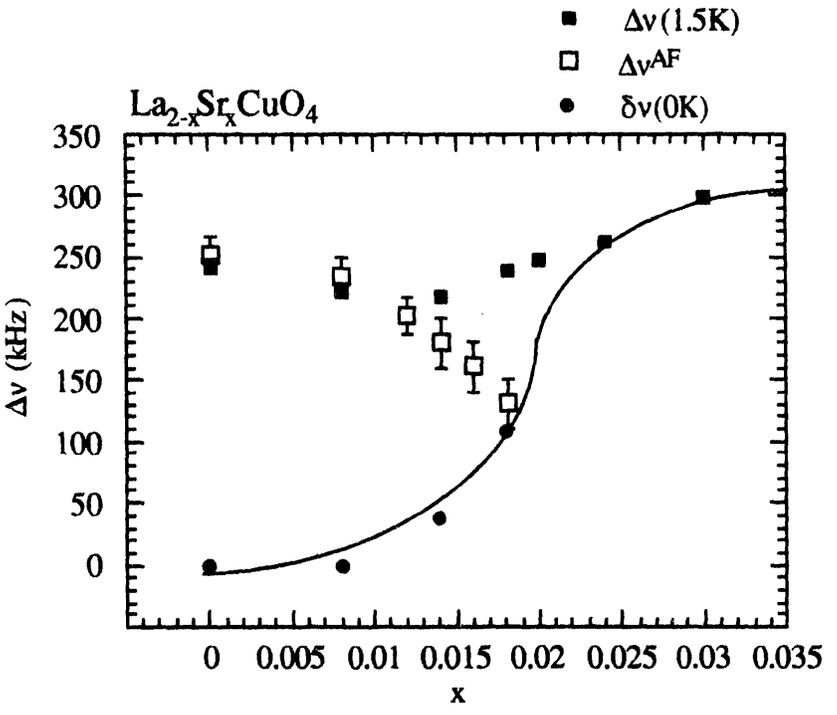

Fig. 4.17 The approximate excess $\delta\nu(0)$ are obtained by subtracting the fitted values of the expected $\Delta\nu^{AF}(0)$ (see Fig. 4.11(d)) from the measured $\Delta\nu(1.5\ K)$(see Fig. 4.13(a)). Solid line is guided for the eyes.

$\Delta\nu^{AF}(0)$ is expected to be zero for $x \geq 0.02$, we can assign the measured $\Delta\nu(1.5K, x \geq 0.02)$ to be solely from the chiral moment contribution. A clear smooth jump of $\delta\nu(0K, x < 0.02)$ to $\Delta\nu(1.5K, x \geq 0.02)$ is found at $x \sim 0.02$, which distinguishes the chiral moment contribution from two different types of magnetic background. It is conceivable that different ground states exist for the ordering chiral moments in the AF or PM background following Gooding's model [Gooding, 1993].

4.5.7. Domain structures

Previous analyses of ^{139}La NQR [Cho, 1992], $T_N(x)$ and $\chi(x,T)$ [Cho, 1993] data for $La_{2-x}Sr_xCuO_4$ ($0 \leq x \leq 0.08$) led to the conclusion that (mobile) doped holes condense into walls in the CuO_2 planes separating undoped domains of linear size $L \propto 1/x$ for $x \leq 0.02$ and $L \propto 1/\sqrt{x}$ for $x \geq 0.02$. L was identified as the zero temperature two-dimensional (2D) AF correlation length ξ_{2D} within the CuO_2 planes. For $x \leq 0.02$, we observe localization of the doped holes below $\approx$ 30 K; $L \propto 1/x$ may crossover to $L \propto 1/\sqrt{x}$ as the holes localize with decreasing T if they redistribute themselves statistically below 30 K. These localized holes should choose the near Sr sites in order to minimize the coulomb repulsion.

4.5.8. Magnetic phase diagram

By combining the present with the previous results [Cho, 1992][Cho, 1993], a detailed magnetic phase diagram for lightly doped ($0 \leq x \leq 0.05$) $La_{2-x}Sr_xCuO_4$ was constructed and is shown in Fig. 4.18(a), where the

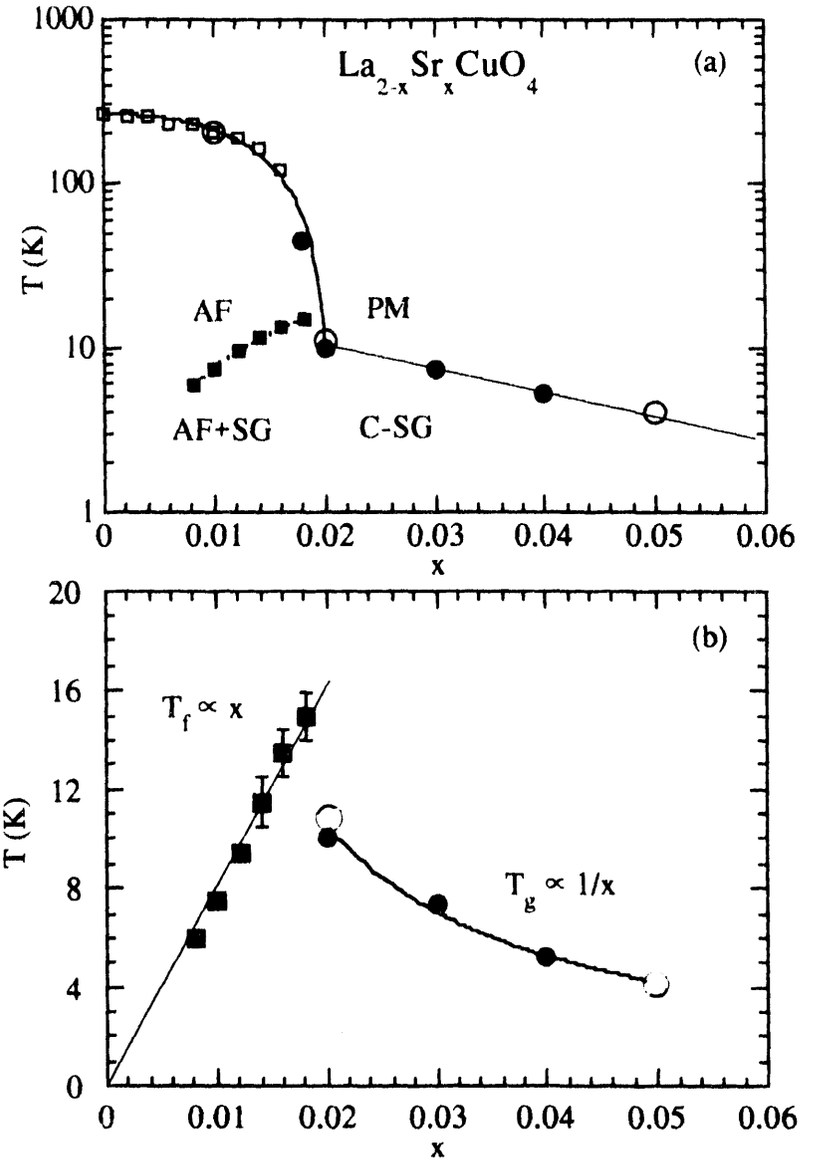

Fig. 4.18(a) The complete magnetic phase diagram of $La_{2-x}Sr_xCuO_4$ temperature T vs. composition x in the low doping region: the closed squares and circles are from NQR; the open squares are from susceptibility [Cho, 1993]; the open circles are from μSR [Harshman, 1988]. (b) x dependence of T_f and the 1/x dependence of T_g as discussed in the text, where data are fitted as T_f = 815x and T_g=0.21/x. C-SG = cluster SG.

spin glass freezing temperature for $x > 0.02$ is denoted by T_g. From Fig. 4.18, a distinct crossover at $x \approx 0.02$ occurs in the composition dependence of the freezing temperature: $T_f \propto x$ for $x < 0.02$, whereas $T_g \propto 1/x$ for $x > 0.02$. This novel behavior indicates that there is a crossover at $x = 0.02$ in the nature of the spin glass transition. According to the above discussion, for $x < 0.02$ the reentrant behavior below T_f should be viewed as the freezing of the spin degrees of freedom associated with the doped holes, superimposed on the pre-existing AF long range order. A similar phase diagram obtained by ^{139}La NQR has been introduced for $La_{2-x}Ba_xCuO_4$ before [Watanabe, 1990]. Our results provide a more detailed look at the phase diagram especially for the $x < 0.02$ range. Instead of three regions with a tricritical point at around $x = 0.02$ as postulated before [Filipkowski, 1990], we can distinguish four regions with different magnetic characteristics as shown in Fig. 4.18(b). Ivanov et al. treat impurities which generate local random strain as fluctuation to the magnetic anisotropy of the CuO_2 planes and has shown that the spin-freezing temperature increases linearly with impurity level x [Ivanov, 1992]. Gooding et al. have obtained a similar linear T_f-x relation based on the excitation of ordered chiral moments in the AF spin texture [Gooding, 1993].

For $x > 0.02$, on the other hand, the system undergoes a collective phase transition from a paramagnetic state, with 2D dynamical correlation in undoped mesoscopic size domains of size $L \propto 1/\sqrt{x}$, to a cluster-spin-glass (C-SG) phase in which these domains freeze due to

their mutual interaction; a static internal magnetic field occurs only below T_g [Cho, 1992]. Thus, $x \approx 0.02$ should be viewed as the composition above which no static AF order can be established independently within each individual domain. By using the molecular field approximation result, $T_N \approx J'(\xi_{2D}/a)^2$, where J' is the CuO_2 interplane coupling and a is the intraplane Cu-Cu distance, one expects $T_g \propto L^2 \propto 1/x$ for a system where ξ_{2D} is limited to a finite size L; from the data in Fig. 4.18, J' is found to be ~ 0.2 K. Whether there is a phase boundary between AF+SG and C-SG is unclear for now. The gradual decrease of $\Delta\nu^{AF}(0)$ as shown in Fig. 4.16 suggests the AF ordered moment decreases as $x \rightarrow 0.02$. A real phase boundary is hard to draw with gradually reduced ordered moments, although there seems a jump at x ~ 0.02 of effective internal field from chiral moment contribution as analyzed in Fig. 4.17.

4.5.9. Indirect exchange interaction

As noted above and shown in Fig. 4.18, T_f is proportional to x with a large slope: $T_f = (815\ K)x$. In Fig. 4.18, there is no discernible threshold in x for spin freezing, in contrast to the usual case where a percolation threshold must first be exceeded. This indicates that the effective interaction between the effective doped hole spins is of long range and that the mean field theory should be applicable, consistent with $T_f \propto x$. Considering the interaction energy in the Heisenberg model, the energy of interaction is

$$U = -2 J S_i \cdot S_j,$$

where J is the nearest-neighbor coupling constant. Defining z as the number of the nearest neighbor sites, the mean field theory result for T_f is [Kittel, 1981]

$$k_B T_f = \frac{2}{3} S(S+1) J z x. \qquad (4.7)$$

The (dilute) Sr doping level x is naturally introduced into Equation (4.7) by noting that the probability to have z n.n. sites occupied is proportional to Sr concentration x. The slope $T_f / x = 815$ K is comparable to the AF exchange interaction between adjacent Cu atoms in the CuO_2 planes (~1500 K), suggesting that the doped hole spin interaction is indirect and mediated by the AF Cu spin system. Indeed, recent microscopic theory predicts that localized holes couple to each other via a long range perturbation introduced in the AF background, leading to freezing of the hole's effective spin with $T_f \propto x$; the predicted T_f values are close to our observed ones [Gooding, 1993]. In Ref. [Gooding, 1993], the spin degrees of freedom associated with the doped holes are the transverse (out-of-plane) components of the Cu spins near the hole which are induced by the presence of the hole on a plaquette of four oxygen ions. In this case, the spin degrees of freedom associated with the doped holes are distinct from the (longitudinal) Cu^{+2} spin degree of freedom which orders below T_N. It is apparently

the localization of the doped holes below 30 K which allows for subsequent observation of their spin degrees of freedom below T_f.

4.6. Summary

In this Chapter, we report a detailed ^{139}La NQR investigation from 4 to 250 K in the AF regime ($0.008 \leq x \leq 0.020$) of $La_{2-x}Sr_xCuO_4$. The data demonstrate localization of the doped holes' charge below ~ 30 K, and constitute the first atomic scale probe of this localization of which we are aware. The hole delocalization with increasing T results in a pronounced decrease of the local magnetic field at the La site for x = 0.012-0.018, reflecting a decrease in the local staggered moment. We find that the spin degree(s) of freedom associated with the doped holes freeze below a temperature $T_f \approx (815\ x)$ K, corresponding to T_f = 16 K for x = 0.02. This spin freezing is superimposed on the background long-range AF order of the CuO_2 planes, and does not significantly affect the local internal field at the La sites. Finally, together with results from previous $\chi(T)$ data for $0 \leq x \leq 0.03$ and ^{139}La NQR data for $0.02 \leq x \leq 0.08$ of Cho et al., a detailed magnetic phase diagram is constructed for $0 \leq x \leq 0.05$. A crossover in the nature of the SG transition at $x \approx 0.02$ is clearly indicated by the totality of the data; an interpretation is given and discussed in the context of related theoretical predictions.

BIBLIOGRAPHY

Abragam, A., *Principles of Nuclear Magnetism* (Oxford, New York, 1961).

Aharony, A., R. J. Birgeneau, A. Conigilio, M. A. Kastner and H. E. Stanley, Phys. Rev. Lett. 60 (1988) 1330.

Ailion, D. C. and W. D. Ohlsen, in *Methods of Experimental Physics*, edited by J. N. Mundy, S. J. Rothman, M. J. Fluss and L. C. Smedskjaer, (Academic Press, Orlando, 1983) pp. 361.

Angerstein-Kozlowska, H., B . E. Conway and B. V. Tilak, Electroanal. Chem. Interfac. Electrochem. 43 (1973) 9.

Bachtler, M., W. J. Lorenz, W. Schindler and G. Saemann-Ischenko, Mod. Phys. Lett. B 2 (1988) 819.

Bean, C. P., Rev. Mod. Phys. 36 (1964) 31.

Bednorz, J. G. and K. A. Müller, Z. Phys. B 64 (1986) 189.

Beille, J., R. Cabanel, C. Chaillout, B. Chevalier, G. Demazeau, F. Deslandes, J. Etourneau, P. Lejay, C. Michel, J. Provost, B. Raveau, A. Sulpice, J. L. Tholence and R. Tournier, C. R. Acad. Sci. (Paris) 304 (1987) 1097.

Bennett, J. C., M. Olfert, G. A. Scholz and F. W. Boswell, Phys. Rev. B 44 (1991) 2727.

Bhat, V., C. N. R. Rao and J. M. Honig, Sol. Stat. Comm. 81 (1992) 751.

Birgeneau, R. J. and G. Shirane, in *Physical Properties of High Temperature Superconductors*, edited by D. M. Ginsberg, (World Scitific, Singapore, 1989) pp. 152.

Blunt, F. J., A. R. Perry, A. M. Campbell and R. S. Liu, Physica C 175 (1991) 539.

Bockris, J. O. and A. K. N. Reddy, *Modern Electrochemistry* (Plenum, New York, 1973).

Bockris, J. O. M. and D. M. Drazic, *Electrochemical Science* (Taylor & Francis, London, 1972).

Borsa, F., M. Corti, T. Goto, A. Rigamonti, D. C. Johnston and F. C. Chou, Phys. Rev. B 45 (1992) 5756.

Borsa, F., M. Corti, T. Rega and A. Rigamonti, Nuovo Cimento D 11 (1989) 1785.

Borsa, F. and A. Rigamonti, J. Mag. Res. 20 (1975) 232.

Borsa, F. and A. Rigamonti, in *Magnetic Resonance of Phase Transition*, edited by F. J. Owens, J. C. P. Poole and H. A. Farach, (Academic Press, New York, 1979) pp. 79.

Braunisch, W., N. Knauf, V. Kataev, S. Neuhausen, A. Grutz, A. Kock, B. Roden, D. Khomskii and D. Wohlleben, Phys. Rev. Lett. 68 (1992) 1908.

Bringley, J. F., S. S. Trail and B. A. Scott, J. Sol. St. Chem. 86 (1990) 310.

Cava, R. J., B. Batlogg, C. H. Chen, E. A. Rietman, S. M. Zahurak and D. Werder, Nature 329 (1987) 423.

Chaddah, P., K. V. Bhagwat and G. Ravikumar, Physica C 159 (1989) 570.

Chaillout, C., S. -W. Cheong, Z. Fisk, M. S. Lehmann, M. Marezio, B. Morosin and J. E. Schirber, Physica C 158 (1989) 183.

Chen, C. Y., R. J. Birgeneau, M. A. Kastner, N. W. Preyer and T. Thio, Phys. Rev. B 43 (1991) 392.

Chen, M. C. and C. P. Slichter, Phys. Rev. B 27 (1983) 278.

Cheong, S. -W., Z. Fisk, J. O. Willis, S. E. Brown, J. D. Thompson, J. P. Remeika, A. S. Cooper, R. M. Aikin, D. Schifer and G. Gruner, Sol. St. Comm. 65 (1988) 111.

Cheong, S. -W., J. D. Thompson and Z. Fisk, Physica C 158 (1989) 109.

Cho, J. H., F. Borsa, D. C. Johnston and D. R. Torgeson, Phys. Rev. B 46 (1992) 3179.

Cho, J. H., F. C. Chou and D. C. Johnston, Phys. Rev. Lett. 70 (1993) 222.

Chou, F. C., J. H. Cho and D. C. Johnston, Physica C 197 (1992) 303.

Chou, F. C., and D. C. Johnston, unpublished (1993)

Chou, F. C., J. H. Cho, D. C. Johnston, S. -W. Cheong and P. C. Canfield, unpublished (1993)

Coffey, T., K. S. Bedell and S. A. Trugman, Phys. Rev. B 42 (1990) 6509.

Dabrowski, B., D. G. Hinks, J. D. Jorgensen and D. R. Richards, Mat. Res. Soc. Proc. 156 (1989) 69.

Dabrowski, B., J. D. Jorgensen, D. G. Hinks, S. Pei, D. R. Richards, K. G. Vandervoort, G. W. Crabtree, H. B. Vanfleet and D. L. Decker, in *Superconductivity and Application*, edited by S. H Kwok et al, (Plenum Press, New York, 1990) pp. 379.

Dabrowski, B., J. D. Jorgensen, D. G. Hinks, S. Pei, D. R. Richards, H. B. Vanfleet and D. L. Decker, Physica C 162-164 (1989) 99.

Daeumling, M., J. M. Seuntjens and D. C. Larbalestier, Nature 346 (1990) 332.

de Gennes, P. G., *Superconductivity in Metals and Alloys* (W. A. Benjamin, New York, 1966).

Dinger, T. R., T. K. Worthington, W. J. Gallagher and R. L. Sandstrom, Phys. Rev. Lett. 58 (1987) 2687.

Doroshev, V. D. and M. M. Savosta, JETP Lett. 50 (1990) 363.

Dzyaloshinsky, I., J. Phys. Chem. Solids 4 (1958) 241.

Emery, V. J., S. A. Kivelson and H. Q. Lin, Phys. Rev. Lett. 64 (1990) 475.

Endoh, Y., K. Yamada, R. J. Birgeneau, D. R. Gabbe, H. P. Jensen, M. A. Kastner, C. J. Peters, P. J. Picone, T. R. Thurston, J. M. Tranquada, G. Shirane, Y. Hidaka, M. Oda, Y. Enomoto, M. Suzuki and T. Murakami, Phys. Rev. B 37 (1988) 7443.

Espinosa, A. M., M. T. S. Jose, M. L. Tascon, M. D. Vazquez and P. S. Batanero, Electrochimica Acta 36 (1991) 1561.

Falck, J. P., A. Levy, M. A. Kastner and R. J. Birgeneau, (1993)

Filipkowski, M. E., J. I. Budnick and Z. Tan, Physica C 167 (1990) 35.

Fukushima, E. and S. B. W. Roeder, *Experimental Pulse NMR: A Nuts and Bolts Approach* (Addison-Wesley, Reading, 1981).

Goodenough, J. B. and A. Manthiram, J. Solid State Chem. 88 (1990) 115.

Gooding, R. J., Phys. Rev. Lett. 66 (1991) 2266.

Gooding, R. J. and A. M ailhot, unpublished (1993)

Grande, B., H. Muller-Buschbaum and M. Schweizer, Z. Anorg. Allg. Chem. 428 (1977) 120.

Grant, P. M., S. S. P. Parkin, V. Y. Lee, E. M. Engler, M. L. Ramirez, J. E. Vazquez, G. Lim, R. D. Jacowitz and R. L. Greene, Phys. Rev. Lett. 58 (1987) 2482.

Grenier, J. -C., N. Lagueyte, A. Wattiaux, J. Doumerc, P. Dordor, J. Etourneau and M. Pouchard, Physica C 202 (1992) 209.

Grenier, J. -C., A. Wattiaux, N. Lagueyte, J. C. Park, E. Marquestaut, J. Etourneau and M. Pouchard, Physica C 173 (1991) 139.

Grenier, J. -C., A. Wattiaux and M. Pouchard, in *Phase Separation in Cuprate Superconductors*, edited by K. A. Muller and G. Benedek, (World Scitific, Singapore, 1992)

Grenier, J.-C., A. Wattiaux, J.-P. Doumerc, P. Dordor, L. Fournes, J.-P. Chaminade and M. Pouchard, J. Sol. Stat. Chem. 96 (1992) 20.

Griessen, R., Phys. Rev. B 38 (1988) 369.

Grover, A. K., R. Kumar and S. K. Malik, Solid. State. Comm. 77 (1991) 723.

Groves, P. D., *Electrochemistry* (John Murray, London, 1974).

Growacki, B. A., R. J. Highmore, K. F. Peters, A. L. Greer and J. E. Evetts, Supercond. Sci. Technol. 1 (1988) 7.

Gurvitch, M. and A. T. Fiory, Phys. Rev. Lett. 59 (1987) 1337.

Hahn, E. L., Phys. Rev. 80 (1950) 580.

Hammel, P. C., E. T. Ahrens, A. P. Reyes, J. D. Thompson, Z. Fisk, P. C. Canfield, J. E. Schirber and D. E. MacLaughlin, in *Phase Separation in Cuperate Superconductors*, edited by K. A. Müller and G. Benedek, (World Scientific, Singapore, 1993)

Harris, D. C. and T. A. Hewston, J. Solid State Chem. 69 (1987) 182.

Harris, D. C. and T. A. Vanderah, Inorg. Chem. 28 (1989) 1198.

Harshman, D. R., G. Aeppli, G. P. Espinosa, A. S. Cooper, J. P. Remeika, E. J. Ansaldo, T. M. Riseman, D. L. Williams, D. R. Noakes, B. Ellman and T. F. Rosenbaum, Phys. Rev. B 38 (1988) 852.

Hidaka, Y., Y. Enomoto and M. Suzuki, Jpn. J. Appl. Phys. 26 (1987) L377.

Hundley, M. F., J. D. Thompson, S.-W. Cheong, Z. Fisk and J. E. Schirber, Phys. Rev. B 41 (1990) 4062.

I. Tarasaki, M. Hase, A. Maeda, K. Uchinokura, T. Kimura, K. Kishio and H. K. I. Yanaka, Physics C 193 (1992) 365.

Ivanov, M. A., V. M. Loktev and Y. G. Pogorelov, Soviet Phys. JETP 74 (1992) 317.

Iye, Y., in *Mechanism of High Temperature Superconductivity*, edited by H. Kamimura and A. Oshiyama, (Springer-Verlag, Berlin, 1989) pp. 263.

Iye, Y., T. Tamegai, T. Sakakibara, T. Goto, N. Miura, H. Takeya and H. Takei, Physica C 153-155 (1988) 26.

Janossy, B., I. Tanaka, H. Kojima, R. Cabannel and L. Fruchter, Physica C 196 (1992) 73.

Johnston, D. C., Phys. Rev. Lett. 62 (1989) 957.

Johnston, D. C., J. Mag. Mag. Mat. 100 (1991) 218.

Johnston, D. C., T. Matsumoto, Y. Yamaguchi, Y. Hidaka and T. Murakami, in *Electronic Properties and Mechanisms of High Tc Superconductors*, edited by T. Oguchi, K. Kadowaki and T. Sasaki, (Elserier Science, B. V., 1992) pp.

Jorgensen, J. D., B. Dabrowski, S. Pei, D. G. Hinks, L. Soderholm, B. Morosin, E. L. Venturini and D. S. Ginley, Phys. Rev. B 38 (1988) 11337.

Jorgensen, J. D., H. B. Schuttler, D. G. Hinks, D. W. Capone, K. Zhang, M. B. Brodsky and D. J. Scalapino, Phys. Rev. Lett. 58 (1987) 1024.

Kastner, M. A., R. J. Birgeneau, C. Y. Chen, Y. M. Chiang, D. R. Gabbe, H. P. Jenssen, T. Junk, C. J. Peters, P. J. Picone, T. Thio, T. R. Thurston and H. L. Tuller, Phys. Rev. B 37 (1988) 111.

Kastner, M. A., R. J. Birgeneau, T. R. Thurston, P. J. Picone, H. P. Jenssen, D. R. Gabbe, M. Sato, K. Fukuda, S. Shamoto, Y. Endoh, K. Yamada and G. Shirane, Phys. Rev. B 38 (1988) 6636.

Kimura, T., K. Kishio, T. Kobayashi, Y. Nakayama, N. Motohira, K. Kitazawa and K. Yamafuji, Physica C 192 (1992) 247.

Kishio, K., Y. Nakayama, N. Motohira, T. Noda, T. Kobayashi, K. Kitazawa, K. Yamafuji, I. Tanaka and H. Kojima, Supercond. Sci. Technol. 5 (1992) S69.

Kitazawa, H. and K. Katsumata, Physica C 185-189 (1991) 1255.

Kitazawa, K., Y. Tomioka, T. Hasegawa, K. Kishio, M. Naito, T. Matsushita, I. Tanaka and H. Kojima, Supercond. Sci. Technol. 4 (1991) S35.

Kittel, C., *Introduction to Solid State Physics* (John Wiley & Sons, New York, 1981).

Kremer, R. K., E. Sigmund, V. Hizhnyakov, F. Hentsch, A. Simon, K. A. Muller and M. Mehring, Z. Phys. B 86 (1992) 319.

Kumagai, K., I. Watanabe, H. Aoki, Y. Nakamura, T. Kimura, Y. Nakamichi and H. Nakajima, Physica B 148 (1987) 480.

Kumar, G. R. and P. Chaddah, Phys. Rev. B 39 (1989) 4704.

Lauer, J. and W. Keune, Phys. Rev. Lett. 48 (1982) 1850.

Lee, W. H., Y. T. Huang, S. W. Lu, K. Chen and P. T. Wu, Sol. St. Comm. 74 (1990) 97.

Li, Q. and M. Suenaga, Phys. Rev. B 47 (1993) 2854.

LI, Q., M. Suenaga, T. Kimura and K. Kishio, Phys. Rev. B (1993)

Lindsey, C. P. and G. D. Patterson, J. Chem. Phys. 73 (1980) 3348.

Lobo, R. C., F. J. Berry and C. Greaves, J. Sol. Stat. Chem. 88 (1990) 513.

Loktev, V. M. and H. M. Yatarenko, Phys. Stat. Sol. (b) 166 (1991) 191.

Longo, J. M. and P. M. Raccah, J. Solid State Chem. 6 (1973) 526.

MacLaughlin, J. P. Vithayathil, H. B. Brom, J. C. J. M. d. Rooy, P. C. Hammel, P. C. Canfield, A. P. Reyes, Z. Fisk, J. D. Thompson and S. -W. Cheong, unpublished (1993)

Matsushita, T., E. S. Otabe and B. Ni, Supercond. Sci. Technol. 5 (1992) S73.

Mattheiss, L. F., Phys. Rev. Lett. 58 (1987) 1028.

McDevitt, J. T., Chemistry of High-temperature Superconductors 2 (1988) 207.

McGuire, T. R., T. R. Dinger, P. J. P. Freitas, W. J. Gallagher, T. S. Plaskett, R. L. Sandstrom and T. M. Shaw, Phys. Rev. B 36 (1987) 4032.

McHenry, M. E., S. Simizu and H. Lessure, Phys. Rev. B 44 (1991) 7614.

McHenry, M. R., B. G. Silbernagel and J. H. Wernick, Phys. Rev. Lett. 27 (1971) 426.

McHenry, M. R., B. G. Silbernagel and J. H. Wernick, Phys. Rev. B 5 (1972) 2958.

Miller, L. L., K. Sun, D. C. Johnston, J. E. Schirber and Z. Fisk, J. Alloys and Compounds 183 (1992) 312.

Montgomery, H. C., J. Appl. Phys. 42 (1971) 2971.

Moriya, T., Phys. Rev. 120 (1960) 91.

Morrison, S. R., *Electrochemistry at semiconductor and oxidized metal electrodes* (Plenum Press, New York, 1980).

Morrison, S. R., *The Chemical Physics of Surfaces* (Plenum, New York, 1990).

Nakamura, Y., S. Uchida, T. Kimura, N. Motohira, K. Kishio and K. Kitazawa, Physica C 185-189 (1991) 1409.

Nishihara, H., H. Yasuoka, T. Shimizu, T. Tsuda, T. Imai, S. Sasaki, S. Kanbe, K. Kishio, K. Kitazawa and K. Fueki, J. Phys. Soc. Jpn. 56 (1987) 4559.

Nücker, N., in *Physics of High-Temperature Superconductors*, edited by S. Maekawa and M. Sato, (Springer-Verlag, Berlin, 1992) pp. 283.

Oda, Y., M. Yamada, H. Ochiai, K. Asayama, T. Kohara, Y. Yamada, K. Koga, S. Kashiwai and M. Motoyama, Solid State Commun. 73 (1990) 725.

Preyer, N. W., M. A. Kastner, C. Y. Chen and R. J. Birgeneau, Phys. Rev. B 44 (1991) 407.

Radaelli, P. G. et al., unpublished (1993)

Radaelli, P. G., J. D. Jorgensen, A. J. Schultz, B. A. Hunter, J. L. Wagner, F. C. Chou and D. C. Johnston, Phys. Rev. B, accepted (1993)

Rega, T., J. Phys. : Condens. Matter 3 (1991) 1871.

Rettori, C., D. Rao, S. B. Oseroff, G. Amoretti, Z. Fisk, S. Cheong, D. Vier, R. D. Zysler and J. E. Schirber, Phys. Rev. B 47 (1993) 8156.

Rigamonti, A., F. Borsa, M. Corti, T. Rega, J. Ziolo and F. Waldner, in *Earlier and Recent Aspects of Superconductivity*, edited by J. G. Bednorz and K. A. Müller, (Springer-Verlag, Berlin, 1990) pp.

Rudolf, P., W. Paulus and R. Schollhorn, Anv. Mater. 3 (1991) 438.

Rudolf, P. and R. Schöllhorn, Chemical Comm., in press (1992)

Ryder, J., P. A. Midgley, R. Exley, R. J. Beynon, D. L. Yates, L. Afalfliz and J. A. Wilson, Physica C 173 (1991) 9.

Sasaki, S., H. Yasuoka, T. Shimizu, H. Nishihara, T. Tsuda, N. Sugii, S. Kambe, K. Kishio, K. Kitazawa and K. Fueki, J. Phys. Soc. Jpn. 57 (1988) 1151.

Sato, M., Physica C 153-155 (1988) 38.

Saylor, J., L. Takacs, C. Hohenemster, J. I. Budnick and B. Chamberland, Phys. Rev. B 40 (1989) 6854.

Schirber, J. E., W. R. Bayless, F. C. Chou, D. C. Johnston, P. C. Canfield and Z. Fisk, submitted to Phys. Rev. B (1993)

Schirber, J. E., B. Morosin, R. M. Merrill, P. F. Hlava, E. L. Venturini, J. F. Kwak, P. J. Nigrey, R. J. Baughman and D. S. Ginley, Physica C 152 (1988) 121.

Schollhorn, R., Angew. Chem. Int. Ed. Engl. 19 (1980) 983.

Selley, N. J., *Experimental Approach to Electrochemistry* (Halsted, New York, 1977).

Senoussi, S., M. Oussena and S. Hadjoudj, J. Appl. Phys. 63 (1988) 4176.

Shafer, M. W., T. Penneyu and B. L. Olson, Phys. Rev. B 36 (1987) 4047.

Shamoto, S., M. Onoda and M. Sato, Sol. Stat. Comm. 62 (1987) 479.

Shannon, R. D., Acta Crystallogr., Sect. A 32 (1976) 751.

Sieburger, R. and J. S. Schilling, Physica C 173 (1991) 403.

Singh, A., Z. Tesanovic, H. Tan, G. Xiao, C. L. Chien and J. C. Walker, Phys. Rev. Lett. 64 (1990) 2571.

Slichter, C. P., *Principles of Magnetic Resonance* (Springer-Verlag, Heideberg, 1990).

Smedskjaer, L. C., J. L. Routbort, B. K. Flandermeyer, S. J. Rothman, D. G. Legnini and J. E. Baker, Phys. Rev. B 36 (1987) 3903.

Sternlieb, B. J., G. M. Luke, Y. J. Uemura, T. M. Riseman, J. H. Brewer, P. M. Gehring, K. Yamada, Y. Hidaka, T. Murakami, T. R. Thurston and R. J. Birgeneau, Phys. Rev. B 41 (1990) 8866.

Suenaga, M., D. O. Welch and R. Budhani, Supercond. Sci. Technol. 5 (1992) S1.

Sun, K., J. H. Cho, F. C. Chou, W. C. Lee, L. L. Miller, D. C. Johnston, Y. Hidaka and T. Murakami, Phys. Rev. B 43 (1991) 239.

Suryanarayanan, R., W. Paulus, M. S. R. Rao, O. Gorochev, L. Ouhammou and G. Heger, Superrcond. Sci. Technol. 5 (1992) 82.

Suzuki, M., Phys. Rev. B 39 (1989) 2312.

Suzuki, M., Physica C 185-189 (1991) 2343.

Suzuki, M. and M. Hikita, Phys. Rev. B 47 (1993) 2913.

T-Muromachi, E., T. Sasaki and Y. Matsui, Physica C 207 (1993) 97.

Takagi, H., B. Batlogg, H. L. Kao, J. Kwo, R. J. Cava, J. J. Krjewski and J. A. F. Peck, Phys. Rev. Lett. 69 (1993) 2975.

Takagi, H., R. J. Cava, M. Marezio, B. Batlogg, J. J. Kraiewski, J. W. F. Peck, P. Bordet and D. E. Cox, Phys. Rev. Lett. 68 (1992) 3777.

Takagi, H., T. Ido, S. Ishibashi, M. Uota, S. Uchida and Y. Tokura, Phys. Rev. B 40 (1989) 2254.

Takahashi, M., T. Nishino and J. Kanamori, J. Phys. Soc. Jpn. 60 (1991) 1365.

Tan, Z., M. E. Filipkowski, J. I. Budnick, E. K. Heller, D. L. Brewe, B. L. Chamberland, C. E. Bouldin, J. C. Woicik and D. Shi, Phys. Rev. Lett. 64 (1990) 2715.

Tarascon, J. M., L. H. Greene, W. R. Mackinnon, G. W. Hull and T. H. Geballe, Science 235 (1987) 1373.

Terasaki, I., M. Hase, A. Maeda, K. Uchinokura, T. Kimura, K. Kishio, I. Tanaka and H. Kojima, Physica C 193 (1992) 365.

Thio, T., T. R. Thurston, N. W. Preyer, P. J. Picone, M. A. Kastner, H. P. Jenssen, D. R. Gabbe, C. Y. Chen, R. J. Birgeneau and A. Aharony, Phys. Rev. B 38 (1988) 905.

Thurston, T. R., R. J. Birgeneau, D. R. Gabbe, H. P. Jenssen, M. A. Kaster, P. J. Picone, N. W. Preyer, J. D. Axe, P. Boni, G. Shirane, M. Sato, K. Fukuda and S. Shamoto, Phys. Rev. B 39 (1989) 4327.

Tilak, B. V., B. E. Conway and H. Angerstein-Kozlowska, Electroanaly. Chem. Interf. Electrochem. 48 (1973) 1.

Tomioka, Y., Y. Nakayama, M. Naito, T. Matsushita, I. Tanaka, H. Kojima, T. Ishii, K. Kishio and K. Yamafuji, Physica C 185-189 (1991) 2163.

Torrance, J. B., A. Bezinge, A. I. Nazzal, T. C. Huang, S. S. P. Parkin, D. T. Keane, S. L. LaPlaca, P. M. Horn and G. A. Held, Phys. Rev. B 40 (1989) 8872.

Tozer, S. W., A. W. Kleinsasser, T. Penney, D. Kaiser and F. Holtzberg, Phys. Rev. Lett. 59 (1987) 1768.

Trasatti, S., *Electrodes of Conductive Metallic Oxides* (Elsevier Scientific, 1981).

Uemura, Y. J., W. J. Kossler, J. R. Kempton, X. H. Yu, H. E. Schone, D. Opie, C. E. Stronach, J. H. Brewer, R. F. Kiefl, S. R. Kreitzman, G. M. Luke, T. Riseman, D. L. Williams, E. J. Ansaldo, Y. Endoh, E. Kudo, Yamada, D. C. Johnston, M. Alvarez, D. P. Goshorn, Y. Hidaka, M. Oda, Y. Enomoto, M. Suzuki and T. Murakami, Physica C 153-155 (1988) 769.

Unoki, H., Y. Nishihara, K. Oka, M. Tokumoto and K. Murata, Physica C 153-155 (1988) 1481.

Vaknin, D., S. K. Sinha, D. E. Moncton, D. C. Johnston, J. M. Newsman, C. R. Safiinya and J. H. E. King, Phys. Rev. Lett. 29 (1987) 2802.

Wang, J., G. Chen, X. Chu, Y. Yan, D. Zheng, Z. Mai, Q. Yang and Z. Zhao, Supercond. Sci. Technol. 1 (1988) 27.

Watanabe, I., K. Kumagai, Y. Nakamura and H. Nakajima, J. Phys. Soc. Jpn. 59 (1990) 1932.

Wattiaux, A., J. C. Grenier, M. Pouchard and P. Hagenmuller, J. Electrochem. Soc. 134 (1987) 1714.

Wattiaux, A., J. Park, J. Grenier and M. Pouchard, C. R. Acad. Sci. (Paris), Series II 310 (1990) 1047.

Wattiaux, A., J. Park, J. Grenier and M. Pouchard, C. R. Acad. Sci. Paris , Series II 310 (1990) 1047.

White, R. M., *Quantum Theory of Magnetism* (Springer-Verlag, Berlin, 1983).

Worthington, T. K., W. J. Gallagher, D. L. Kaiser, F. H. Holtzberg and T. R. Dinger, Physica C 153-155 (1988) 32.

Yamada, K., E. Kudo, Y. Endoh, Y. Hidaka, M. Oda, M. Suzuki and T. Murakami, Sol. Stat. Comm. 64 (1987) 753.

Yamada, N. and M. Ido, Physica C 203 (1992) 240.

Yamafuji, K., Y. and Mawatari, Supercond. Sci. Technol. 5 (1992) S204.

Yamaguchi, Y., M. Tokumoto, S. Waki, Y. Nakagawa and Y. Kimura, J. Phys. Soc. Jpn. 58 (1989) 2256.

Yang, Z. J., K. Kishio, T. Kobayashi, T. Kimura and S. L. Yuan, J. Phys.: Condens. Matter 5 (1993) 1883.

Zalesskii, A. V., V. G. Krivenko, A. P. Levanyuk, I. E. Lipinski, Y. G. Metlin and T. A. Sivokon, Superconductivity 3 (1990) 202.

Zhang, H. and H. Sato, Phys. Rev. Lett. 70 (1993) 1697.

Zhou, J., S. Sinha and J. B. Goodenough, Phys. Rev. B 39 (1989) 12231.

Ziolo, J., F. Borsa, M. Corti and A. Rigamonti, Physica C 153-155 (1988) 725.

Ziolo, J., F. Borsa, M. Corti, A. Rigamonti and F. Parmigiani, J. Appl. Phys. 67 (1990) 5864.

ACKNOWLEDGMENTS

I have been very fortunate to have completed my graduate research work under the guidance of Professor David Johnston. Being an open-minded advisor and a good friend, he encourages me to try out new ideas and shares the excitement of discovery with me. I am grateful to Professor Ferdinando Borsa's constant support on NMR works. It is always a rewarding experience to have stimulating discussions with him.

I wish to express my appreciation to Jin Hyung Cho who generously guided me in my early research period. All the works we collaborated are the major learning lessons for me. I would like to thank Dr.'s James Jorgensen, Chris Hammel and Robert Gooding for many valuable discussions. I am indebted to many colleagues in our new materials lab and NMR lab for their help and cooperation, especially Zhaorong Wang, Beongki Cho, Jerzi Ziolo, Alexandra Lascialfari, Kyung Han Kim, Byoungjin Suh, Ananda Shastri and David Torgeson.

Many friends have helped me transform the journey in the United States enjoyable: many thanks to Chiao-ling and May-yin Wu, Shu-shin and Lee-wan Hsu, Tseng-yen and Ru-yin Chung, Leon and Nancy Razaitis and Micky and Jan Krug-Fite. Special thanks goes to Paul and Sunny Rutherford, Jr. for their hospitality during our stay in Iowa and Paul's helpful correction on my writing.

I am deeply appreciative to my mother, Shu-Huei Yang, and my wife, Shi-Jiuan, for being there in every way. I am grateful to my

father and mother-in-law and my brothers and sisters for their encouragement and assistance.

This work was performed at Ames Laboratory under contract no. W-7405-eng-82 with the U. S. Department of Energy. The United States government has assigned the DOE Report number IS-T 1661 to this thesis.

DATE
FILMED
2/23/94
END